To the Graduate Council :

I am submitting herewith a thesis written by M. Satishchandra Arya entitled "Convective Heat Transfer in a Sealed Vertical Storage Cask Containing Spent–Fuel Canisters." I have examined the final copy of this thesis for form and content and recommend that it be accepted in partial fulfilment of the requirements for the degree of Master of Science, with a major in Mechanical Engineering.

Majid Keyhani

Majid Keyhani, Major Professor

We have read this thesis
and recommend its acceptance :

Rao V. Arimilli

Accepted for the Council :

C W Minkel

Vice Provost
and Dean of The Graduate School

STATEMENT OF PERMISSION TO USE

In presenting this thesis in partial fulfilment of the requirements for a Master's degree at The University of Tennessee, Knoxville, I agree that the Library shall make it available to borrowers under rules of the Library. Brief quotations from this thesis are allowable without special permission, provided that accurate acknowledgment of the source is made.

Permission for extensive quotation from or reproduction of this thesis may be granted by my major professor, or in his absence, by the Head of Interlibrary Services when, in the opinion of either, the proposed use of the material is for scholarly purposes. Any copying or use of the material in this thesis for financial gain shall not be allowed without my written permission.

signature [illegible]

Date 05-19-1988

Convective Heat Transfer in a Sealed Vertical Storage Cask Containing Spent–Fuel Canisters

A Thesis

Presented for the

Master of Science

Degree

The University of Tennessee, Knoxville

M. Satishchandra Arya

August 1988

Acknowledgments

The author wishes to express his appreciation to his advisor Dr. M. Keyhani for his excellent support, guidance and willingness to help in completing this project.

Acknowledgment should also be made to his committee members Dr. R. V. Arimilli and Dr. J. R. Parsons for their valuable suggestions.

This research was sponsored by Energy, Environment and Resources center, The University of Tennessee, Knoxville, under the Center of Excellence – Waste Management – Needs Assessment Project RO1–2532–20. The author would also like to express his thanks to Dr. Wm. Colglazier, Director, EERC, and Dr. Helen Hafford, Associate Director, EERC.

Abstract

An experimental study of natural convection heat transfer in a one–twelfth scaled model of a sealed storage cask of the Integral Monitored Retrievable Storage (MRS) facility containing twelve canisters is performed. A uniform power dissipation per unit length is supplied to each canister (heater rod) and the cask (outer cylinder) is maintained at a constant temperature. Correlations representing the convective Nusselt number as a function of Rayleigh number for each rod as well as one for the rod–bundle as a whole are reported. Two outer cylinders in a vertical position with exactly the same dimensions, one with internal fins and the other without the fins are used in these experiments. Comparison of the heat transfer data obtained for these two show that the conduction regime terminates at a much lower Rayleigh number in case of the cylinder without internal fins. Moreover, the critical Rayleigh number (onset of convection) obtained for this case is in a good agreement with the one predicted by a general correlation for square array of rod–bundles as reported previously. A significant result of the present study is that, once, the rod–bundles reach their respective convective flow regime, the heat transfer can be predicted with a single correlation. Using a length scale recommended in this study, the correlation predicts the convective Nusselt number for all the available rod–bundle data (present and previously reported results) with an accuracy of 7.2%.

Contents

List of Tables

List of Figures

List of Abbreviations and Symbols

Abbreviations

A_d	Area of heater rod, m^2
A_T	Total outer surface area, (including fin area if present), m^2
C_p	Specific heat at constant pressure, $KJ/Kg-K$
d	Diameter of heater rod, m
d_i	Diameter of an equivalent fictitious inner cylinder, $(M)^{\frac{1}{2}}d$. m
D	Diameter of the outer cylinder, m
D^*	Equivalent outer cylinder diameter based on A_T, $(\frac{A_T}{\pi L})^{\frac{1}{2}}$, m
g	Gravitational constant, m/s^2
h_d	Convective heat transfer coefficient on each rod, $\frac{q_c}{A_d(T_{MR}-T_{MC})}$, W/m^2-K
h_{Td}	Total heat transfer coefficient on each rod, $\frac{q}{A_d(T_{MR}-T_{MC})}$, W/m^2-K
h_D	Overall convective heat transfer coefficient on the outer cylinder, $\frac{Q_c}{A_T(T_{MR1}-T_{MC})}$, W/m^2-K
h_{TD}	Overall total heat transfer coefficient on the outer cylinder, $\frac{Q}{A_T(T_{MR1}-T_{MC})}$, W/m^2-K
H	Aspect ratio of the equivalent annulus, $\frac{L}{l}$
k	Thermal conductivity, $W/m-K$
K	Radius ratio of the equivalent annulus, $\frac{r_o}{r_i}$
l	Annular gap of the equivalent annulus, r_o-r_i, m

L	Height of the rod–bundle, m
M	Total number of rods in the bundle
Nu_d	Convective Nusselt number, $\frac{h_d d}{k}$
Nu_{Td}	Total Nusselt number, $\frac{h_{Td} d}{k}$
Nu_D	Overall convective Nusselt number, $\frac{h_D D}{k}$
Nu_{TD}	Overall total Nusselt number, $\frac{h_{TD} D}{k}$
p	Pitch, m
P	Pressure, $atm.$ ($1 atm. = 1.01325\ KN/m^2$)
Pr	Prandtl number
q	Power per rod, W
q_c	Energy transferred by convection for a given heater rod, W
Q	Total power input, W
Q_c	Energy transferred by convection by all the rods, W
r	Radius, m
Ra_d	Rayleigh number based on the diameter of the rods, $\frac{g\beta}{\alpha\nu} d^3 (T_{MR} - T_{MC})$
Ra_D	Rayleigh number based on the diameter of the outer cylinder, $\frac{g\beta}{\alpha\nu} D^3 (T_{MR} - T_{MC})$
$R1$	Rod-position 1 (four–rods)
$R2$	Rod-position 2 (eight–rods)
T_f	Reference fluid temperature for evaluating thermophysical properties, $T_{MC} + 0.25(T_{MR} - T_{MC})$, C
T_{MC}	Mean temperature of the outer cylinder , C
T_{HP}	Temperature measured from Hewlett–Packard's Data Acquisition unit
T_{hR}	Temperature on the hot side of the rods, C
T_{cR}	Temperature on the cold side of the rods, C
T_{MR}	Mean temperature of a given rod, C

T_{MR1}	Mean temperature of R1, C
T_{NBS}	Temperature measured from NBS calibrated thermometer
ΔT	Characteristic temperature difference between the rod-bundle and the outer cylinder, $T_{MR} - T_{MC}$, C
y	Co-ordinate (measured from the bottom of the rod-bundle), m

Symbols

α	Thermal diffusivity, $\frac{k}{\rho C_p}$, m^2/s
β	Isobaric coefficient of thermal expansion, K^{-1}
ν	Kinematic viscosity, m^2/s
ρ	Density, Kg/m^3

Subscripts

c	Convection
cr	Critical value
d	Based on the diameter of the rods
D	Based on the diameter of the outer cylinder
i	Inner
o	Outer
r	Radiation
R	Rod
T	Total value

Chapter 1

INTRODUCTION

1.1 Background

Spent–fuel refers to nuclear fuel that has been used in a reactor to produce heat to generate electricity. After several years, its ability to produce heat is diminished to a point where it must be replaced. The fuel is in the form of small ceramic pellets of uranium, which are sealed in 12 to 13 feet long tubes. After removal from the reactor, these assemblies are stored in concrete storage pools lined with stainless steel. The water in the pool shields against radiation emissions and removes heat produced by radioactive decay of the spent–fuel. According to Newman [9], the Department of Energy will begin accepting spent–fuel from the utilites for final disposal deep underground in 1998. By that time, the quantity of spent–fuel, currently 13,000 metric tons of uranium (MTU), would have tripled to almost 41,000 MTU. Requirements for additional on–site storage will increase to about 11 % of the inventory (4850 MTU). Some plants have been already experiencing a shortage for storage capacity.

According to the Department of Energy, by 1998, the operating 39 Light Water Reactor Plants (LWR) would accumulate more spent–fuel than their pools are licensed to store, even after extensive modification. There is a possibility in the future that dry storage casks, approximately 8 feet in diameter, 16 feet long, which can hold about 10 MTU of unconsolidated spent–fuel would be constructed for dry storage of spent–fuel, that is, to provide a permanent disposal method posing no threat to people or the environment. Dry storage casks could be deployed at nearly all reactor sites. They are generally designed for adequate cooling of spent–fuel from the reactor core for five years or more.

A conceptual design report [1] of Integral Monitored Retrievable storage facility has been completed and is under review by the Department of Energy. The proposed details of the design for the storage of Pressurized Water Reactor spent–fuel are given in Fig. 1.1. As shown, a unit storage cell consists of a concrete cask, a carbon steel liner with dividers to facilitate the placement of twelve canisters inside the liner. Each canister contains fuel rods from three Westinghouse 17 $\times$ 17 PWR spent–fuel assemblies.

1.2 Literature Review

Larson et al. [7] conducted a numerical and experimental study of natural convection heat transfer in a horizontal enclosure formed by an inner heated circular or a hexagonal cylinder which is centrally placed in a rectangular isothermal box. The two selected models represent nuclear spent–fuel shipping casks. In their numerical approach, the assumption of incompressibility and the Boussinesq approximation were invoked. Two solution algorithms were formed, one using finite differences and the other for the finite element method. In order to check the accuracy of the numerical method, an experimental study involving Laser Interferometry was conducted. The temperature field in the test cells set up to simulate the two geometric configurations of a fuel element in the shipping cask was determined. Air was used as a fluid in both the tests. They were not able to make measurements and perform numerical analyses at high Grashof numbers ($> 10^8$) with moderate to high Prandtl

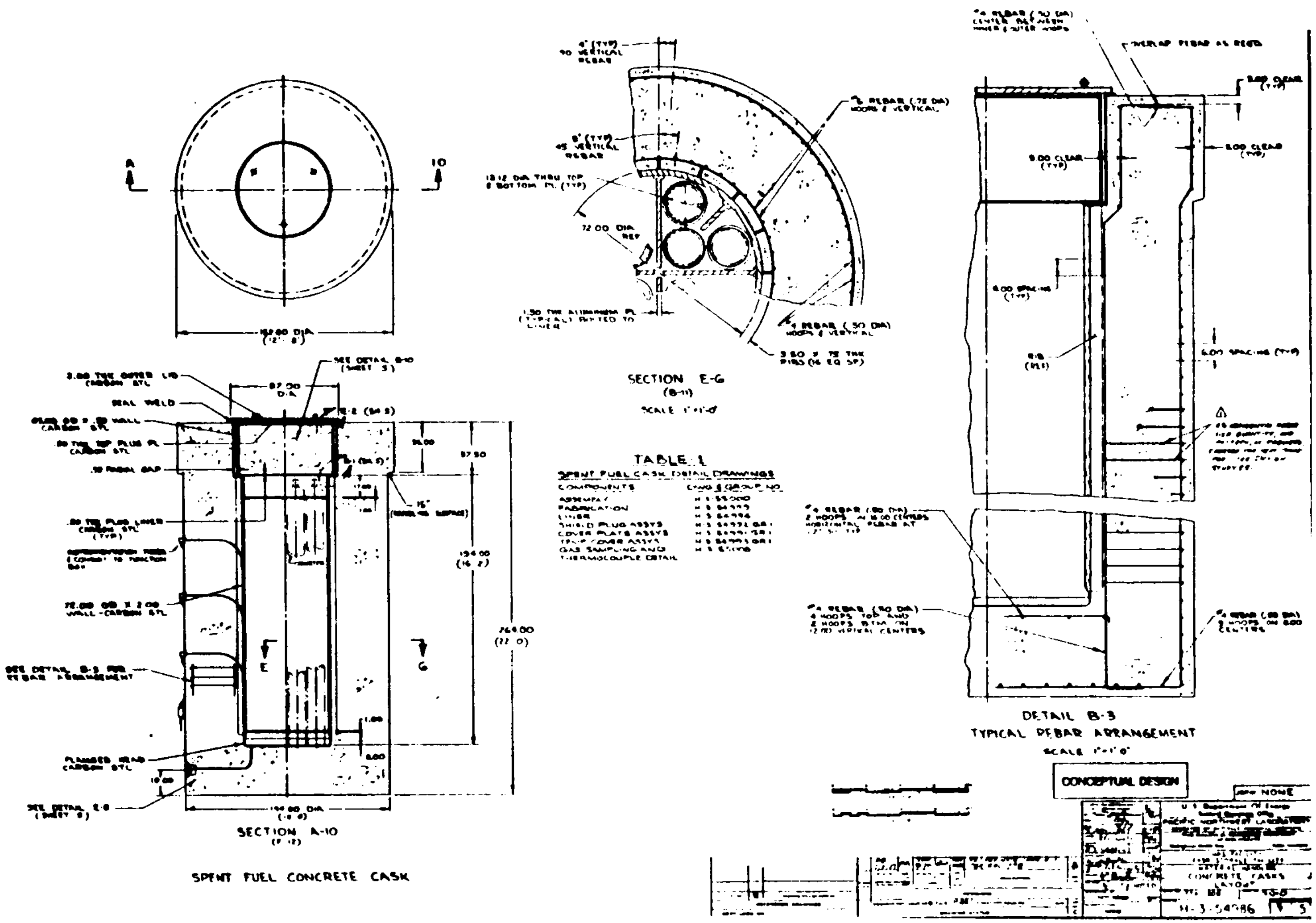

Figure 1.1: Spent fuel cask detail drawings

number (> 10). The experimental and computational results are qualitatively comparable, but there is a problem of parallax when viewing a holometrogram which is a projection of three–dimensional field (unlike classical intereferometry which deals with two dimensional fields). They have reported another possible source of error which is due to the fact that the boundary temperatures in the test sections were not truly isothermal as assumed in the numerical model.

Wong and Chen [11] have developed the analytical techniques to obtain closed–form solutions for the two–dimensional fluid flow and heat transfer problems in a finite rod bundle system. They have shown that this system can be effectively handled by augmenting the effects of all the cylindrical rods. The method is applicable for both symmetrical rod arrangements and for rods with arbitrary dimensions and orientations. They have illustrated the solution method by formulating the solutions for both Poisson and the Helmholtz equations in a finite rod bundle system and presented the numerical equation in a circular flow channel containing a center rod and a ring with six peripheral rods and with Dirichlet boundary conditions specified on the wall surfaces. The Helmholtz equation describes the vapor temperature distribution in non–equilibrium dispersed droplet laminar flow in rod bundles under emerging core cooling reactor operating conditions. The conclusion of their analysis is that the asymmetrical geometries tends to reduce the overall heat transfer of a finite rod bundle system, and the hot spots occur at the narrow gaps between adjacent rods.

McCann [8] has developed a finite difference code, Hydra–I, that simulates the three–dimensional performance of a spent–fuel assembly contained within a canister. The convection heat transfer contribution is determined by calculating the velocity and pressure fields consistent with the conservation laws of mass and momentum. The nearest and next–nearest neighbor rods are considered for radiation exchange within the spent–fuel assembly. Also, the radiation exchange between the fuel assembly and support structure and canister are included. The code is quite versatile, since it can handle coupled modes of conduction, convection and radiation heat transfer and permits spatially varying boundary conditions, thermophysical properties and power generation rates. A major assumption in his study was to treat the rod–bundle as a porous media with directional permeabilities. Nearly two dozen cases have been examined using this code. From the results presented, the maximum and various local temperatures and heat fluxes illustrating the changing importance of the three modes of heat transfer and the thermal time dependence of a fuel assembly to a transient imposed on the canister has been shown. Since, the calculations performed were not verified against experimental data, the numerical code that has been developed cannot be completely relied upon. In particular, he has emphasized that the convection heat transfer modelling can be more adequately assessed when complete air data is available and also the thermal radiation heat transfer modelling can be verified by examining a well–defined vacuum system.

Cox [2] has experimentally and theoretically investigated the radiative heat transfer in enclosed rod–bundles for two different geometries, a square array on a square pitch and a hexagonal array on a equilateral triangular pitch. He has shown two different methods to be adapted for treating radiative exchanges with diffuse grey enclosures, one for the steady–state and the other for the transient problem. For the steady–state problem, the net radiation method [10] was found to be the most convenient, while for the transient one, either Gebhart's [3] or Hottel's [4] equations were the most suitable.

Keyhani et al. [5, 6] have experimentally investigated free convection in two vertical rod–bundles; a 3×3 array with $p/d = 3.08$, $L/d = 138$ and $L/D = 10.62$, and a 5×5 array with $p/d = 2.25$, $L/d = 92.42$ and $L/D = 5.79$, covering a wide range of Rayleigh numbers with helium, air and water as the convective media. They have shown that, when the air and water results are compared, for a fixed Rayleigh number, an increase in Prandtl number results in a reduction in Nusselt number, which is contrary to what has been previously observed for the vertical cavities, attributing this difference to the curvature effects. They have proposed an equivalent annulus model for the enclosed rod–bundles, and based on this, reported a general correlation for predicting the critical Rayliegh number for the onset of convective flow.

1.3 Motivation

The heat transfer processes that are taking place inside the liner enclosure are conduction, convection and thermal radiation heat transfer. All the three modes are strongly three–dimensional. It is indeed, extremely complicated for the complete analysis of the problem.

The thermal analysis of this problem contained in the Conceptual Design Report [1] (Volume IV Book XIV – Calculations) is very simplistic and indeed unrealistic. The thermal radiation and convection heat transfer from each canister are simplified by assuming that they are equivalent to the heat transfer across an imaginary annulus formed by the canister and an imaginary cylinder, concentric with the canister, placed half–way between the adjacent canisters. Then, the convection heat transfer coefficient across the imaginary annulus was calculated by using the available empirical correlations. The radiation heat transfer across the imaginary annulus was calculated with the assumption that the view factor is unity. Based on these unrealistic calculations, the effective thermal conductivity of air inside the cask was calculated. Finally, the temperature field was solved by using a two–dimensional conduction heat transfer numerical code. Here, it has to be emphasized that even though the three modes of heat transfer present are strongly three–dimensional and interdependent, a two–dimensional conduction heat transfer analysis was performed.

This discussion clearly indicates that the existing analysis cannot be relied upon for the accurate prediction of the spent-fuel temperature. It is necessary to obtain an accurate predictive scheme for removal of the generated energy by the spent-fuel to the outside surface of the concrete cask. One of the conclusions in the above report is that the heat transfer through the cask wall could be enhanced through the use of radial rebar or other means. Thus, positioning of the fins or ribs within the cask cavity were recommended in order to enhance the heat transfer from the canisters to the cask liner. In order to quantify the effect of fins on heat transfer, in addition to the cask with the fins present, another cask with exactly the same dimensions, but without the fins was also considered for the thermal analysis of this problem.

1.4 Objectives

The objectives sought to complete this project were :

- To develop the engineering correlations for convective Nusselt number as a function of Rayleigh number.

  1. Nu_d versus Ra_d for each rod in the bundle.
  2. Nu_D versus Ra_D for the overall rod-bundle.

- To determine the effect of presence of fins on heat transfer from the canisters to the cask.

- To find and compare the radiation contribution of both the casks and with different convective media (helium and air).

- To determine the extent of conduction flow regime so as to obtain the critical Rayleigh number ($Ra_{D_{cr}}$) for the onset of convection and to compare with the one predicted by a general correlation for a square array of rod–bundles as reported by Keyhani et al. [5, 6].

1.5 Method of Attack

As shown in Figs. 1.2a and 1.2b, a one–twelfth scaled model of the actual liner–canister arrangement has been designed and fabricated in order to conduct heat transfer experiments in a controlled environment with the specific objective of obtaining the maximun temperature of each canister and empirical relations that can be used to predict convective Nusselt number for each canister inside the enclosure as well as for the overall case. Then, the maximum temperatures on the surface of the canisters for the actual model (atmospheric pressure) at various heat generations and radiation heat transfer contributions can be predicted.

The convective heat transfer coefficient or non–dimensional Nusselt number for a given surface in an enclosure is governed by the relevant non–dimensional geometric parameters as well as a non–dimensional flow parameter (Rayleigh number). Hence, the results obtained from this model with the geometric parameters being the same as those of the actual liner can be extended to the actual case by either extrapolating the data, if the required Rayleigh number range is not covered or without extrapolating, if the range is covered. The range of Rayleigh number in the experiments can be extended by either varying the temperature field and/or pressurizing the enclosure. The radiative component of the total heat transfer can be obtained through a series of experiments conducted in a vacuum environment. The thermal radiation heat transfer effects will also be the same as long as the absolute values of the temperature field in the model are comparable to the values in the actual liner enclosure. This can

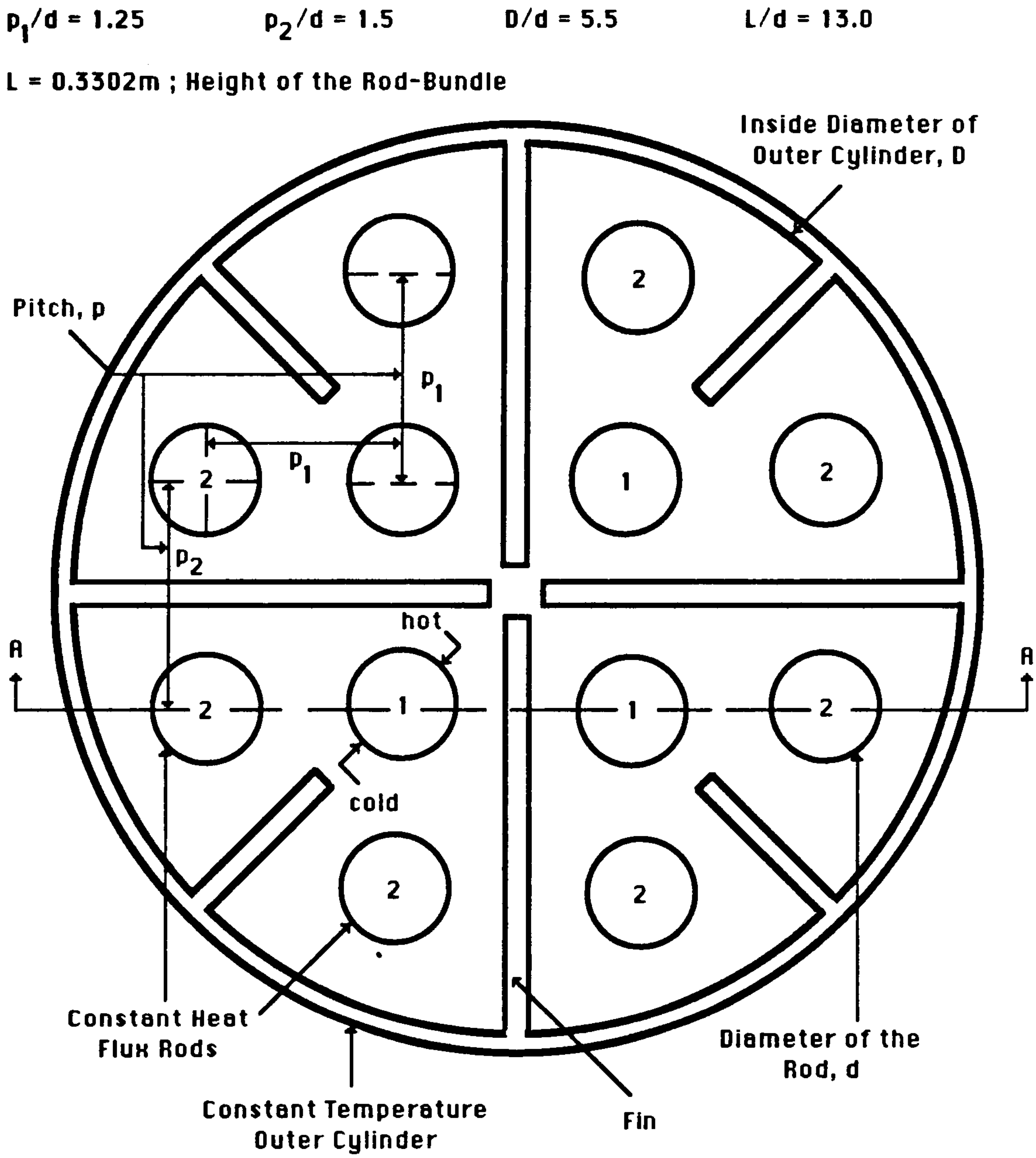

Figure 1.2: Schematic of experimental apparatus (a) Sectional top-view (b) Sectional front-view (A–A plane of 2a)

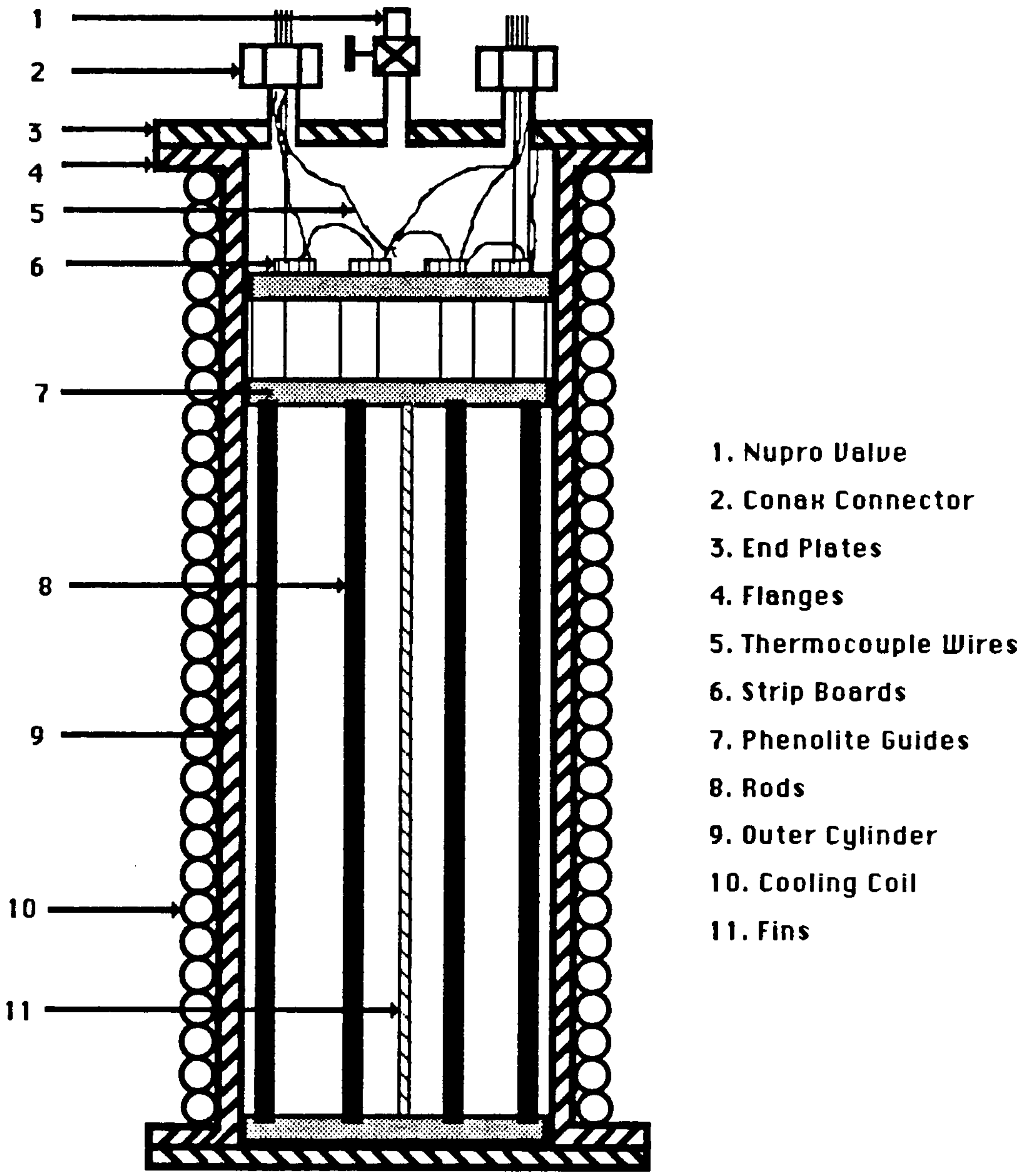

Figure 1.2 (Continued)

be achieved by imposing the heat flux on the surface of the canisters as are actually generated by the spent–fuel.

Chapter 2

EXPERIMENTAL APPARATUS AND PROCEDURE

2.1 Apparatus

The experimental set-up is a one-twelfth scaled model of an actual MRS cask configuration, excluding the outer concrete component. It consists of an outer cylinder in the vertical position, end-plates, rod-bundle and power supply with associated circuitry as can be seen in the Figs. 1.2b and 2.1. The detailed discussion of all the components is presented below.

The brass outer cylinder is a 13.97 cm in inner diameter with a wall thickness of 0.32 cm and a length of 48.57 cm. Two brass flanges of 20.0 cm in diameter and 0.95 cm in thickness are silver soldered to each end of the cylinder with sixteen equally spaced, threaded holes (azimuthal, angular direction) in order to facilitate the attachment of the end-plates as seen in Fig. 2.2. To provide a tight sealing between the end-plates and flanges, o-rings made of Ethylene Propylene Rubber of 14.92 cm inner diameter and 0.48 cm in width are placed in grooves cut in the flanges. Two separate segments of soft copper tubing, each covering one-half of the cylinder height are soft soldered to the outer cylinder.

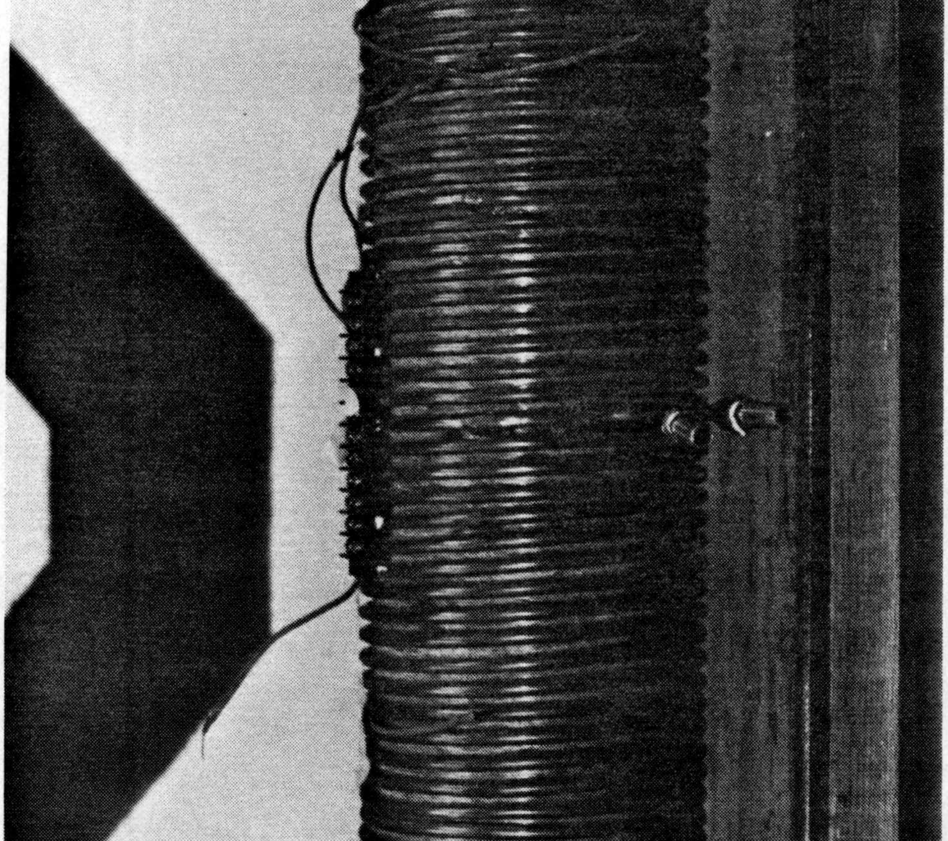

Figure 2.1: Outer cylinder

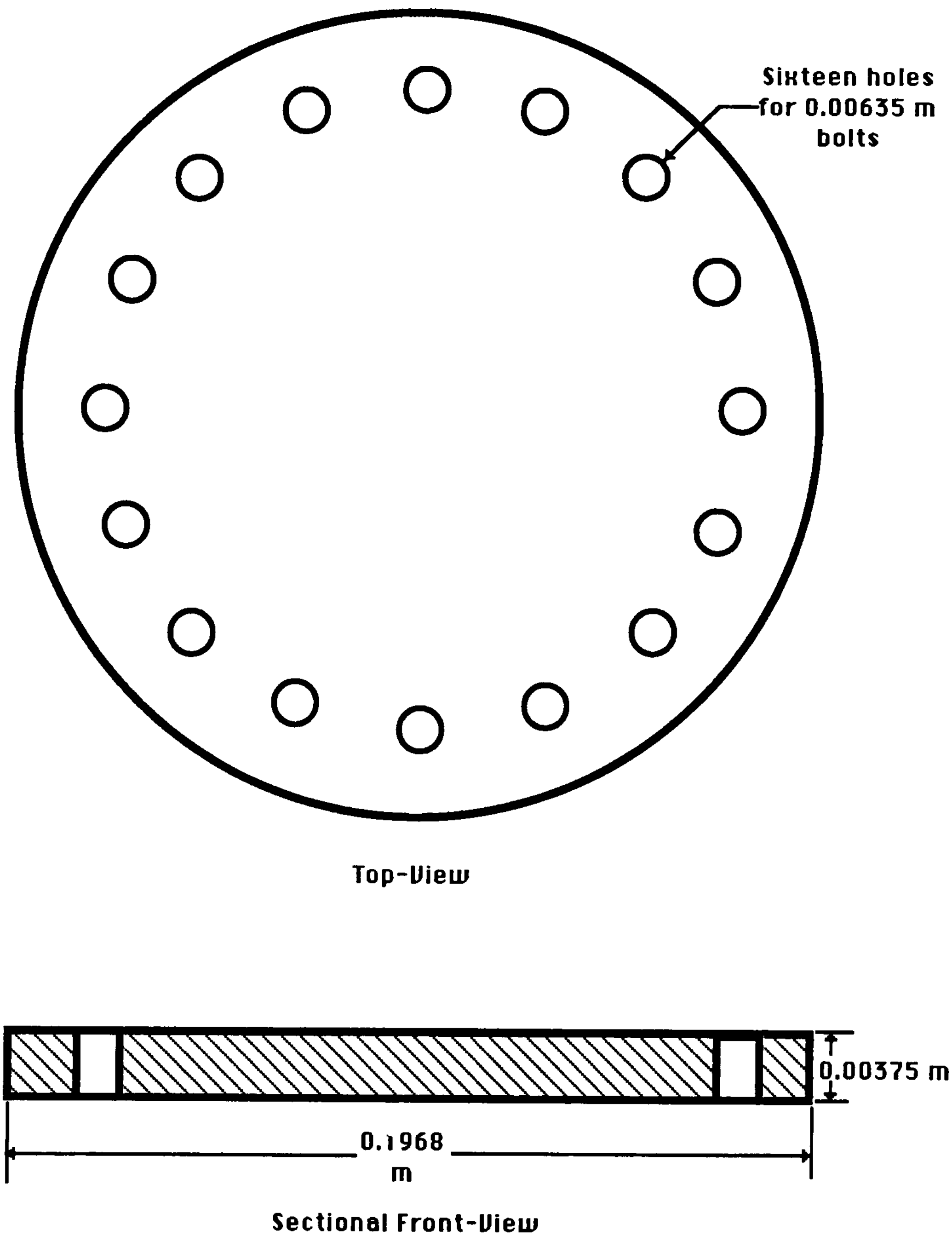

Figure 2.2: Top and bottom end-plates

Two constant temperature circulators (MGW LAUDA MT 6) supply water to the cooling coils in order to maintain a constant surface condition. Finally, two sets of brass fins are soft soldered to the inside surface of the cylinder as shown in Fig. 2.3 The first set are 34.92 cm in width, 0.32 cm in thickness and 6.84 cm in length are aligned along the imaginary center line (θ–direction) and the second set with a smaller length of 2.59 cm are each placed at forty–five degrees from the imaginary center line in the θ–direction.

The two end–plates provide an air tight sealing to the apparatus. The top end–plate is a 0.95 cm thick piece of brass with a diameter of 20.0 cm. Four 1.91 cm holes are tapped and threaded in this plate to accomodate the conax connectors. Three of these connectors are used to send through the leads of twenty–four thermocouples and one for the power leads as shown in Fig. 2.4. On the outer surface of the plate, exactly at the center, a thermocouple at a depth of 0.32 cm is glued to help in the determination of the convective heat loss. The bottom end–plate is similar to the top end–plate with the exception that there are no holes leading into the enclosure.

The spent–fuel canisters are represented by twelve 2.54 cm in diameter and 34.29 cm long Watlow Fire Rod Cartridge heaters as can be seen in Figs. 2.5a and 2.5b respectively. The heaters are spaced in four symmetrical arrangements inside the cylinder (please see Fig. 1.2a). The spacing of heaters according to the specifications of the original model are held in place with the aid of two guides, made of phenolite of 1.27 cm in thickness and 13.94 cm in diameter. A steel disk of 0.32 cm in thickness is fastened to the bottom of the lower guide in order to provide a support for the rod–bundle assembly. Twelve holes of 2.54 cm in diameter are drilled on each guide to assemble the heaters. The whole assembly can easily slide past the fins and after it is completely inside the cylinder, a gap of 11.43 cm is available above the top–guide to facilitate the connection to the heaters and thermocouple leads.

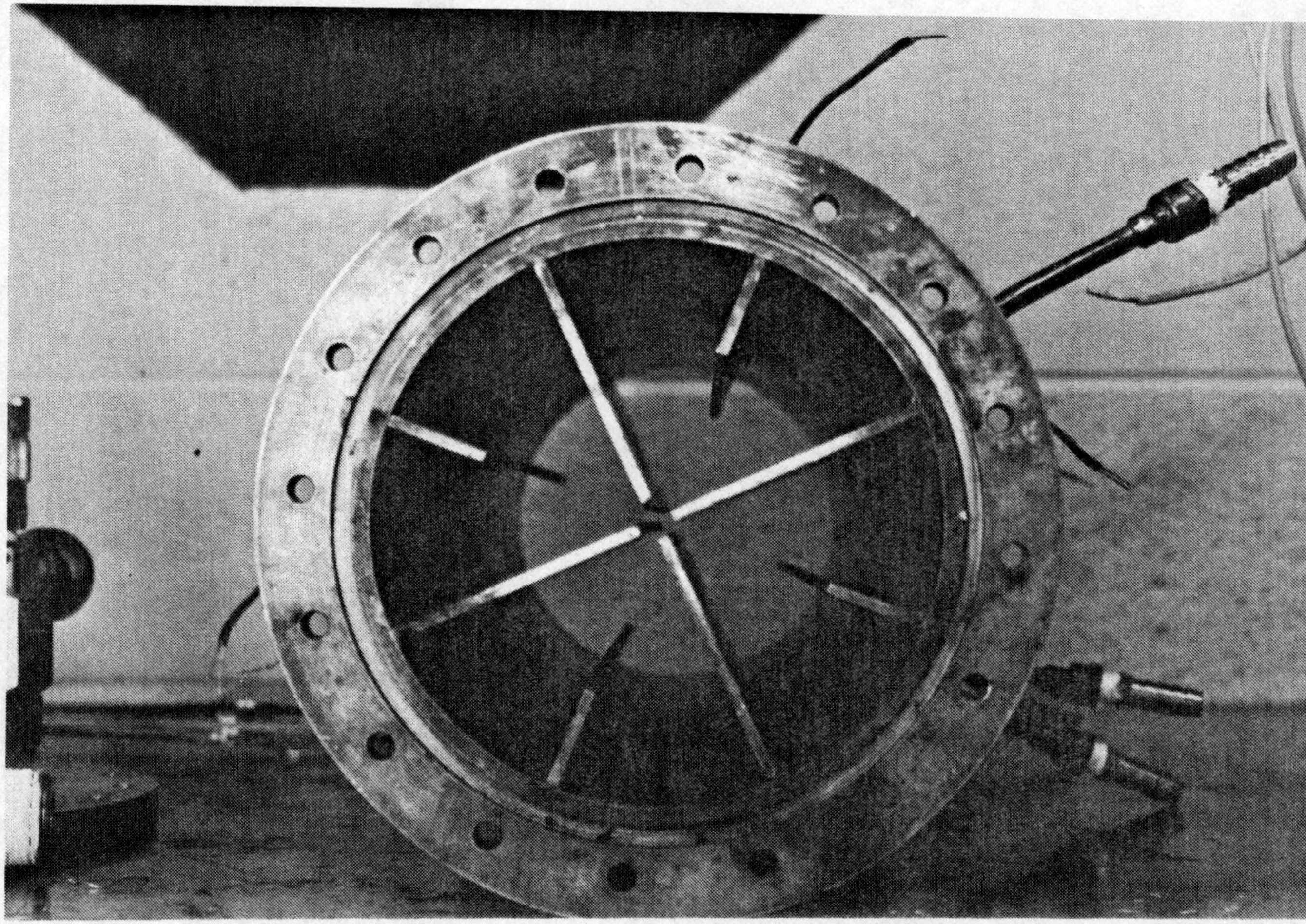

Figure 2.3: Location of brass fins inside the outer cylinder

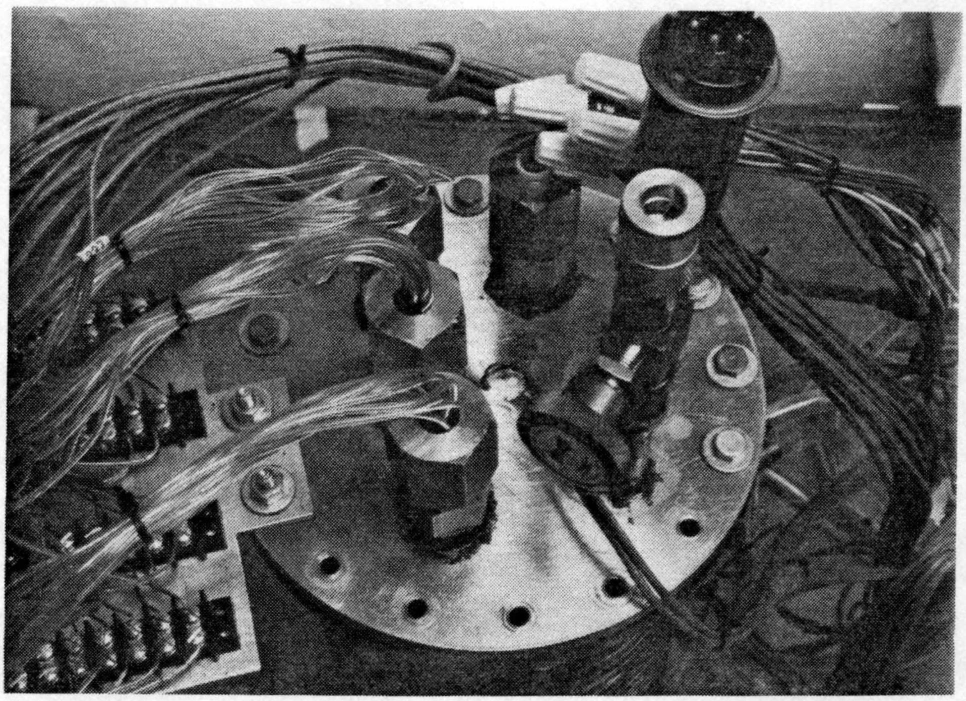

Figure 2.4: Top end–plate with conax connectors, quick connect and vacuum gage

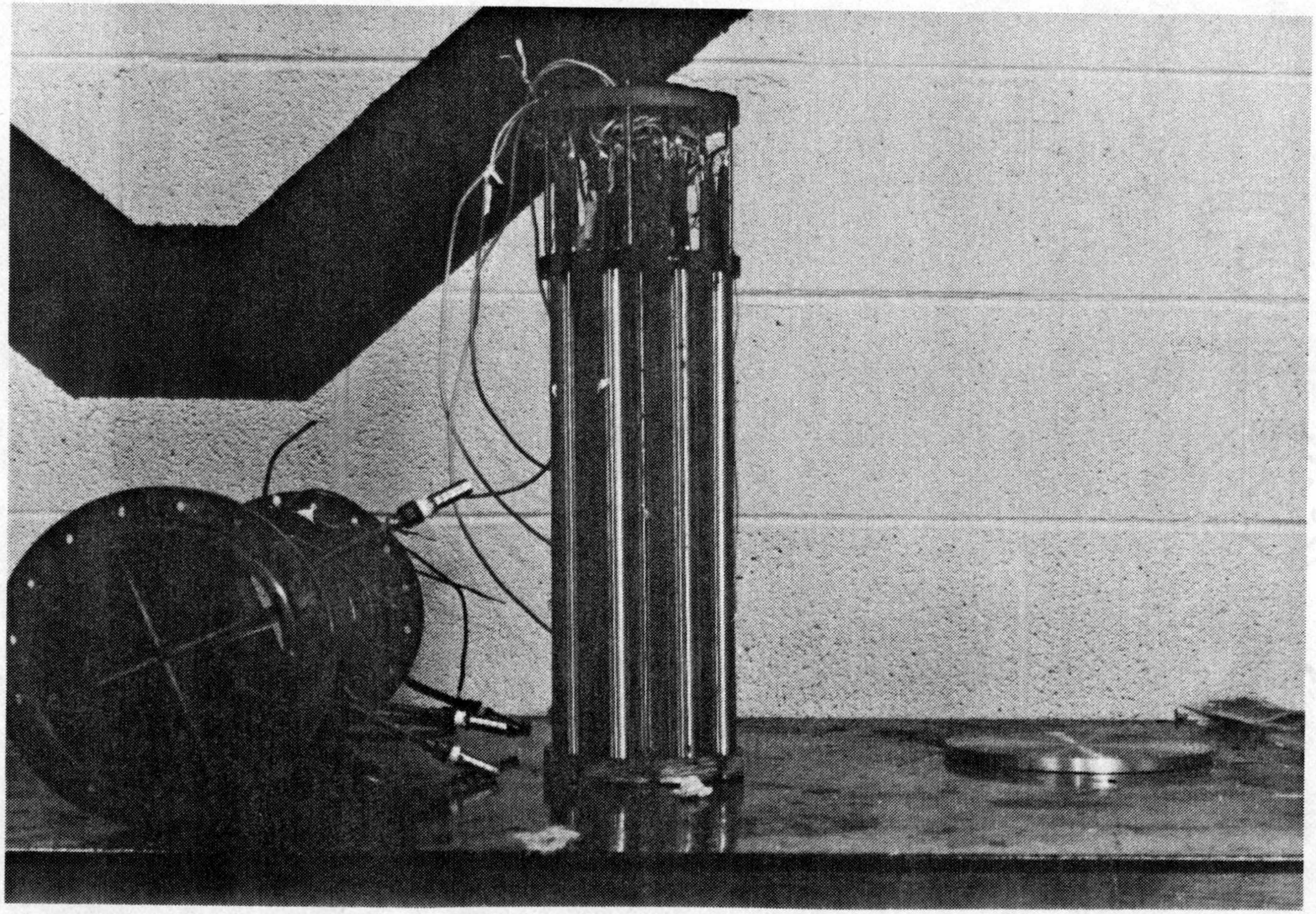

Figure 2.5: Watlow fire rod cartridge heaters (a) Rod–bundle assembly with circuitry (b) Gluing of thermocouples on rods

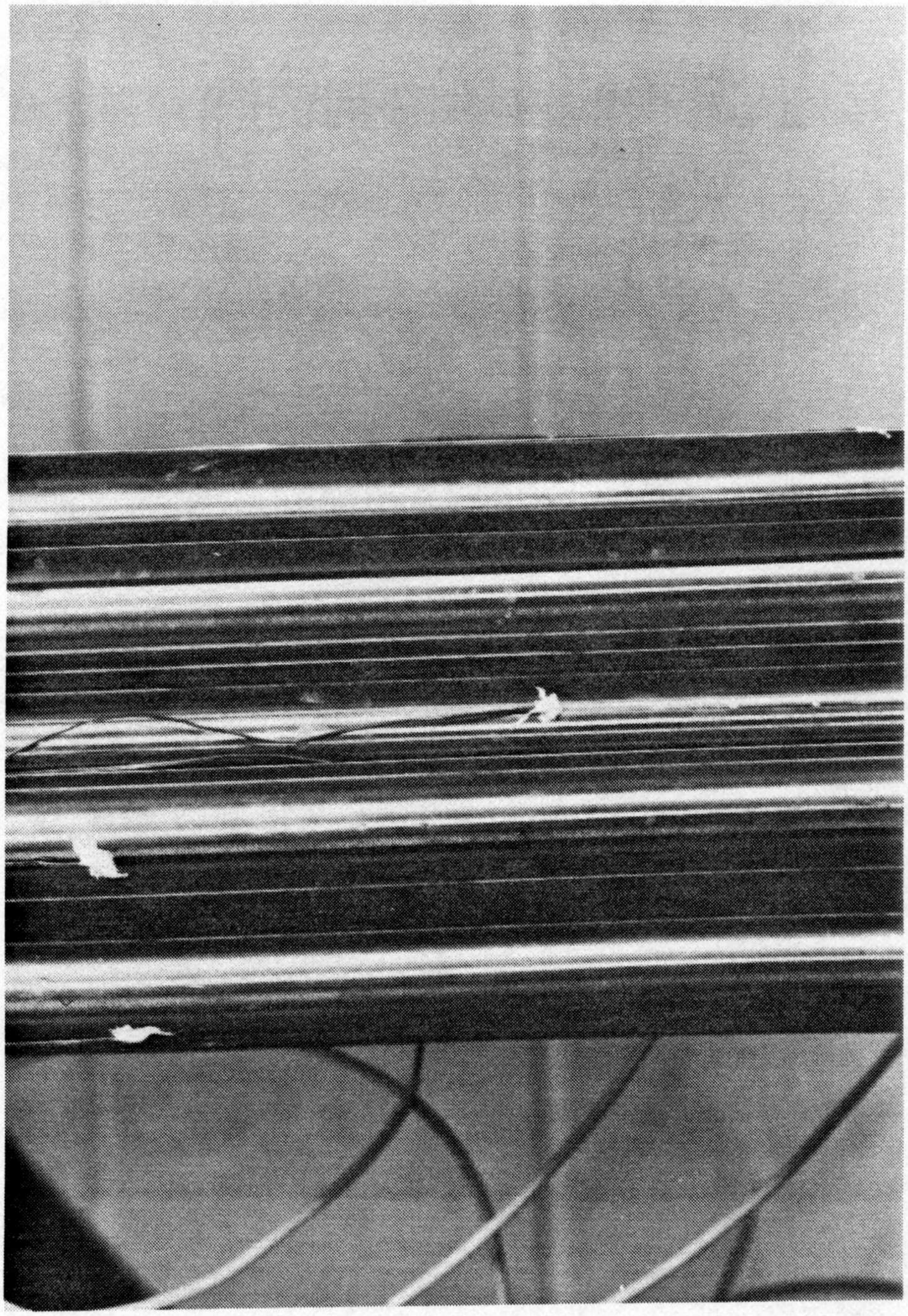

Figure 2.5 (Continued)

A Sargent–Welch mechanical pump (model–1400) having a capacity of 0.9 cubic feet per minute coupled with a water cooled diffusion pump as shown in the Fig. 2.6 is used to pull the vacuum in the cylinder. It is possible to obtain an absolute pressure as low as 0.025mm of Hg ($3.28 \times 10^{-5} atm.$).

2.2 Instrumentation

The arrangement of thermocouples (copper–constantan, 30 gage) for the measurement of surface temperature consists of twenty–four on the heaters, ten on the outer cylinder and one on the top end–plate.

The twenty–four thermocouples are glued to the surface of the heaters, utilizing the quarter symmetry of the rod–bundle. The arrangement is five–equally spaced 5.72 cm apart on the hot side (facing the center) and three–equally spaced 8.57 cm apart on the cold side (180 degrees in the θ–direction from the hot side). Since, the heaters are symmetrically arranged, only fifteen thermocouples are required to face the hot side and nine on the cold side. To ensure that the heat transfer due to radiation is not affected by the wires, the thermocouples are distributed to all the heaters in the assembly. The other end of the thermocouple wires are connected to a set of strip–boards on a phenolite support attached to the top guide as shown in Fig. 2.7. Four conax connectors are used to feed through the wire leads needed for the thermocouples and the heater rods. The thermocouples on the outside surface of the cylinder are arranged with three–spaced (Fig. 2.8a), 11.83 cm apart, along the 6.65 cm width fin and seven–spaced (Fig. 2.8b), 5.91 cm apart, along the 2.59 cm width fin. All the thermocouples are secured with epoxy cement.

The external leads from the twenty–four thermocouple wires (eight pairs per conax connector) are attached to an aluminium plate, which is bolted to the top end–plate for support. The extension thermocouple wires from the strip–boards

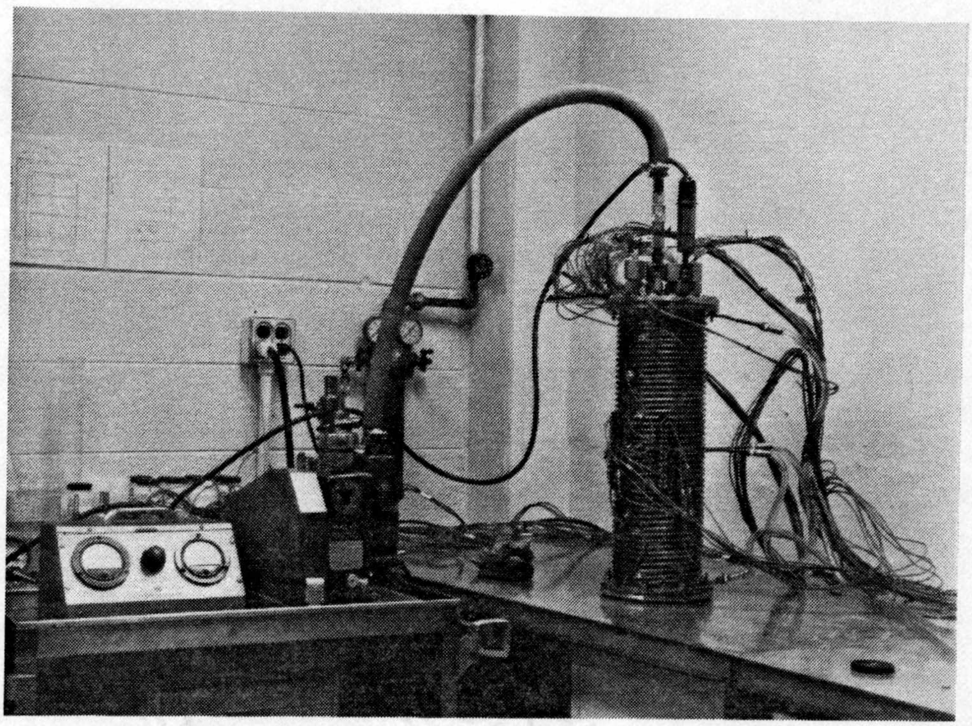

Figure 2.6: Vacuum pump and vacuum gage control

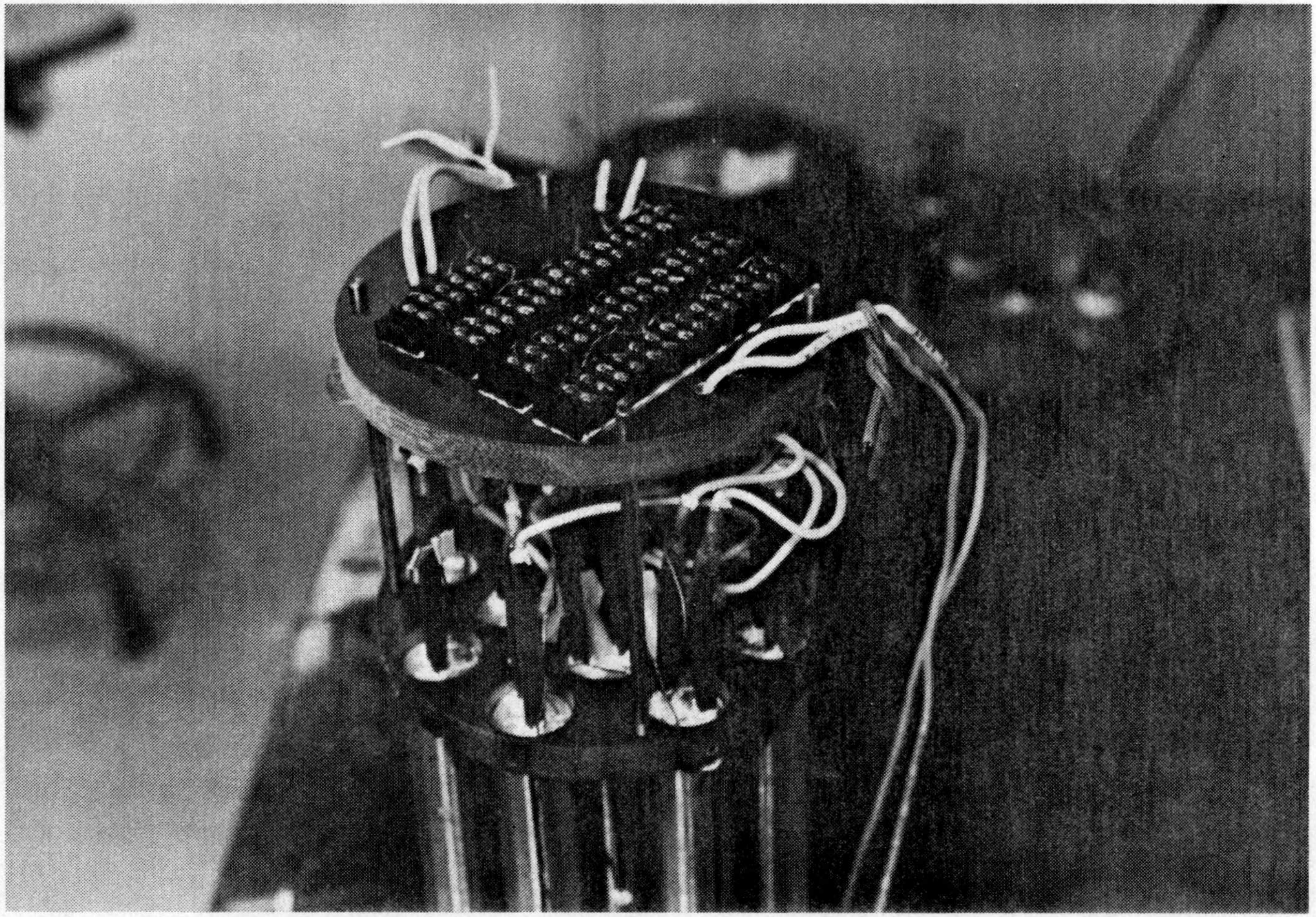

Figure 2.7: Top guide and phenolite support with strip–boards

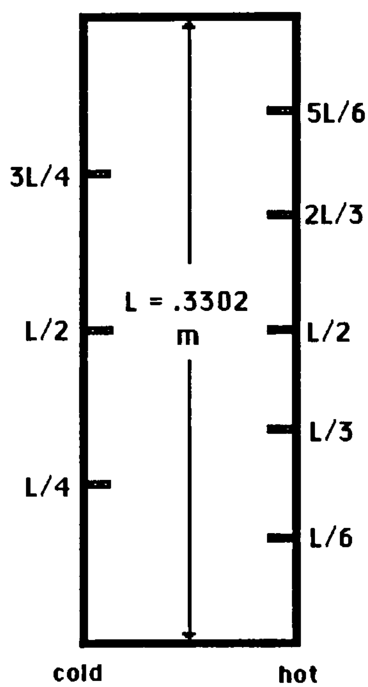

Figure 2.8: Location of thermocouples (a) Rods (b) Outer cylinder

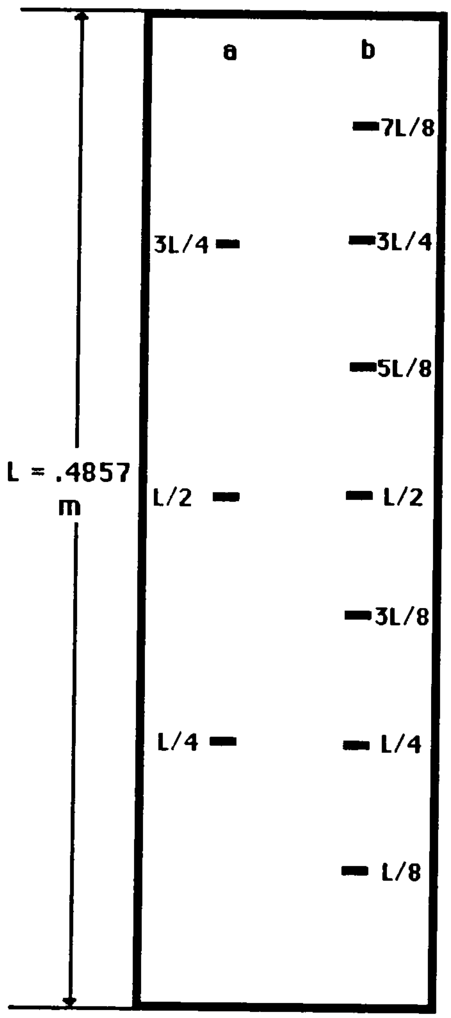

a = Thermocouples aligned along the fins

b = Thermocouples aligned between the fins

Figure 2.8 (Continued)

carry the signals to the Hewlett–Packard's 3497A data acquisition/control unit.

The power leads are connected to a regulated power control panel which has nine variacs. The panel has a switching arrangement that permits the measurement of current and voltage supplied by each variac. The voltages are measured with a Hewlett–Packard's 3456A Digital Voltmeter. The ice–point reference voltage for the thermocouples are provided by an electronic ice point reference cell (Kaye Instruments, model K-140/4). This instrument has a maximum deviation of $\pm$ 0.05^0C from 0^0C.

2.3 Procedure

The important factors affecting the experiments are the power input to each circuit, pressure of the test gas inside the cylinder, temperature of the outer cylinder and the corresponding steady state conditions.

2.3.1 Air Experiments

In case of air as the test gas, pressures ranging from 1 to 7.0 atmospheres with different power inputs to each rod (1 to 22 watts) are covered.

Once, the system has been pressurized to the desired value and the rods are supplied with the required power, it would take about six hours to reach a steady state. It is assumed that the system has reached a steady state when the difference in temperature readings between successive recordings were within 0.1% of the previous ones. The outer cylinder is maintained at a constant temperature approximately equal to the ambient temperature by periodically adjusting the constant temperature baths.

At higher Rayleigh number, more cooling is required at the top section of the cylinder in order to maintain a constant temperature. The observed difference between the top and bottom section of the cylinder is about 1^0C to 1.6^0C. This problem could be eliminated by the use of two circulators, one supplying the cooling water from the top to the mid–height and the other from the mid–height to the bottom of the cylinder.

2.3.2 Helium Experiments

In case of helium as the test gas, pressures ranging from 1 to 8 atmospheres, with different power inputs to each rod (1 to 30 watts) are covered.

In order to ensure that the system is completely filled with helium, the following procedure is adapted. Both the vacuum pump and the helium bottle are connected to the system through two different lines, each having a control valve. With the valve in the helium line closed, the system is evacuated to an absolute pressure of 0.025mm Hg (3.28×10^{-5} atm.). Helium is introduced into the system by releasing the control valve open and then the vacuum pump is shut off.

In this case, also, the experimental procedure is basically the same as that followed with air. Since, the thermal conductivity of helium is approximately 5.6 times that of air, the highest Rayleigh number that could be reached was closer to the Rayleigh number that was reached for air as the test gas at lower pressures. Hence, it is possible to maintain the outer cylinder at a constant temperature from the top to the bottom section with the use of a single constant temperature bath. The time for achieving the steady state condition for helium was about 9 hours.

2.3.3 Vacuum Experiments

These are performed in order to reproduce the same temperature fields (within 1% on an average basis) as those observed with air and helium present as the test gas. This could be done by trial and error. The typical time for reaching the steady state condition was about 24 hours. For example, after the system had reached a steady state, without varying the power input to the heaters, by merely changing the outer cylinder temperature (using the constant temperature bath) by about 1.5%, it would take about 4 hours for the system to reach a steady–state.

As stated earlier the evacuation of the system is achieved by using a mechanical pump and a diffusion pump. Here, it would be appropriate to give a brief surmise of the operating procedure of these pumps.

The mechanical pump consists of a stationary housing, an eccentrically mounted rotor with two spring loaded vanes, an inlet and a discharge port. Air enters the pump from the vacuum chamber through the inlet port. This air is trapped, compressed and ejected into the atmosphere through the discharge port by means of the rotor arrangement.

The electric heater at the bottom of the diffusion pump heats the pump oil until it boils and gives off oil vapor (molecules of oil in the gaseous state). These molecules of oil then rise up the jet stack and are forced through the nozzles forming a high velocity vapor stream. This stream is directed downward and outward toward the wall of the pump. Molecules of gas which diffuse from the vacuum region toward the jet stream are struck by oil vapor molecules.

After performing its function, the oil vapor condenses on the wall of the pump which is cooled to a temperature below the condensation point of the oil. The condensed oil then runs back down into the boiler while the gas molecules are directed to successively lower stages. The gas thus directed toward the bottom of the pump is further pumped by oil vapor jets directed from the lower nozzles and then pumped through the foreline by the mechanical pump. After the oil drops to the bottom of the pump, it is reboiled and the cycle repeats.

2.4 Measurement Uncertainty

A Hewlett–Packard 3497A Data Acquisition/Control system connected to a HP 9000 series 200 computer is used for the collection of data. The thermocouple outputs are measured to $0.1\mu V$, which results in a sensitivity of 0.0025 C. The accuracy of temperature measurements are within ± 0.2 C, which consists of errors introduced by reference junction compensation (± 0.01 C), temperature difference along the terminals, thermal offset, voltage to temperature conversion error and Digital Voltmeter accuracy. The voltage input to each circuit is measured with a sensitivity of $1mV$ and an accuracy of 0.1%. The voltages and currents recorded from all the runs indicate that the heater resistances are highly stable, resulting in a maximum uncertainty of $\pm 0.08\%$ in the resistance of each circuit. The power input is evaluated by using the measured voltage drop across each circuit and its respective resistance. This procedure gives an uncertainty of $\pm 1.3\%$ in the calculated power inputs. An uncertainty of $\pm 0.254mm$ in the length scale is used for the data reduction. The thermophysical properties for air and helium are obtained from the National Bureau of Standards and Thermophysical Properties Research Center tables, hence, the uncertainty in these are negligible.

The uncertainty in the Nusselt and Rayleigh numbers vary with the power input. Smaller power inputs result in a higher uncertainty due to a lower temperature difference between the rods and the outer cylinder. As the power input increases, the uncertainty in the experimental data decreases. The heat loss from the top and bottom end–plates are negligible as both the plates are insulated from the rods. The estimated uncertainities in Nu_{Td} and Ra_d are 1.72 to 3.09% and 3.04 to 3.98%, respectively. The uncertainty in the convective Nusselt number, Nu_d, is somewhat higher than that of Nu_{Td}, due to uncertainty in the radiation correction. The added uncertainty, however, should be a smaller fraction of the radiation heat transfer contribution.

Chapter 3

RESULTS AND DISCUSSION

Convective heat transfer results are presented for a rod–bundle with two enclosing outer cylinders in a vertical position, one with the internal fins present and the other without the fins. The rod–bundle enclosure has pitch to diameter ratios of $p_1/d = 1.25$ and $p_2/d = 1.50$, (please see Fig. 1.2a), and a height to diameter ratio of $L/d = 13.0$; with an outer cylinder of $D/d = 5.50$, with $d = 2.54\ cm$. The position and numbering of rods, and the position of the fins inside the enclosure are shown in the Fig. 1.2a. Sectional front–view showing the height of the rod–bundle, thermocouples, conax connectors, valves, etc are shown in Fig. 1.2b. A uniform power dissipation per unit length is supplied to each rod and the outer cylinder is maintained at a constant temperature. The results consists of indvidual rod temperature distributions, and correlations of the Nusselt number as a function of Rayleigh number for both of the outer cylinders.

A total number of 73 runs are conducted for air experiments. These data points cover a pressure range of 1 to 7.0 atmospheres with the variation in the power input per rod of 1 to 22 watts. With helium, a total number of 36 runs are conducted covering a pressure range of 1 to 8 atmospheres, with the variations in the power input per rod of 1 to 30 watts. Also, a total of 50 runs under vacuum are conducted for reproducing the average temperature fields observed with the gas present.

The characteristic temperature difference of the rod-bundle, $T_{MR1} - T_{MC}$, is plotted as a function of power input to the rods as shown in Figs. 3.1a and 3.1b, respectively. For a given test gas and power input, as the pressure is increased, there is an increase in Rayleigh number and consequently a lower temperature difference is observed. This observation is made for the convection flow regime. It should be noted that these temperature differences are a result of combined processes of conduction, convection and radiation heat transfer. A good example of the interdependent effects of these processes are given by comparing the following two data points. For, air at a pressure of 1 atm., a temperature difference of 18.93^0C is obtained with a power input of 2.98 W/rod. Whereas, under vacuum (a pressure of 3.28×10^{-5} atm.) with the same power input, a temperature difference of 73.69^0C is observed. These data points correspond, respectively, to a conduction dominated heat transfer process and to one in which radiation is the primary mode of energy transfer.

At lower Rayleigh numbers, corresponding to the conduction and transition flow regimes (transition from conduction to convection) with helium as the convective medium, the temperature distributions from the bottom to the top of the rods 1 and 2 are nearly uniform. As the Rayleigh number increases, corresponding to the convection flow regime with air as the convective medium, the temperature profiles show a steady increase from the leading edge to the top of a given heater rod. This can be seen from Figs. 3.2a and 3.2b, where the temperature difference as a function of local height is presented for rods 1 and 2, respectively. At the same axial location, the rods in position 1 (which are closer to the center) have higher temperatures compared to those in the position 2. This effect is more pronounced in the conduction regime. As the Rayleigh number increases, boundary layers are formed from the bottom to the

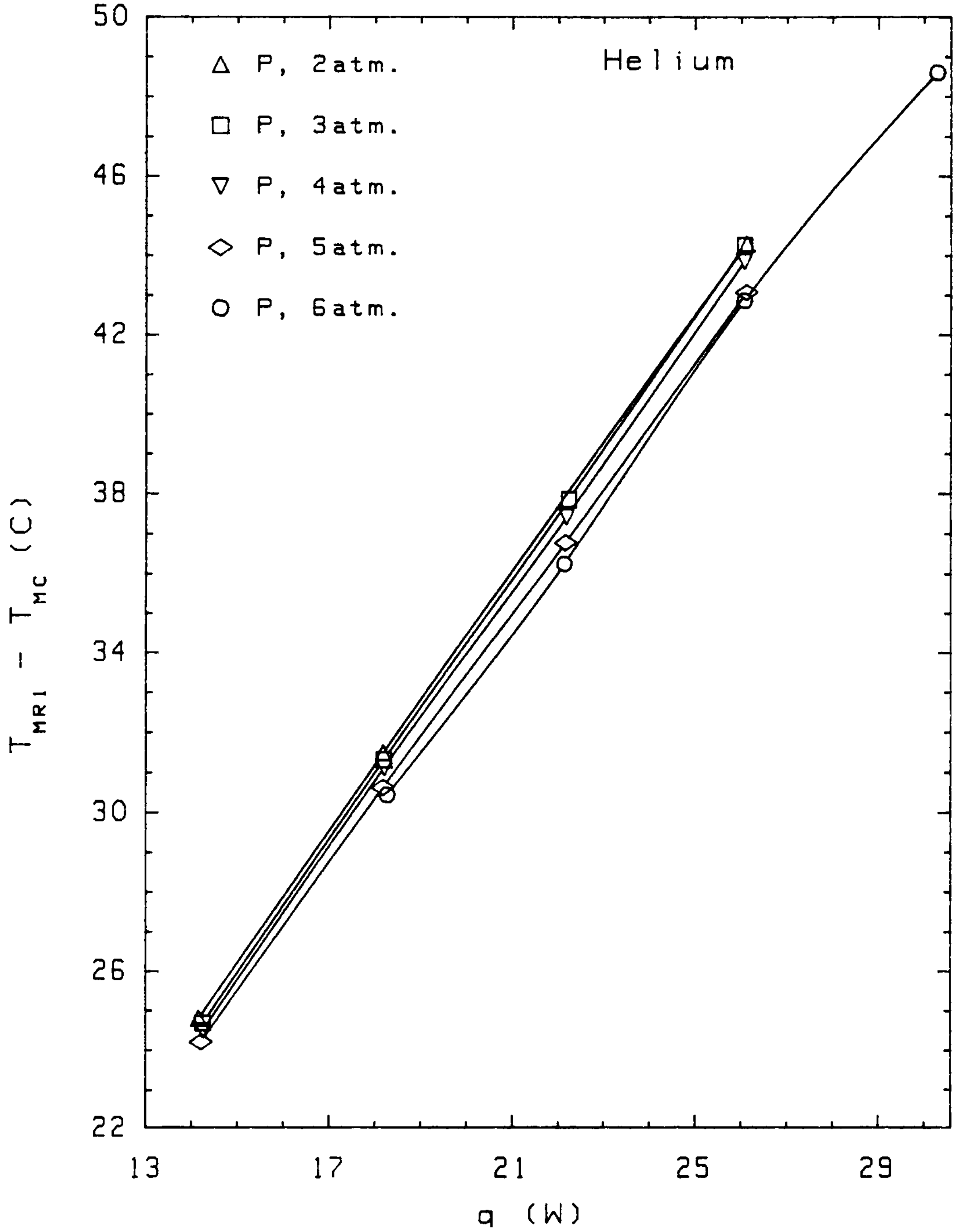

Figure 3.1: Average temperature difference on rod 1 as a function of total power input per rod (a) Helium data (b) Air data

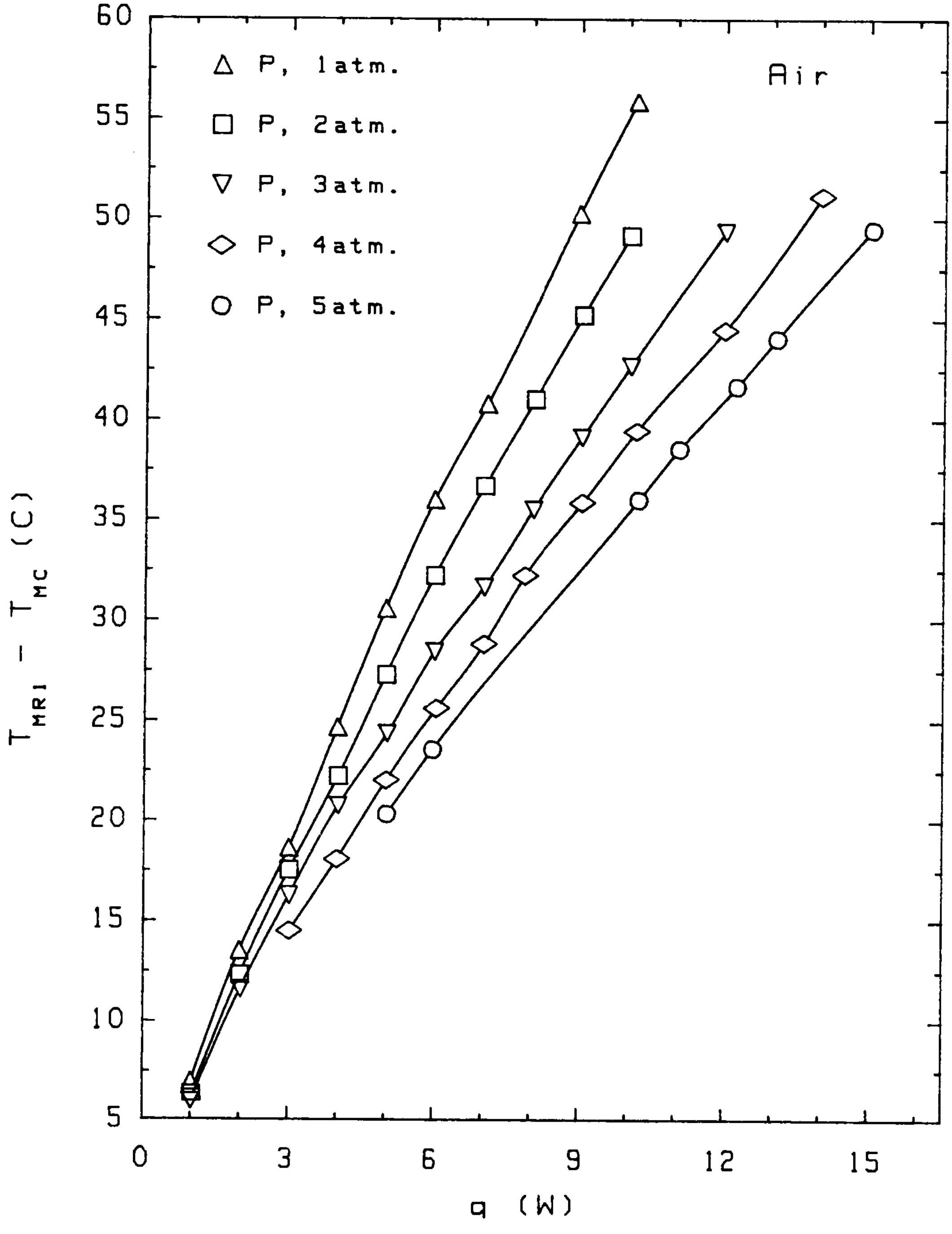

Figure 3.1 (Continued)

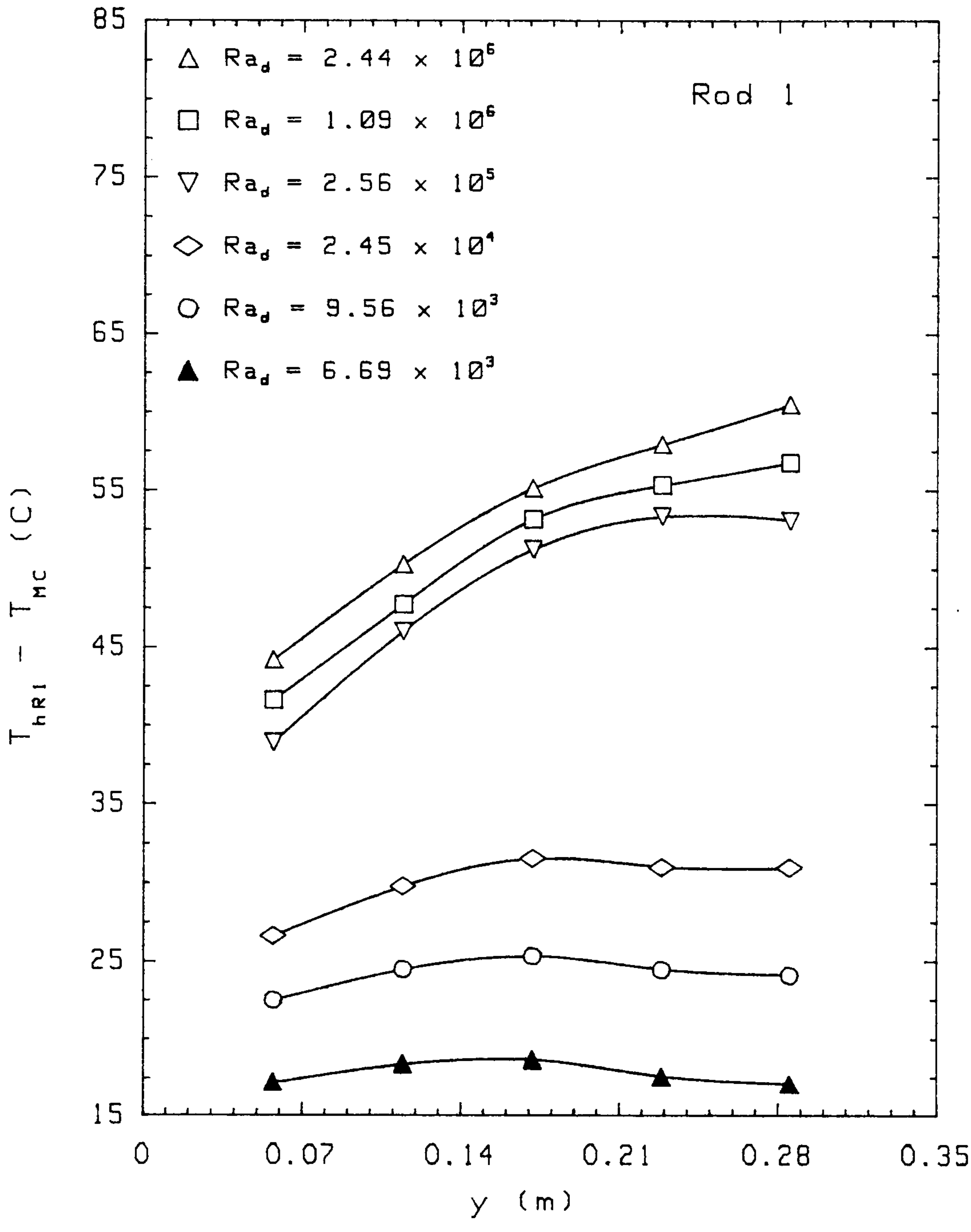

Figure 3.2: Local temperature differences on the hot–side of rods at various Rayleigh numbers (a) Rod 1 (b) Rod 2

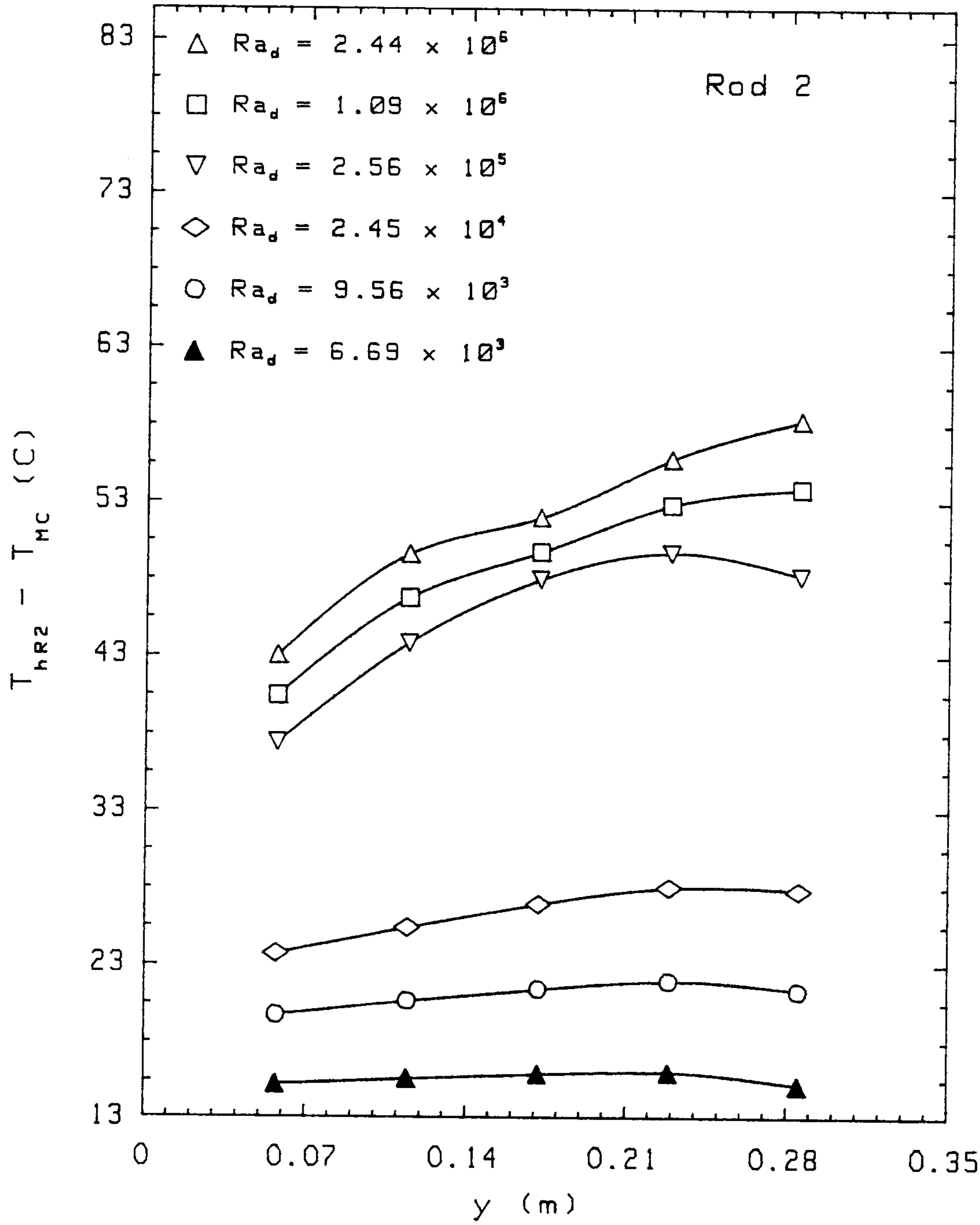

Figure 3.2 (Continued)

top of the rods. Each rod will have a distinct temperature profile depending on its position in the rod–bundle. However, their average temperature at very high Rayleigh numbers are nearly the same.

The following procedure is adapted in order to obtain the convective Nusselt number. For air and helium as the test gas and a given power input per rod, the mean temperatures of rods 1 and 2 are measured. Then, the cylinder is completely evacuated. The power inputs to the rods 1 and 2 are simultaneously adjusted until the mean temperatures are the same as those obtained when the convection heat transfer was present. The outer cylinder is also maintained at the same temperature as that when the gas was present. These power inputs are considered to be the radiation contribution to the heat transfer process. Fig. 3.3 shows the temperature distributions on rods 1 and 2 obtained from a typical experiment under vacuum, (a pressure of 3.28×10^{-5} atm.). The temperature profiles observed with convection heat transfer present are superimposed in this figure. The average temperatures of rods 1 and 2, under vacuum are reproduced to within 1% of the values observed with the test gas present.

3.1 Cask with Fins

The total and convective Nusselt numbers Nu_{Td} and Nu_d as a function of Rayleigh number, Ra_d, for rods 1 and 2 are graphically presented in Figs. 3.4 and 3.5, respectively. The engineering correlations Nu_d versus Ra_d for each rod in the bundle for pure conduction, conduction flow and convection flow regimes are :

Rod 1

$$Nu_{d1} = 3.259, \qquad Ra_{d1} < 4.64 \times 10^3 \tag{3.1}$$

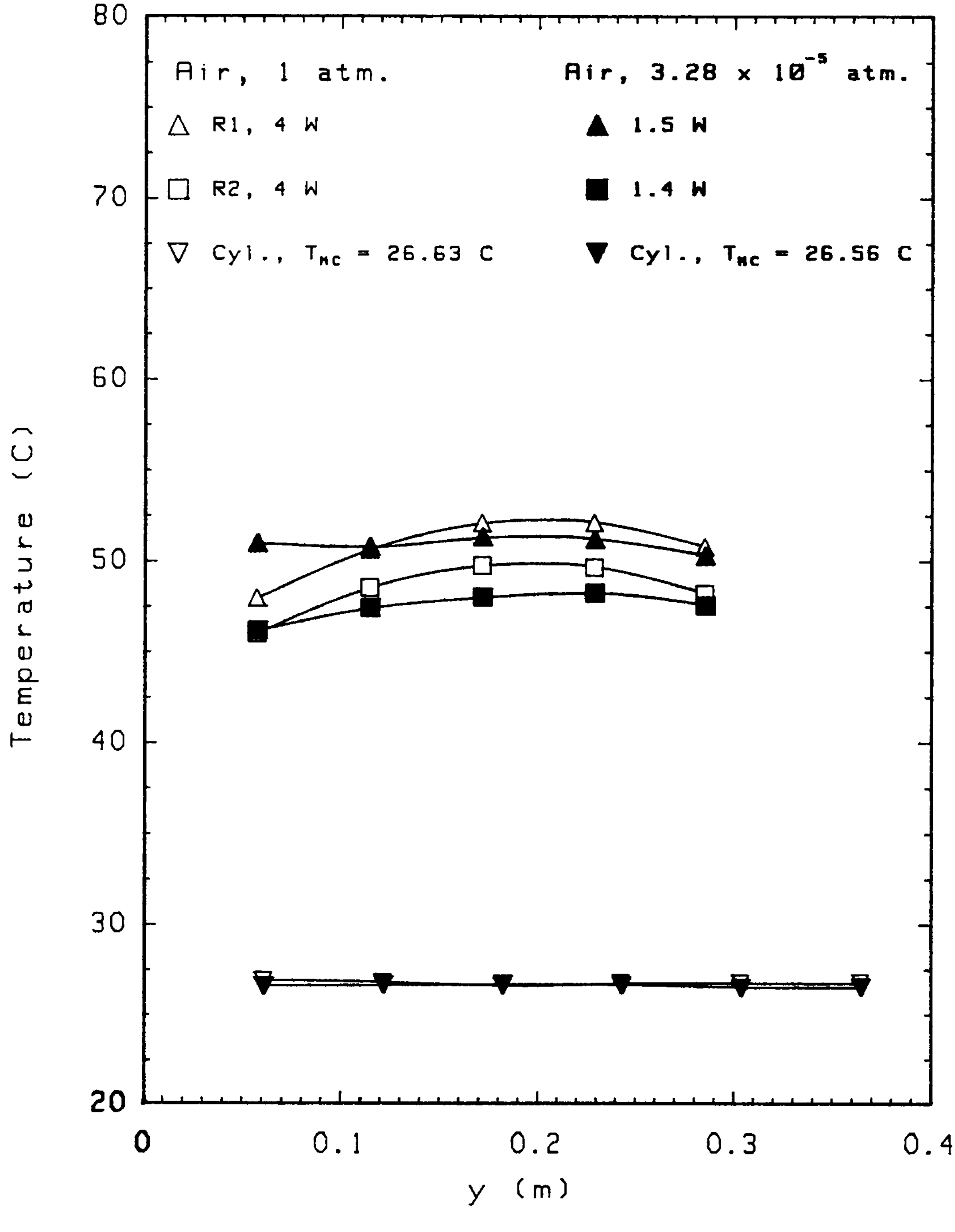

Figure 3.3: Comparison of temperature distribution on rods 1 and 2 with air and under vacuum conditions

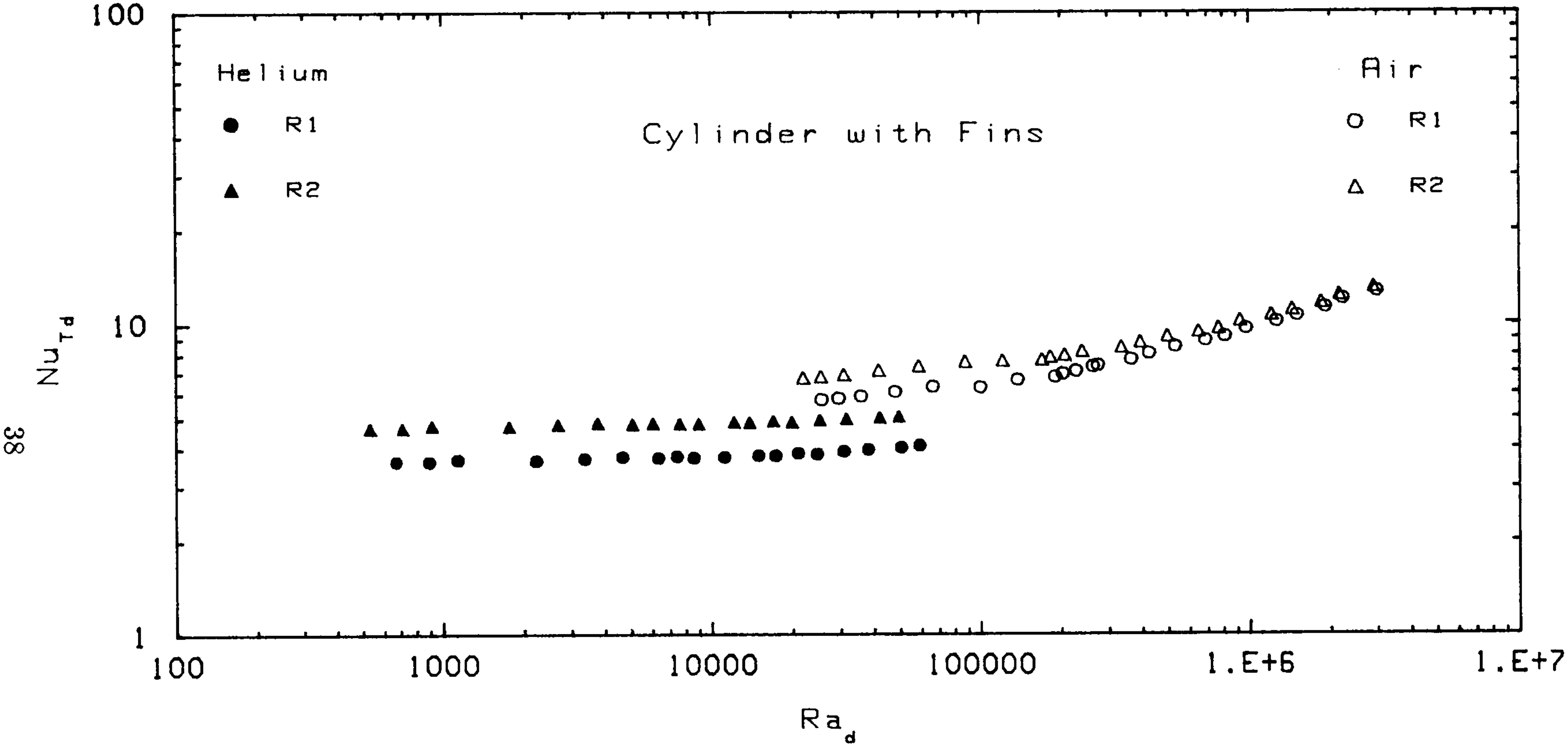

Figure 3.4: Total Nusselt numbers for individual rods in the 3×4 (fins) rod–bundle

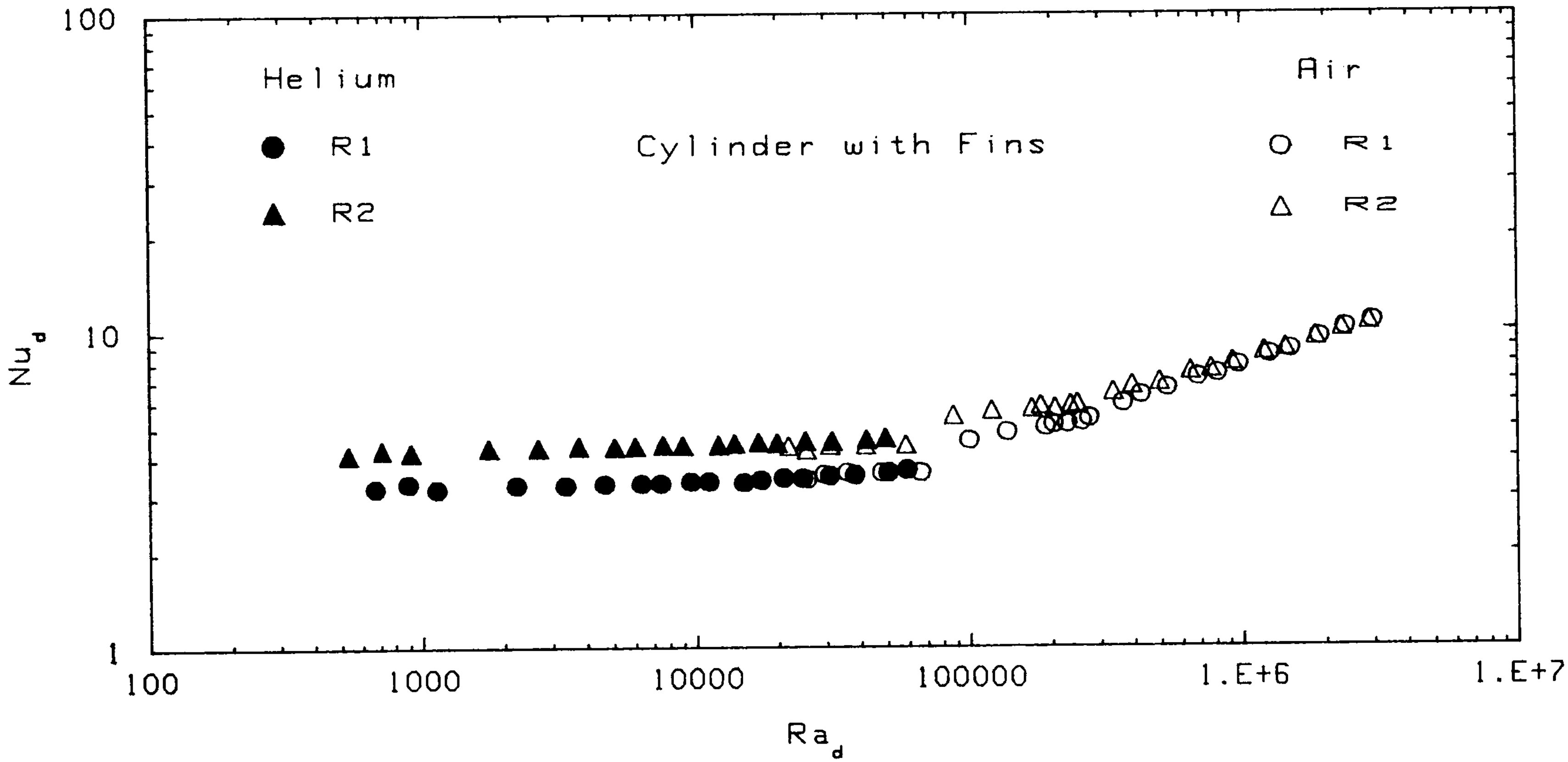

Figure 3.5: Convective Nusselt numbers for individual rods in the 3 × 4 (fins) rod–bundle

$$Nu_{d1} = 2.360 Ra_{d1}^{0.0378}, \quad 4.64 \times 10^3 < Ra_{d1} < 5.04 \times 10^4 \quad (3.2)$$

$$Nu_{d1} = 0.157 Ra_{d1}^{0.2830}, \quad 5.04 \times 10^4 < Ra_{d1} < 2.36 \times 10^6 \quad (3.3)$$

Rod 2

$$Nu_{d2} = 4.254, \quad Ra_{d2} < 3.75 \times 10^3 \quad (3.4)$$

$$Nu_{d2} = 3.597 Ra_{d2}^{0.0220}, \quad 3.75 \times 10^3 < Ra_{d2} < 4.20 \times 10^4 \quad (3.5)$$

$$Nu_{d2} = 0.339 Ra_{d2}^{0.2300}, \quad 4.20 \times 10^4 < Ra_{d2} < 1.85 \times 10^6. \quad (3.6)$$

The overall convective and total Nusselt numbers Nu_D and Nu_{TD} as a function of Rayleigh number Ra_D is graphically presented in Fig. 3.6. The correlations for Nu_D as a function of Ra_D are :

$$Nu_D = 39.973, \quad Ra_D < 7.71 \times 10^5 \quad (3.7)$$

$$Nu_D = 23.25 Ra_D^{0.0388}, \quad 7.71 \times 10^5 < Ra_D < 8.39 \times 10^6 \quad (3.8)$$

$$Nu_D = 0.489 Ra_D^{0.2770}, \quad 8.39 \times 10^6 < Ra_D < 4.94 \times 10^8, \quad (3.9)$$

and Nu_{D^*} as a function of Ra_{D^*} are :

$$Nu_{D^*} = 39.973, \quad Ra_{D^*} < 2.45 \times 10^7 \quad (3.10)$$

$$Nu_{D^*} = 20.57 Ra_D^{0.0388}, \quad 2.45 \times 10^7 < Ra_{D^*} < 1.96 \times 10^8 \quad (3.11)$$

$$Nu_{D^*} = 0.204 Ra_D^{0.2770}, \quad 1.96 \times 10^8 < Ra_{D^*} < 1.15 \times 10^{10}. \quad (3.12)$$

The correlation of the ratio of maximum temperature to mean temperature of the heater rod as a function of Rayleigh number in the convection flow regime is given as,

$$\frac{T_{MAX} - T_{MC}}{T_{MR} - T_{MC}} = 0.656 Ra_{D^*}^{0.0236}. \quad (3.13)$$

The average deviation of these correlations from experimental data is less than 3.0%.

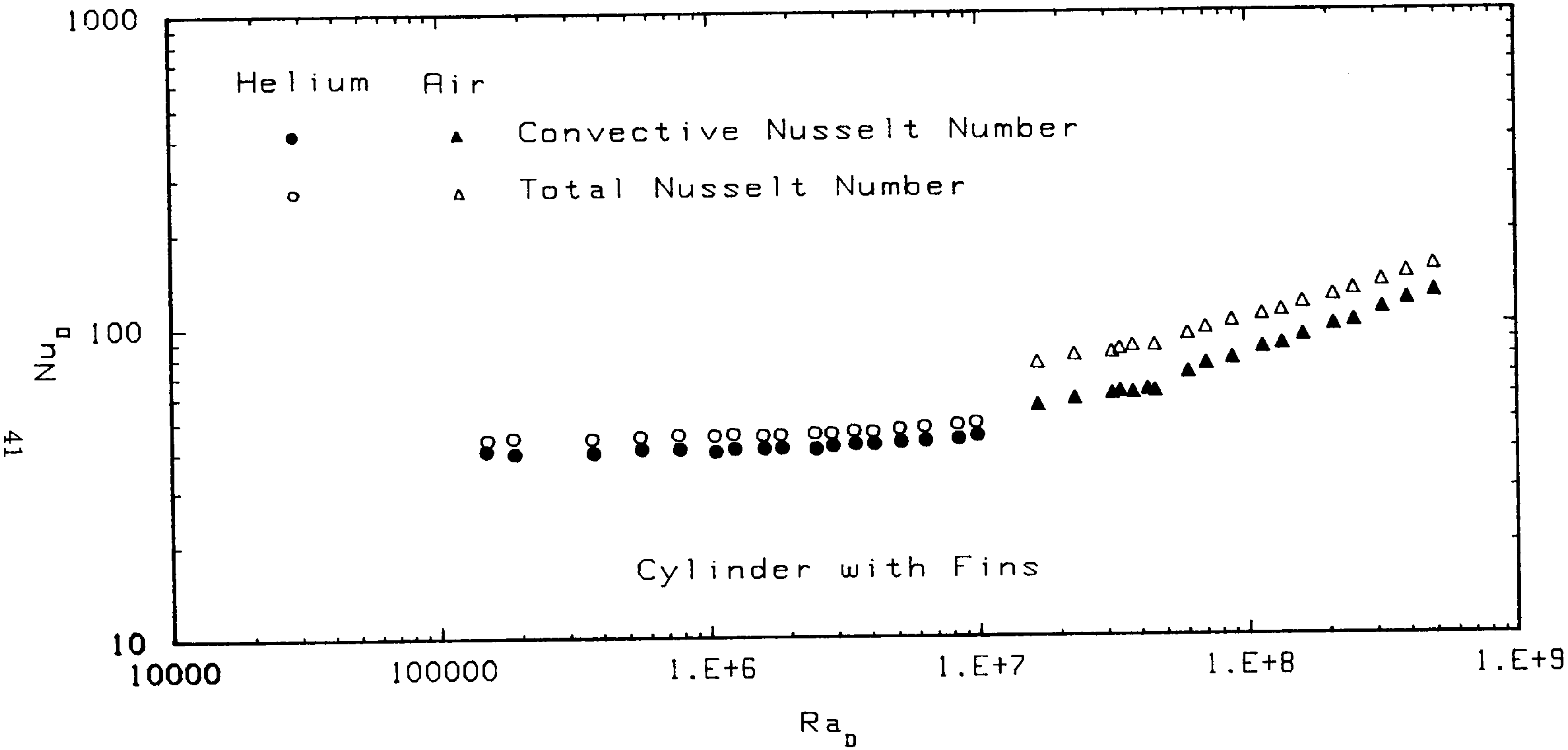

Figure 3.6: Overall and total convective Nusselt numbers for the 3 × 4 (fins) rod–bundle

3.2 Cask without Fins

The total and convective Nusselt numbers are presented in Figs. 3.7 and 3.8 respectively. As the radiation heat transfer contributions are different for the two gases, there is a discontinuity in the slopes and the absolute values as observed in Fig. 3.7 (also Fig. 3.4) of the Nu_{Td} versus Ra_d graphs. The radiation heat transfer contribution with air as the test gas is a higher percentage of the total heat transfer when compared to that of helium. Under a given condition of uniform power input per rod, the individual rods in the bundle exchange energy with the working fluid via different but co–existing flow regimes. At a power input of 10 W, with helium, rod 1 has a Ra_d of 8.42×10^3, which can be classified as a transition flow regime and the rod 2 has a Ra_d of 5.90×10^3, which can be classified as a conduction regime (Fig. 3.8). The departure from conduction flow regime is classified as the case where the Nu_d of a given rod exceeds its pure conduction value by 10% or more. As can be seen from this figure (also Fig. 3.5), the conduction flow regime ends at a lower Rayleigh number for rod 1 than rod 2. Also, rod 2 has a higher convective Nusselt number than rod 1, which is a direct consequence of its proximity to the outer cylinder. This difference is more pronounced in the conduction and transition flow regimes, but, as the Rayleigh number increases (convection flow regime), the Nusselt numbers for the rods are nearly the same.

The engineering correlations for each rod in the bundle are :

Rod 1

$$Nu_{d1} = 0.860, \qquad Ra_{d1} < 2.80 \times 10^3 \qquad (3.14)$$

$$Nu_{d1} = 0.206 {Ra_{d1}}^{0.1970}, \quad 2.80 \times 10^3 < Ra_{d1} < 2.56 \times 10^4 \qquad (3.15)$$

$$Nu_{d1} = 0.068 {Ra_{d1}}^{0.2940}, \quad 2.56 \times 10^4 < Ra_{d1} < 2.70 \times 10^6 \qquad (3.16)$$

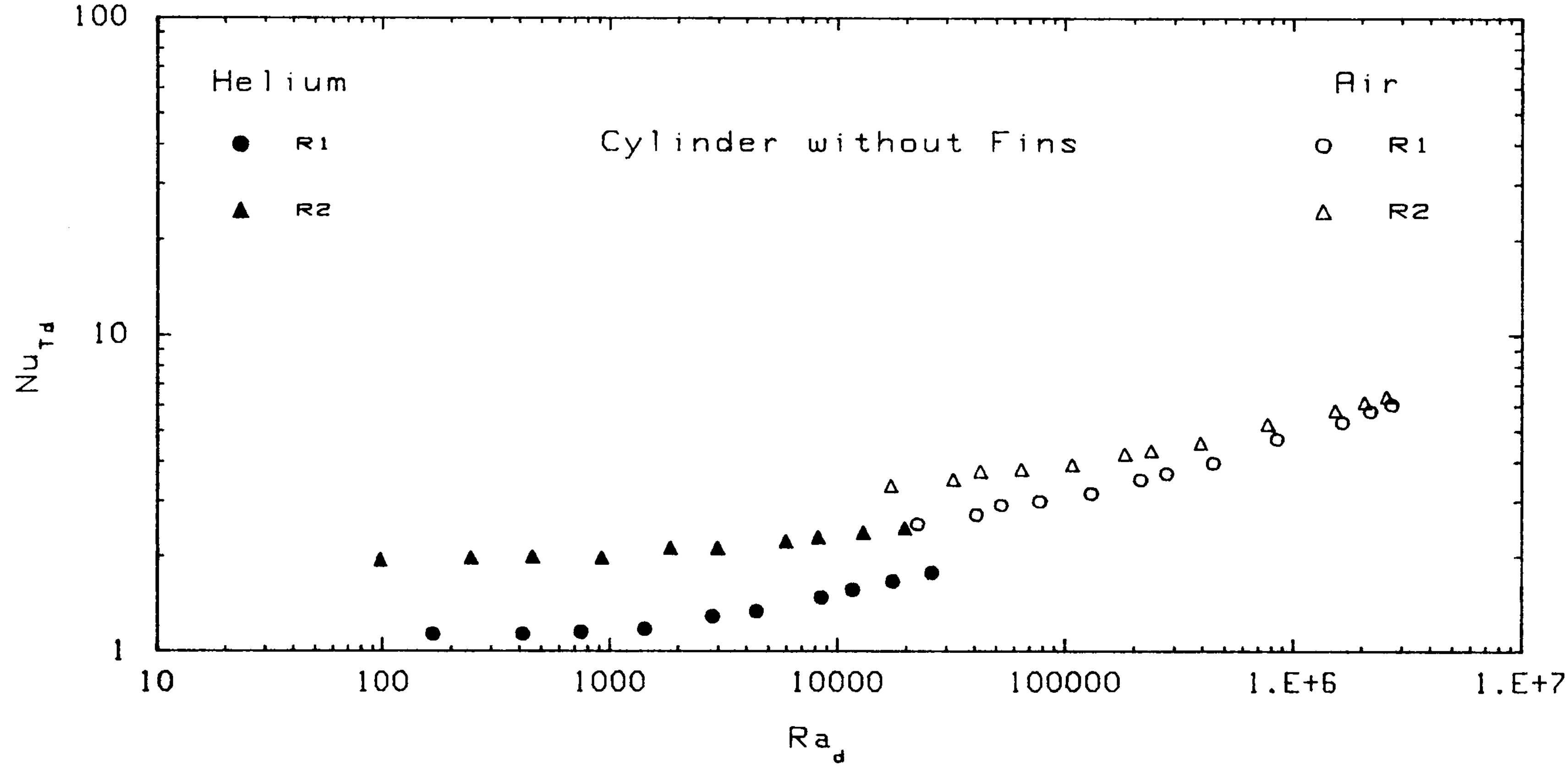

Figure 3.7: Total Nusselt numbers for individual rods in the 3 × 4 (no fins) rod–bundle

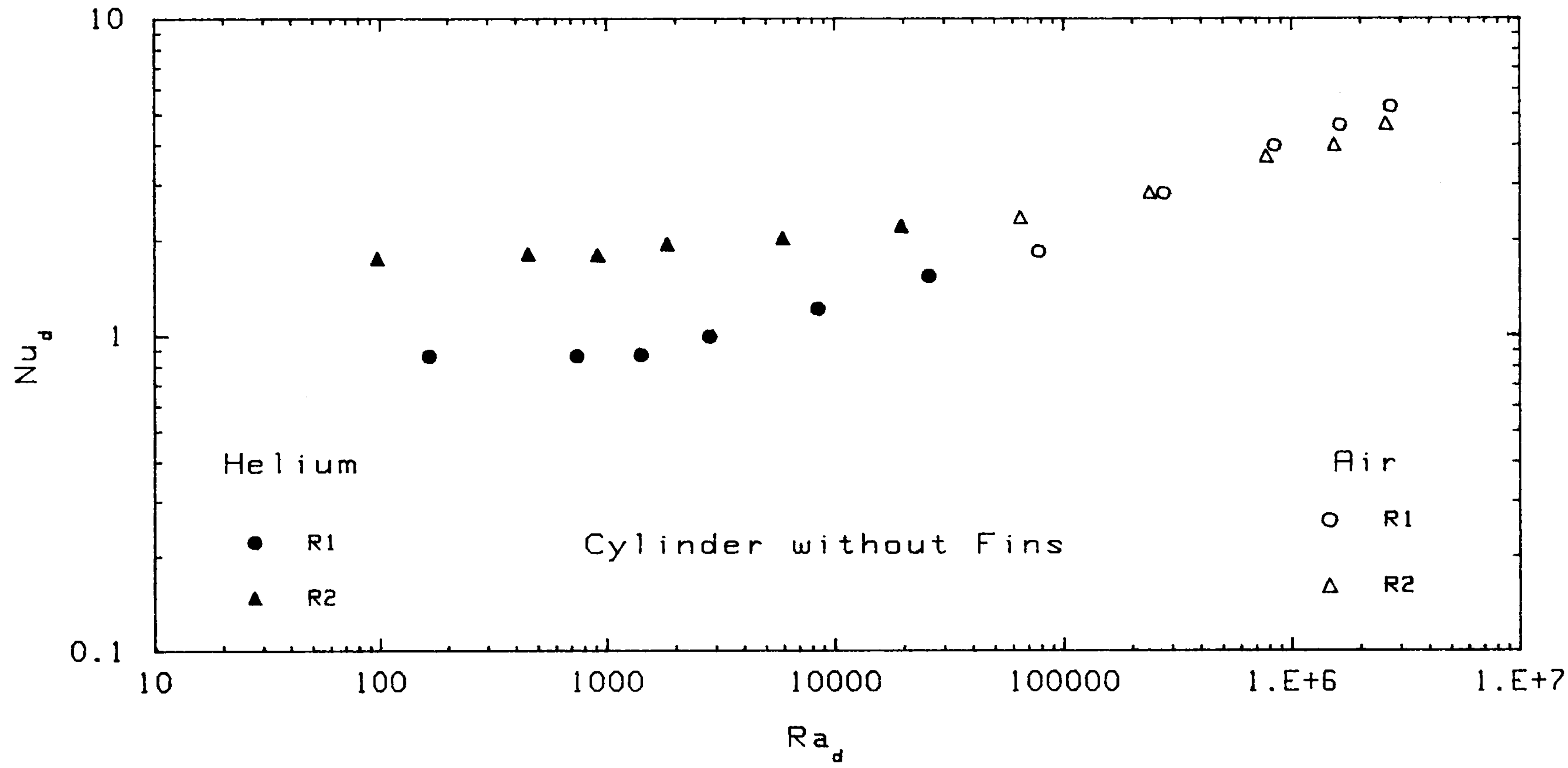

Figure 3.8: Convective Nusselt numbers for individual rods in the 3×4 (no fins) rod–bundle

Rod 2

$$Nu_{d2} = 1.780, \qquad Ra_{d2} < 1.84 \times 10^3 \tag{3.17}$$

$$Nu_{d2} = 1.275 {Ra_{d2}}^{0.0549}, \quad 1.84 \times 10^3 < Ra_{d2} < 1.95 \times 10^4 \tag{3.18}$$

$$Nu_{d2} = 0.286 {Ra_{d2}}^{0.1880}, \quad 1.95 \times 10^4 < Ra_{d2} < 2.58 \times 10^6. \tag{3.19}$$

The overall convective and total Nusselt numbers are presented in Fig. 3.9. The correlations for overall and total Nusselt numbers are :

$$Nu_D = 11.794, \qquad Ra_D < 2.35 \times 10^5 \tag{3.20}$$

$$Nu_D = 1.7320 {Ra_D}^{0.156}, \quad 2.35 \times 10^5 < Ra_D < 4.26 \times 10^6 \tag{3.21}$$

$$Nu_D = 0.3097 {Ra_D}^{0.261}, \quad 4.26 \times 10^6 < Ra_D < 4.50 \times 10^8. \tag{3.22}$$

The maximum temperature correlation is given as,

$$\frac{T_{MAX} - T_{MC}}{T_{MR} - T_{MC}} = 0.5436 {Ra_D}^{0.0338}. \tag{3.23}$$

The average deviation of these correlations from experimental data is less than 3.0%.

3.3 Comparison

The radiation heat transfer contributions of the rods 1 and 2 vary with the test gas, Rayleigh number and the outer cylinder (please see Tables 3.1 and 3.2). For example, for rod 1 with helium as the working fluid, the radiation contributions at an approximate Ra_d of 7.0×10^2, are 11.0% (cylinder with fins) and 25.3% (cylinder without fins). When the Ra_d increases to about 2.5×10^4, the corresponding values gets reduced to 9.5% and 13.5%. The radiation contribution for rod 2 also follows the same pattern as above.

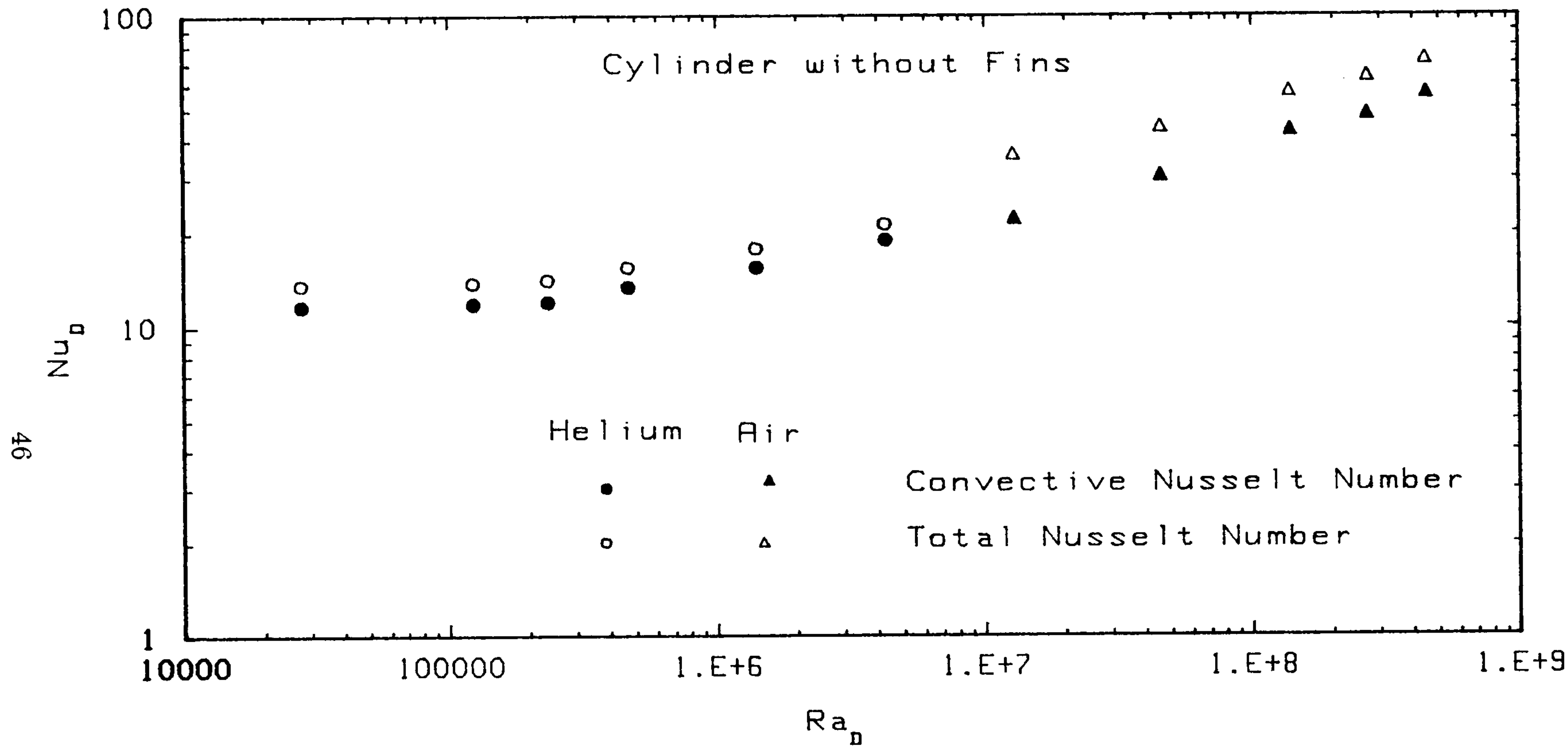

Figure 3.9: Overall and total convective Nusselt numbers for the 3×4 (no fins) rod–bundle

Table 3.1: Radiation contributions as percentages of power input per rod : with internal fins

Gas	Power W	Rod 1 %	Rod 2 %	Ra_{d1}	Ra_{d2}
Helium	22	12.97	10.99	1.13×10^3	9.12×10^2
	22	9.82	7.76	3.08×10^4	2.51×10^4
Air	9	43.34	40.64	6.62×10^4	5.86×10^4
	12	16.13	18.66	1.90×10^6	1.84×10^6

Table 3.2: Radiation contributions as percentages of power input per rod : without internal fins

Gas	Power W	Rod 1 %	Rod 2 %	Ra_{d1}	Ra_{d2}
Helium	1	24.11	10.11	1.64×10^2	0.96×10^2
	10	18.23	9.24	8.43×10^3	5.91×10^3
Air	5	38.59	37.82	7.73×10^4	6.45×10^4
	10	12.63	27.60	2.70×10^6	2.58×10^6

The presence of internal fins alter the flow regime spectrum with respect to Ra_D. At $Ra_D = 1 \times 10^6$, the rod–bundle is exhibiting a pure conduction flow regime for the cylinder with fins (Fig. 3.6), and is in the convection flow regime for the one without fins (Fig. 3.9). As seen from these figures, there is a difference in absolute values of Nu_D, which is higher in case of the cylinder with internal fins. This is due to the fact that the cylinder with internal fins provides a greater cooling surface area for the heat transfer from the rod–bundle and consequently a lower characteristic temperature difference is observed when compared with the one without fins. In order to see the effect of presence of fins on individual rods in the bundle, with repect to the onset of convection and absolute values of Nusselt numbers, the set of equations representing the individual rod correlations (Nu_d versus Ra_d) are shown graphically in Figs. 3.10a (rod 1) and 3.10b (rod 2). As already discussed for the overall bundle, in case of individual rods also, due to the presence of fins, there is a delay in the onset of convection which can be clearly seen in these figures.

The overall convective Nusselt numbers Nu_{D^*} as a function of Ra_{D^*} are shown graphically in Fig. 3.11 for the 3×3 and 5×5 rod–bundle of Keyhani et al. [5, 6] and 3×4 rod–bundle for the present cases. D^* represents the diameter of an equivalent outer cylinder, whose surface area is equal to the outer cooling area including the area of the fins if present. The experimental critical Rayleigh number for departure from the conduction flow regime ($Ra_{D_{cr}}$, $D = D^*$ in this case) for the case of 3×4 rod–bundle without fins is 4.03×10^5. This value is calculated from Eq. (3.21) for a Nusselt number whose value is 10% higher than the pure conduction value (Eq. (3.20)). Keyhani et al. [5, 6] have proposed the following relation for the prediction of critical Rayleigh number for the onset of convection in enclosed vertical rod–bundles without internal fins,

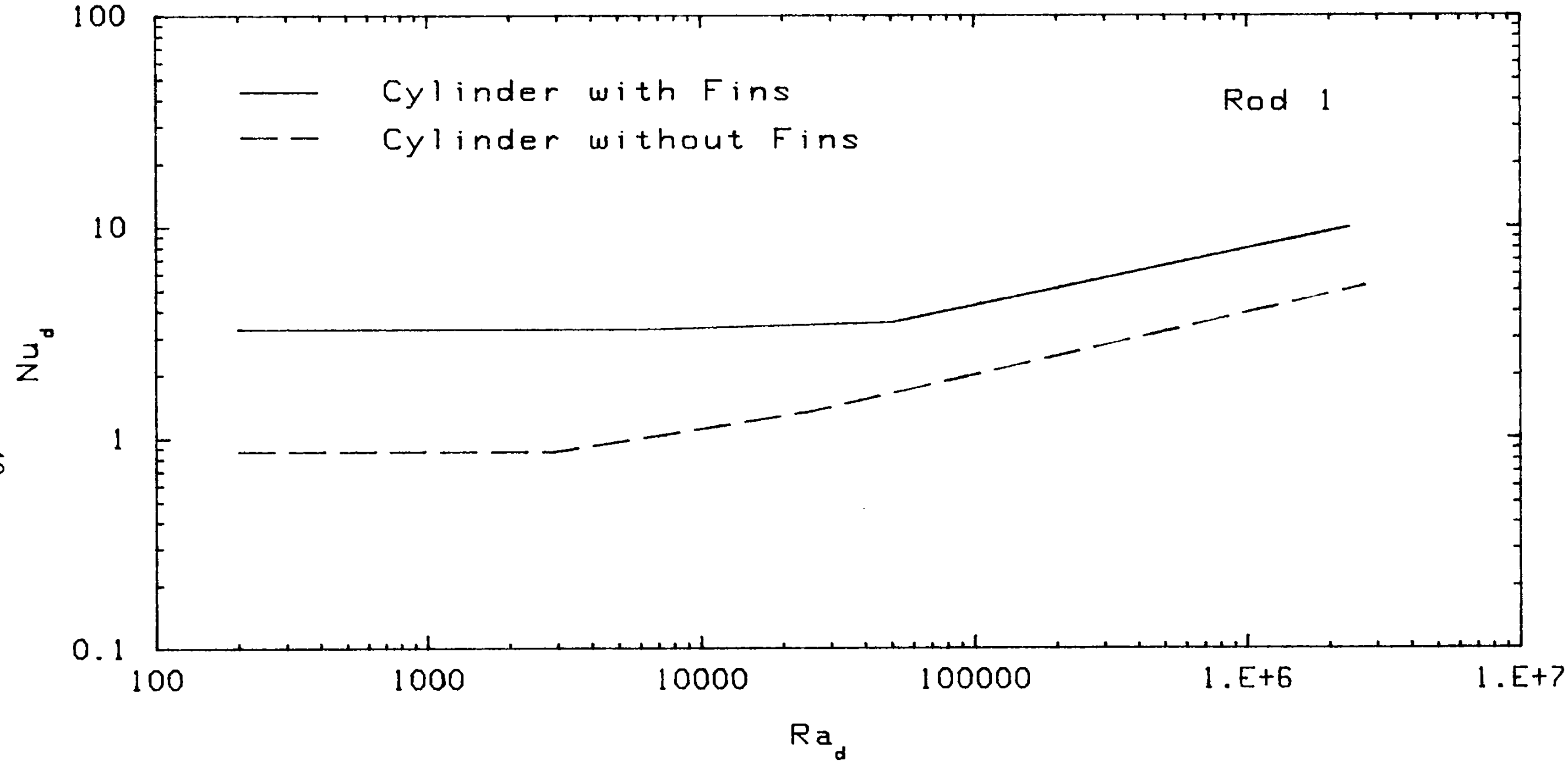

Figure 3.10: Graphical representation of the individual rod correlations (a) Rod 1 (b) Rod 2

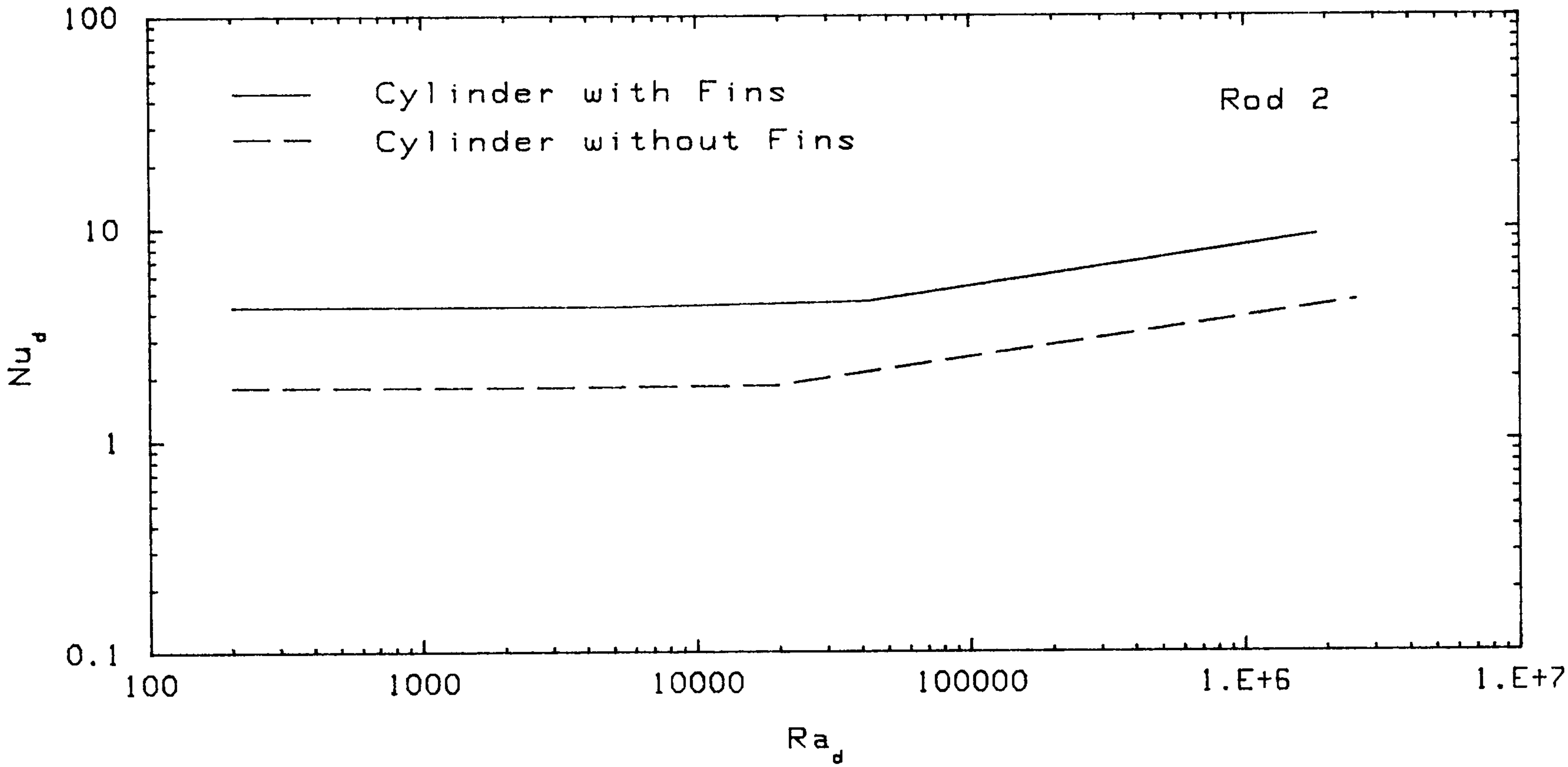

Figure 3.10 (Continued)

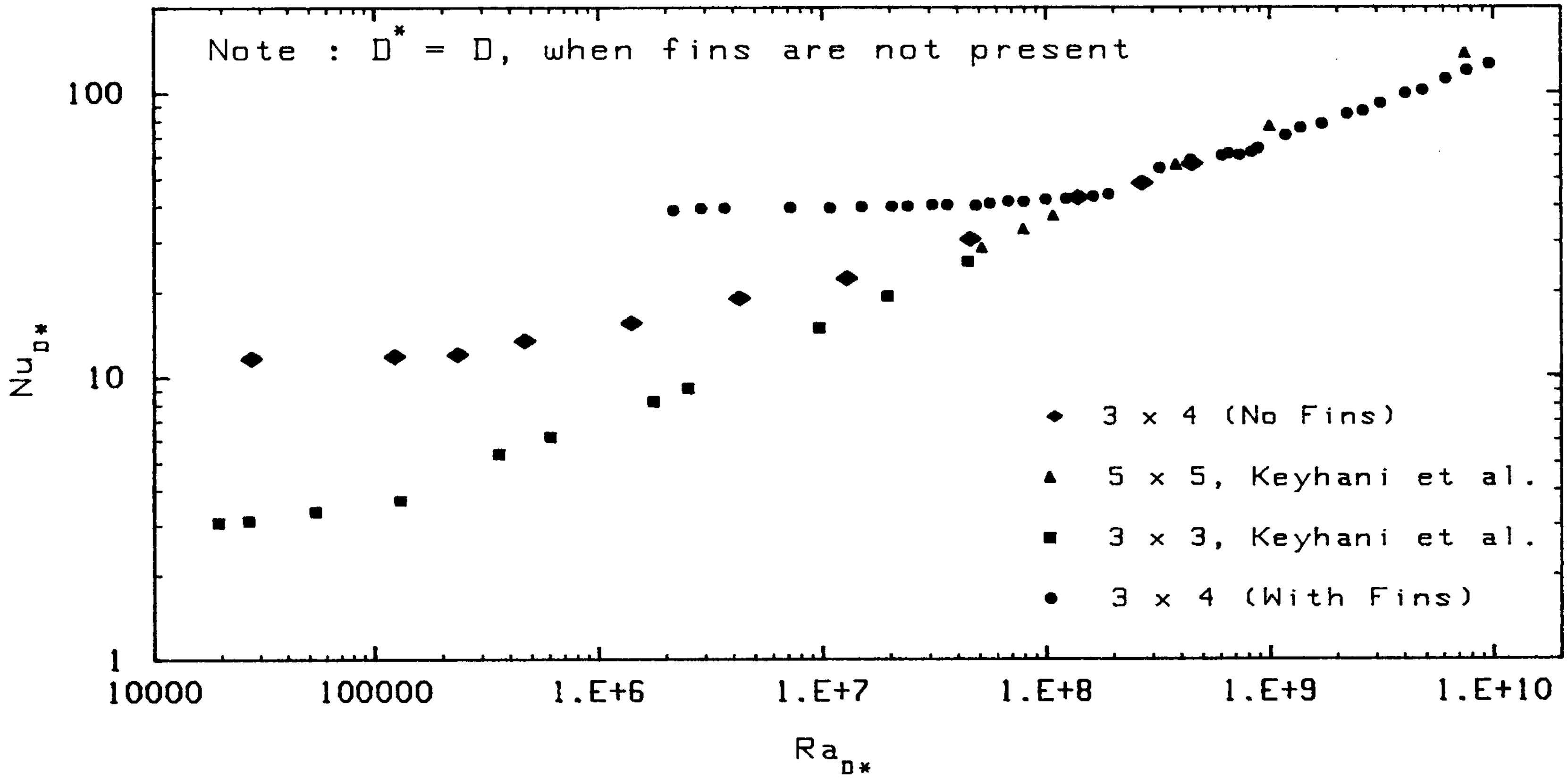

Figure 3.11: Comparison of the overall convective Nusselt numbers for all the rod–bundles

$$Ra_{D_{cr}} = 363[\frac{D}{d_i}]^{0.25} [\frac{2L}{(D-d_i)}]^{0.76} [\frac{2D}{(D-d_i)}]^3. \quad (3.24)$$

For the 3 × 4 rod–bundle without internal fins, Eq. (3.24) predicts a critical Rayleigh number of $Ra_{D_{cr}} = 4.42 \times 10^5$, which is within 10% of the experimentally determined value of 4.03×10^5. Also, as seen from this figure, in case of 3 × 4 (fins), the conduction regime is extended to a higher Rayleigh number and the onset of convection is considerably delayed. Here, it should be emphasised that the results for the 3 × 4 (fins) are based on a fictitious outer cylinder. Unfortunately, it is not possible to compare the experimental critical Rayleigh number for this case with the one obtained from Eq. (3.24) as it has been proposed only for the rod–bundle without internal fins. Another significant result of the present study is the fact, that, once the rod–bundles reach their respective convective flow regimes (that is at different Rayleigh number), the slopes of the Nusselt number versus Rayleigh number curves are very close to each other, as evident from Fig. 3.11, though the absolute values of the Nusselt numbers are different. But as the Rayleigh number increases ($Ra_{D^*} \geq 2.0 \times 10^8$), the Nusselt number of all the rod–bundles are nearly the same. Hence, the data points for all the rod–bundles are put together and a general correlation is proposed for the convective flow regime in vertical enclosed rod–bundles (with or without internal fins and whether a square array of rod–bundles or not). The correlation is given as,

$$Nu_{D^*} = 0.1131 Ra_{D^*}^{0.309}, \; 1.28 \times 10^7 \leq Ra_{D^*} \leq 9.56 \times 10^9. \quad (3.25)$$

Eq. (3.25) predicts all the experimental data in the convective flow regime with an average deviation of 7.2%.

The range of Rayleigh numbers, Ra_{D^*}, (at atmospheric pressure) encountered for the actual model at various power generations (500, 1000 and 2000 watts) and radiation heat transfer contributions (0%, 20% and 50%) are 5.89×10^{10} to 1.84×10^{11} in case of the liner with fins and 4.69×10^{9} to 1.39×10^{10} in case of the one without fins. Thus, Eq. (3.25) can be used for the actual model with an extrapolation to $Ra_{D^*} = 2.0 \times 10^{11}$. The extrapolation of this correlation to the higher Rayleigh number range is not expected to result in any significant error. The maximum temperature of the canisters in this Rayleigh number range are calculated using Eqs. (3.12) and (3.13) (with fins) and Eqs. (3.22) and (3.23) (without fins). The range of maximum temperatures on the canisters vary from 299.32 K to 356.59 K (with fins) and 304.58 K to 386.84 K (without fins), respectively, at various sink temperatures (liner) of 293.16, 303.16, 313.16 and 323.16 K. Figs. 3.12a (with fins) and 3.12b (without fins) show the characteristic temperature difference as a function of power generation for the lowest and highest sink temperatures considered. As seen from these figures, in the convective flow regime, the heat transfer has no dependency on the variation of the sink temperatures for both the cases.

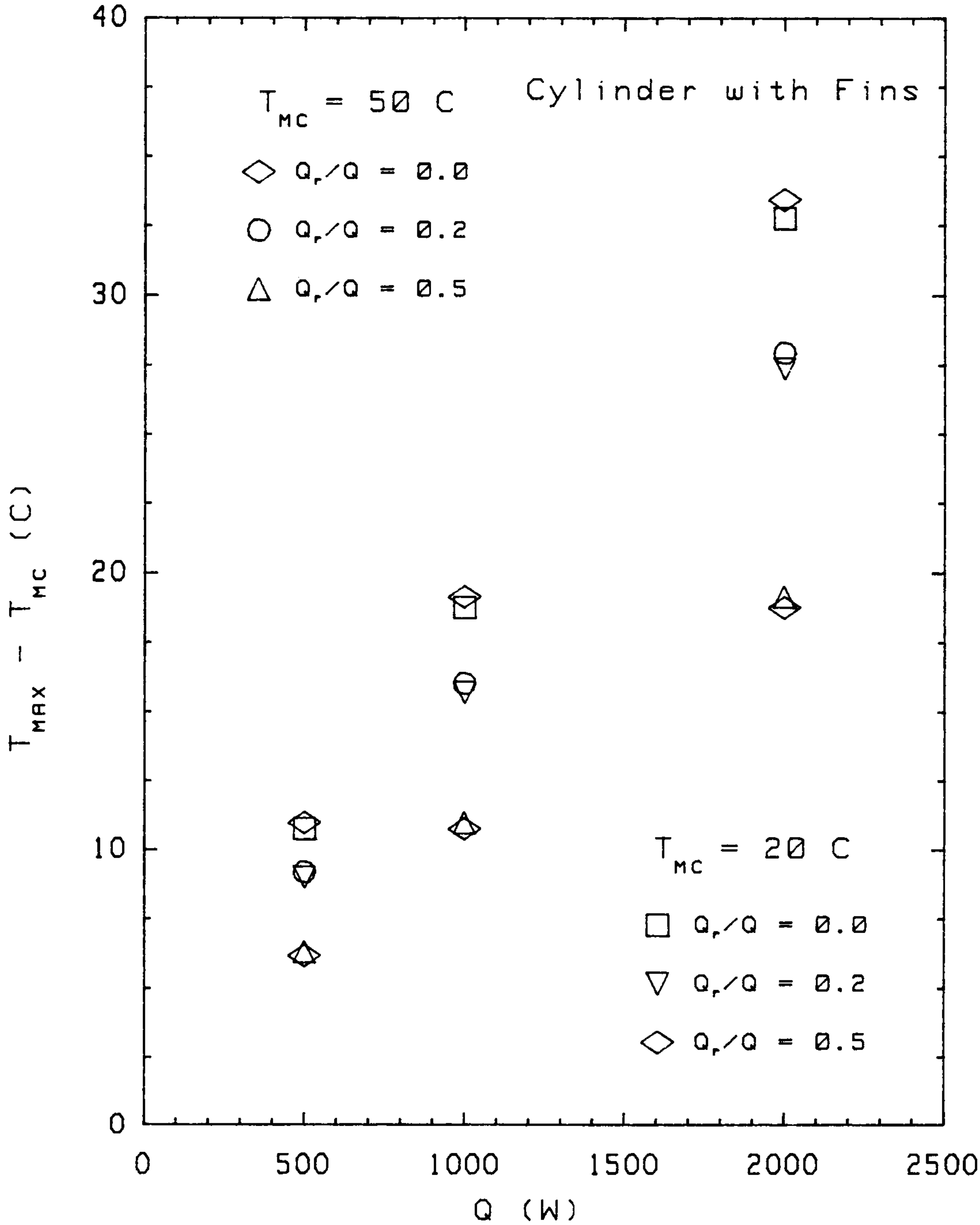

Figure 3.12: Maximum temperature difference as a function of power generation (a) Fins (b) No fins

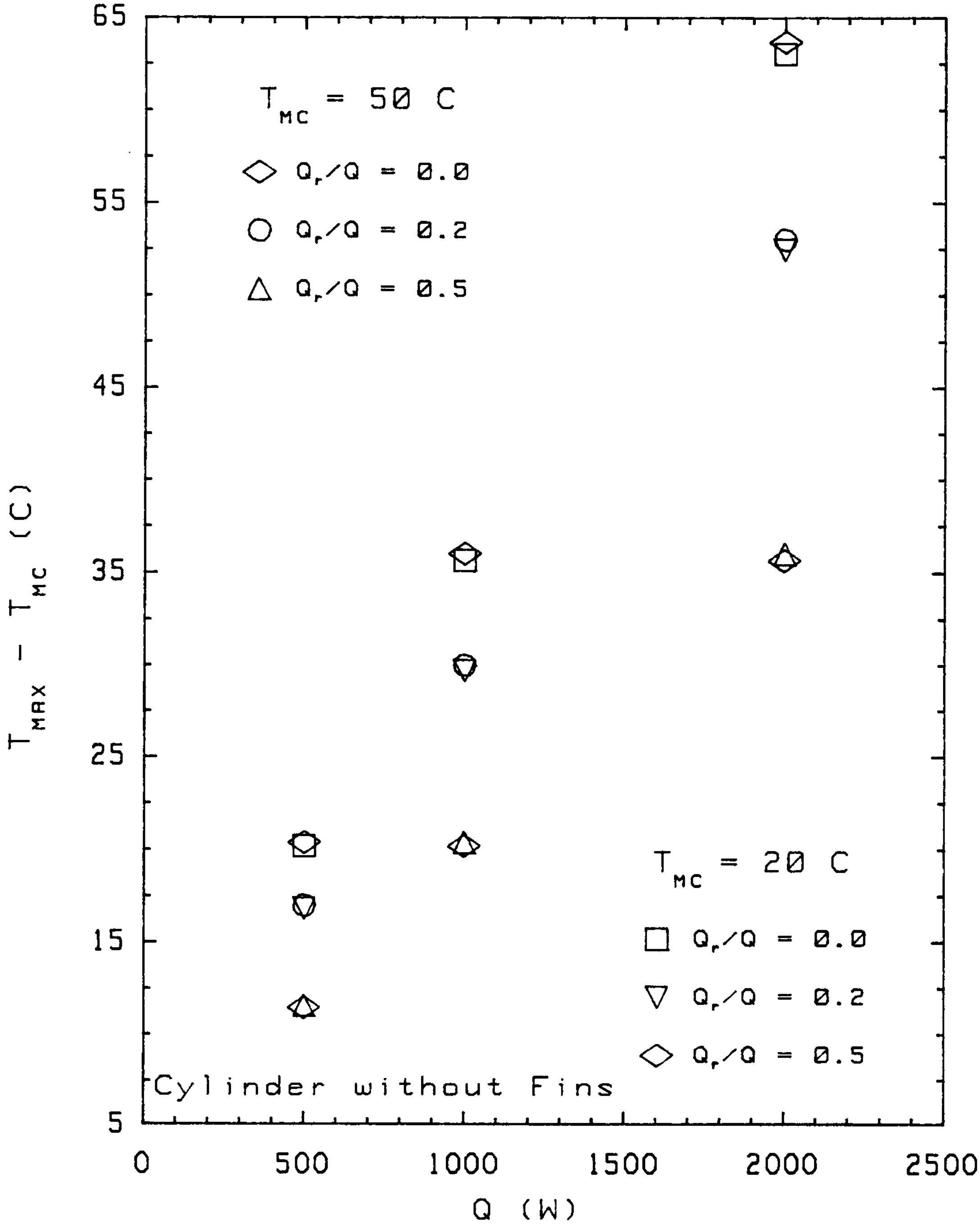

Figure 3.12 (Continued)

Chapter 4

CONCLUSIONS AND RECOMMENDATIONS

The following conclusions are drawn from the present study :

- The 3×4 rod–bundle, in case of outer cylinder with internal fins clearly shows that the extent of conduction regime is extended to a higher Rayleigh number and the onset of convection is delayed when compared with the one without fins. It can be concluded that, the fins which are present in this configuration are retarding convection heat transfer from the rod–bundle to the outer cylinder while increasing conduction heat transfer.

- The experimental $Ra_{D_{cr}}$ obtained for the 3×4 rod–bundle without internal fins on the outer cylinder is in a very good agreement with the one predicted by the relation, proposed by Keyhani et al. [5, 6] for a square array of rod–bundles. Hence, in general, this relation (Eq. (3.24)) may be used to predict the onset of convection for all the vertical rod–bundles (whether a square array or not), where the outer cylinder has no internal fins. Since, this relation is applicable to only vertical, cylindrical enclosures without internal fins, for the case of enclosing cylinder with internal fins a different relation is needed for predicting the critical Rayleigh number $Ra_{D^*_{cr}}$ and unfortunately, sufficient data is not available for proposing a similar criterion.

- Once, the convective flow regime is attained, the convective heat transfer for all the available rod–bundle data can be predicted with a single correlation given by Eq. (3.25).

- The final conclusion is that, in order to cover the higher Rayleigh number range encountered for the actual model with or without fins, Eq. (3.25) needs to be extrapolated, expecting, this will not result in any substantial error.

BIBLIOGRAPHY

BIBLIOGRAPHY

1. Conceptual Design Report, "Integral Monitored Retrievable Storage (MRS) Facility," Prepared for United States Department of Energy, Richlands Operation Office under Contract *No. DE-AC06-84RI,* Sep, 1985.

2. Cox, R. L., 1976, "Radiative Heat Transfer in Arrays of Parallel Cylinders," *Ph.D. dissertation*, The University of Tennesee.

3. Gebhart, B., 1961, "Surface Temperature Calculations in Radiation Surroundings of Arbitrary Complexity for Gray and Diffuse Radiation," *Internal Journal of Heat and Mass Transfer*," vol. 3, pp. 341–346.

4. Hottel, H. C., 1954, "Radiant Heat Transmission," Heat Transmission, 3^{rd} Ed., W. H. McAdams, Chapter–4, Ed., McGraw–Hill, New York.

5. Keyhani, M., Kulacki, F. A. and Christensen, R. N., 1985, "Experimental Investigation of Free Convection in a Vertical Rod–Bundle – a General Correlation for Nusselt Numbers," *Journal of Heat Transfer - Transactions of the ASME*, vol. 107, no. 3, pp. 611–623.

6. Keyhani, M., Kulacki, F. A. and Christensen, R. N., 1987, "Heat Transfer Within Spent-Fuel Canisters: An Experimental Laboratory Study – Final Report, " *Office of Nuclear Waste Isolation*, Battele Memorial Institute, Columbus, BMI/ONWI–530.

7. Larson, David W., Gartling, David K. and Schimmel, Walter P. Jr., 1978, "Natural Convection Studies in Nuclear Spent–Fuel Shipping Casks : Computation and Expt.," *Journal of Energy*, vol. 2, no. 3, pp. 147–154.

8. McCann, R. A., 1980, "Thermohydraulic Analysis of a Spent–Fuel Assembly Contained Within a Canister," *Heat Transfer in Nuclear Waste Disposal*, ed. F. A. kulacki and R. Lyczkowski, HTD Vol. 11, *ASME.*

9. Newman, Darrell F., 1985, "Spent–Fuel Management : Near–Term Aspects," *Mechanical Engineering*, August, pp.28–31.

10. Siegel, R. and Howell, J. R., 1972, "Thermal Radiation Heat Transfer, McGraw–Hill, New York.

11. Wong S. and Chen, K., 1981, "On the Two–Dimensional Analysis of Fluid Flow and Heat Transfer in Rod–Bundles with Arbitrary Arrangement," *Journal of Nuclear Science and Engineering*, vol. 77, no. 1, pp. 92–106.

APPENDIXES

Appendix A

EXPERIMENTAL DATA FOR CASK WITH FINS

Table A.1: Temperature data for helium experiments

Run *no.*	P *atm.*	q W	T_{MC} C	T_{MR1} C	T_{MR2} C	ΔT_1 C	ΔT_2 C
64	1.23	10	23.67	41.70	37.80	18.02	14.12
65	1.22	14	23.82	49.02	43.56	25.19	19.73
66	1.18	18	23.49	55.12	48.14	31.62	24.64
67	1.14	22	24.36	62.74	54.39	38.38	30.03
68	2.02	22	23.97	61.90	53.63	37.92	29.85
69	1.94	14	23.69	48.49	42.97	24.79	19.28
70	2.14	18	23.52	55.00	48.05	31.48	24.52
71	2.18	26	24.12	68.42	58.73	44.29	34.61
72	2.76	26	24.04	68.30	58.79	44.26	34.74
73	2.98	14	23.14	47.83	42.30	24.68	19.15
74	2.95	18	23.60	54.91	48.08	31.30	24.47
75	2.97	22	23.85	61.71	53.60	37.85	29.74
76	4.05	21	23.82	61.24	53.30	37.41	29.47
77	4.04	14	23.17	47.66	42.25	24.49	19.07
78	3.92	18	23.26	54.37	47.64	31.10	24.38
79	3.93	26	24.15	68.00	58.52	43.84	34.36
80	5.00	26	23.76	66.83	57.78	43.06	34.01
81	4.95	14	22.94	47.15	41.93	24.20	18.98
82	4.93	18	23.56	54.17	47.55	30.61	23.98
83	5.00	22	23.62	60.39	52.65	36.77	29.03
84	6.10	22	23.44	59.68	52.29	36.23	28.84
85	5.88	18	23.33	53.76	47.40	30.42	24.06
86	6.03	26	24.02	66.87	58.21	42.85	34.19
87	6.00	30	23.73	72.33	62.66	48.59	38.92
88	6.97	30	23.92	71.61	62.39	47.68	38.46
89	7.57	30	23.90	71.10	62.14	47.20	38.24

Table A.2: Temperature data for air experiments

Run no.	*P* atm.	*q* W	T_{MC} C	T_{MR1} C	T_{MR2} C	ΔT_1 C	ΔT_2 C
1	1.00	1	22.11	29.08	27.97	6.96	5.86
2	1.16	2	26.52	39.34	37.43	12.81	10.90
3	1.04	3	26.48	45.41	42.61	18.93	16.13
4	1.02	4	26.63	51.06	47.48	24.42	20.84
5	1.00	5	23.52	54.08	49.43	30.55	25.91
6	1.01	6	28.11	63.26	58.19	35.15	30.08
7	1.00	7	23.41	64.20	58.39	40.79	34.98
8	1.00	8	23.56	64.58	60.17	41.02	36.61
9	1.02	9	27.29	77.68	70.79	50.39	43.49
10	1.00	10	23.80	79.66	71.99	55.86	48.19
11	1.91	1	21.98	28.35	27.35	6.36	5.36
12	1.89	2	22.11	34.43	32.69	12.31	10.57
13	1.89	3	22.91	40.42	38.04	17.51	15.12
14	2.03	4	23.17	45.39	42.52	22.22	19.35
15	2.03	5	23.61	50.89	47.50	27.28	23.88
16	2.03	6	23.95	56.17	52.37	32.21	28.41
17	1.98	7	23.78	60.47	56.29	36.68	32.51
18	2.00	8	23.58	64.61	60.19	41.03	36.60
19	2.01	9	24.18	69.40	64.83	45.21	40.65
20	1.97	10	23.92	73.09	67.98	49.16	44.05
21	2.89	1	23.39	29.33	28.45	5.94	5.06
22	2.97	2	23.43	35.00	33.59	11.56	10.15
23	2.97	3	23.32	39.56	37.75	16.24	14.42
24	2.96	4	23.22	43.95	41.86	20.72	18.63
25	2.96	5	23.24	47.59	45.44	24.34	22.20
26	2.97	6	23.62	52.03	49.60	28.40	25.98
27	3.05	7	23.46	55.11	52.62	31.64	29.15
28	3.00	8	23.36	58.85	56.13	35.49	32.76
29	3.00	9	23.56	62.68	59.76	39.12	36.20
30	3.00	10	23.35	66.03	62.98	42.67	39.62
31	3.00	12	23.67	73.02	69.54	49.34	45.87

Table A.2 (Continued)

Run no.	*P* atm.	*q* W	T_{MC} C	T_{MR1} C	T_{MR2} C	ΔT_1 C	ΔT_2 C
32	1.44	3	22.27	40.41	37.83	18.13	15.56
33	1.52	4	21.99	45.80	42.34	23.81	20.35
34	1.52	5	22.36	51.55	47.58	28.19	25.22
35	1.51	6	23.77	57.34	52.65	33.56	28.88
36	1.50	7	24.19	63.03	57.73	38.83	33.53
37	1.54	8	24.04	67.41	61.98	43.37	37.94
38	3.97	3	22.69	37.17	35.93	14.47	13.24
39	3.98	4	23.47	41.52	40.13	18.05	16.65
40	4.02	5	24.01	46.02	44.39	22.01	20.38
41	4.16	6	24.38	49.99	48.29	25.60	23.90
42	4.04	7	23.09	51.89	50.09	28.80	26.99
43	3.93	8	23.91	56.13	54.19	32.21	30.28
44	4.00	9	23.71	59.56	57.53	35.84	33.81
45	4.00	10	23.29	62.73	60.45	39.43	37.16
46	3.99	12	23.52	67.99	65.54	44.46	42.01
47	4.00	14	23.71	74.84	72.10	51.12	48.38
48	4.95	5	24.45	44.75	43.58	20.29	19.13
49	4.94	6	24.92	48.47	47.17	23.54	22.25
50	4.94	10	23.69	59.66	57.99	35.97	34.30
51	5.01	11	23.47	62.00	60.21	38.53	36.74
52	5.00	12	23.42	65.09	63.40	41.67	39.97
53	4.99	13	23.92	67.98	66.11	44.05	42.18
54	4.99	15	23.87	73.34	71.26	49.47	47.39
55	5.99	10	23.50	56.86	55.66	33.35	32.15
56	5.93	12	23.80	62.64	61.30	38.83	37.50
57	5.97	14	24.11	67.74	66.18	43.63	42.07
58	5.96	16	24.12	72.72	71.14	48.60	47.02
59	5.93	18	24.86	78.57	76.66	53.71	51.79
60	6.36	14	23.29	65.48	64.24	42.18	40.95
61	6.39	16	23.65	70.84	69.33	47.18	45.67
62	6.31	18	23.92	75.91	74.33	51.98	50.41
63	6.37	20	23.75	79.86	78.05	56.10	54.29

Table A.3: Convective and total Nusselt numbers for helium experiments

Run no.	Ra_{d1}	Nu_{Td1}	Nu_{d1}	Ra_{d2}	Nu_{Td2}	Nu_{d2}
64	6.69×10^2	3.61	3.21	5.32×10^2	4.81	4.11
65	8.9×10^2	3.60	3.26	7.11×10^2	4.61	4.25
67	1.13×10^3	3.66	3.18	9.12×10^2	4.69	4.18
69	2.21×10^3	3.63	3.28	1.75×10^3	4.68	4.31
70	3.34×10^3	3.68	3.27	2.67×10^3	4.74	4.31
71	4.63×10^3	3.73	3.30	3.74×10^3	4.79	4.36
74	6.31×10^3	3.70	3.31	5.05×10^3	4.75	4.34
72	7.42×10^3	3.74	3.31	6.02×10^3	4.79	4.36
77	9.56×10^3	3.70	3.35	7.59×10^3	4.77	4.40
78	1.11×10^4	3.72	3.35	8.94×10^3	4.76	4.38
79	1.49×10^4	3.76	3.33	1.21×10^4	4.82	4.38
82	1.72×10^4	3.75	3.39	1.38×10^4	4.81	4.44
83	2.09×10^4	3.82	3.44	1.69×10^4	4.86	4.48
85	2.45×10^4	3.80	3.44	1.98×10^4	4.82	4.45
84	3.08×10^4	3.88	3.50	2.51×10^4	4.89	4.51
87	3.80×10^4	3.93	3.52	3.15×10^4	4.93	4.50
88	5.04×10^4	4.00	3.58	4.20×10^4	4.98	4.55
89	5.90×10^4	4.05	3.65	4.93×10^4	5.02	4.61

Table A.4: Convective and total Nusselt numbers for air experiments

Run no.	Ra_{d1}	Nu_{Td1}	Nu_{d1}	Ra_{d2}	Nu_{Td2}	Nu_{d2}
2	2.55×10^4	5.72	3.42	2.18×10^4	6.73	4.33
3	2.94×10^4	5.77	3.53	2.54×10^4	6.78	4.21
4	3.57×10^4	5.86	3.57	3.09×10^4	6.89	4.35
6	4.78×10^4	6.06	3.57	4.17×10^4	7.10	4.36
9	6.62×10^4	6.30	3.56	5.86×10^4	7.33	4.35
34	8.98×10^4	6.26	4.52	8.75×10^4	7.27	5.41
14	1.37×10^5	6.63	4.98	1.20×10^5	7.63	5.76
16	1.89×10^5	6.76	4.97	1.69×10^5	7.69	5.69
17	2.02×10^5	6.93	5.07	1.82×10^5	7.84	5.81
18	2.26×10^5	7.07	5.09	2.05×10^5	7.95	5.69
20	2.56×10^5	7.30	5.16	2.34×10^5	8.17	5.85
24	2.73×10^5	7.07	5.30	3.35×10^5	7.88	5.89
26	3.63×10^5	7.69	5.90	3.35×10^5	8.43	6.41
27	4.23×10^5	8.05	6.26	3.93×10^5	8.75	6.73
30	5.29×10^5	8.47	6.58	4.97×10^5	9.14	6.88
42	6.85×10^5	8.86	7.13	6.47×10^5	9.46	7.46
44	8.08×10^5	9.13	7.31	7.69×10^5	9.70	7.56
46	9.68×10^5	9.68	7.76	9.23×10^5	10.26	7.96
50	1.25×10^6	10.19	8.38	1.20×10^6	10.70	8.59
53	1.49×10^6	10.63	8.68	1.44×10^6	11.12	8.82
56	1.90×10^6	11.31	9.49	1.84×10^6	11.73	9.54
60	2.35×10^6	12.03	10.19	2.30×10^6	12.41	10.16
63	2.97×10^6	12.71	10.65	2.89×10^6	13.15	10.66

Table A.5: Convection and radiation contributions for helium experiments

Run *no.*	*q* *W*	Ra_{D^*}	Nu_{TD^*}	Nu_{D^*}	*RAD*1 %	*CON*1 %	*RAD*2 %	*CON*2 %
64	10	2.60×10^6	43.31	43.01	11.13	88.87	10.87	89.13
65	14	3.46×10^6	43.24	40.07	9.62	90.38	7.77	92.23
67	22	4.40×10^6	43.87	39.25	12.97	87.03	11.00	89.00
69	14	8.62×10^6	43.54	39.52	9.66	90.34	7.86	92.14
70	18	1.30×10^7	44.14	40.53	11.13	88.87	8.95	91.05
71	26	1.80×10^7	44.73	40.49	11.43	88.57	9.04	90.96
74	18	2.45×10^7	44.38	39.71	10.50	89.50	8.65	91.35
72	26	2.88×10^7	44.88	40.52	11.49	88.51	8.98	91.02
77	14	3.72×10^7	44.43	40.58	9.43	90.57	7.68	92.32
78	18	4.33×10^7	44.63	40.77	9.79	90.21	7.99	92.01
79	26	5.81×10^7	45.13	40.43	11.42	88.58	9.10	90.90
82	18	6.71×10^7	45.05	41.33	9.71	90.29	7.72	92.28
83	22	8.13×10^7	45.88	41.81	9.91	90.09	7.92	92.08
85	18	9.53×10^7	45.58	41.84	9.52	90.48	7.69	92.31
84	22	1.20×10^8	46.53	42.48	9.82	90.18	7.76	92.24
87	30	1.48×10^8	47.16	42.76	10.49	89.51	8.70	91.30
88	30	1.96×10^8	47.98	43.33	10.41	89.59	8.55	91.45
89	30	2.30×10^8	48.56	44.33	9.84	90.16	8.19	91.81

Table A.6: Convection and radiation contributions for air experiments

Run *no.*	*q* *W*	Ra_{D^*}	Nu_{TD^*}	Nu_{D^*}	*RAD*1 %	*CON*1 %	*RAD*2 %	*CON*2 %
4	4	1.39×10^8	70.42	43.69	39.07	60.93	36.82	63.17
6	6	1.86×10^8	72.74	43.93	41.06	58.94	38.61	61.38
9	9	2.57×10^8	75.60	44.11	43.34	56.65	40.64	59.35
34	5	3.88×10^8	75.17	55.18	27.85	72.15	25.61	74.39
14	6	5.34×10^8	79.55	59.83	24.88	75.11	24.48	75.51
16	6	7.36×10^8	81.13	59.89	26.44	73.56	26.02	73.98
17	7	7.88×10^8	83.13	60.94	26.79	73.21	25.92	74.07
18	8	8.82×10^8	84.80	60.27	28.03	71.97	28.34	71.66
20	10	9.99×10^8	87.58	61.66	29.33	70.67	28.48	71.52
24	4	1.06×10^9	84.86	60.96	25.06	74.94	25.23	74.77
26	6	1.41×10^9	92.32	70.08	23.35	76.64	23.96	76.04
27	7	1.65×10^9	96.56	74.51	22.20	77.80	23.11	76.89
30	11	2.06×10^9	101.63	77.51	22.25	77.75	24.72	75.28
42	7	2.67×10^9	106.28	83.96	19.52	80.47	21.10	78.89
44	9	3.15×10^9	109.60	86.01	19.96	80.03	22.00	78.00
46	12	3.76×10^9	116.13	91.54	19.77	80.22	22.39	77.60
50	10	4.88×10^9	122.30	99.03	17.74	82.25	19.74	80.25
53	13	5.80×10^9	127.61	101.66	18.34	81.65	20.70	79.30
56	12	7.40×10^9	135.78	111.59	16.13	83.87	18.66	81.33
60	14	9.17×10^9	144.41	119.31	15.35	84.64	18.13	81.87
63	20	1.15×10^{10}	152.54	125.80	16.19	83.81	18.94	81.06

Appendix B

EXPERIMENTAL DATA FOR CASK WITHOUT FINS

Table B.1: Temperature data for helium experiments

Run *no.*	*P* *atm.*	*q* *W*	T_{MC} *C*	T_{MR1} *C*	T_{MR2} *C*	ΔT_1 *C*	ΔT_2 *C*
1	1.14	10	27.82	81.20	59.97	53.38	32.15
2	2.12	10	27.90	74.96	57.86	47.05	29.96
3	1.67	10	27.49	76.44	57.52	48.94	30.02
4	1.09	1	26.41	32.06	29.70	5.65	3.29
5	1.02	3	27.00	43.96	36.78	16.96	9.78
6	1.01	6	26.90	59.68	46.00	32.78	19.09
7	3.07	10	27.81	70.27	56.17	42.46	28.36
8	4.04	8	27.78	60.23	50.00	32.45	22.21
9	4.04	14	28.42	80.88	65.45	52.46	37.04
10	5.04	14	28.57	78.18	64.62	49.61	36.05

Table B.2: Temperature data for air experiments

Run *no.*	*P* *atm.*	*q* *W*	T_{MC} *C*	T_{MR1} *C*	T_{MR2} *C*	ΔT_1 *C*	ΔT_2 *C*
1	1.03	1	26.82	41.17	37.64	14.34	10.82
2	1.03	3	27.07	63.88	55.98	36.80	28.90
3	1.04	5	27.22	85.81	73.97	58.58	46.74
5	1.99	2	26.32	49.35	45.07	23.03	18.75
6	1.99	4	26.88	67.57	60.80	40.69	33.93
7	3.10	2	26.29	46.20	43.20	19.91	16.91
8	3.02	4	26.71	62.89	58.07	36.17	31.35
9	4.07	5	26.89	65.19	61.34	38.30	34.45
10	4.99	8	28.17	81.42	77.12	53.26	48.96
11	5.98	8	28.64	77.62	74.58	48.98	45.94
12	6.16	10	27.61	85.84	82.46	58.22	54.84

Table B.3: convective and total Nusselt numbers for helium and air experiments

Run no.	Ra_{d1}	Nu_{Td1}	Nu_{d1}	Ra_{d2}	Nu_{Td2}	Nu_{d2}
4	1.64×10^2	1.13	0.86	0.96×10^2	1.94	1.74
6	7.40×10^2	1.15	0.86	4.52×10^2	1.99	1.80
1	1.41×10^3	1.18	0.87	9.13×10^2	1.97	1.79
3	2.80×10^3	1.29	0.99	1.83×10^3	2.12	1.94
7	8.43×10^3	1.48	1.21	5.91×10^3	2.23	2.02
10	2.56×10^4	1.77	1.53	1.96×10^4	2.45	2.21
3	7.73×10^4	2.98	1.83	6.45×10^4	3.77	2.34
7	2.74×10^5	3.69	2.80	2.37×10^5	4.32	2.82
9	8.37×10^5	4.76	3.97	7.71×10^5	5.24	3.67
10	1.64×10^6	5.30	4.49	1.53×10^6	5.79	4.12
12	2.70×10^6	6.03	5.27	2.58×10^6	6.42	4.65

Table B.4: Convection and radiation contributions for helium and air experiments

Run *no.*	q W	Ra_D	Nu_{TD}	Nu_D	$RAD1$ %	$CON1$ %	$RAD2$ %	$CON2$ %
4	1	2.74×10^4	13.57	11.60	24.11	75.89	10.11	89.89
6	6	1.23×10^5	13.81	11.80	25.31	74.69	9.12	90.88
1	10	2.35×10^5	14.12	11.98	26.28	73.72	9.28	90.72
3	10	4.66×10^5	15.48	13.37	23.18	76.82	8.58	91.42
7	10	1.40×10^6	17.76	15.42	18.23	81.77	9.24	90.76
10	14	4.26×10^6	21.26	18.88	13.51	86.49	10.01	89.99
3	5	1.29×10^7	35.80	22.17	38.59	61.41	37.82	62.18
7	2	4.56×10^7	44.33	30.41	24.11	75.89	34.62	65.38
9	5	1.39×10^8	57.09	42.58	16.53	83.47	28.95	70.05
10	8	2.73×10^8	63.65	48.20	15.32	84.68	28.74	71.26
12	10	4.50×10^8	72.37	55.97	12.63	87.37	27.60	72.40

Appendix C

TEMPERATURE PROFILES FOR THE 3X4 ROD-BUNDLE

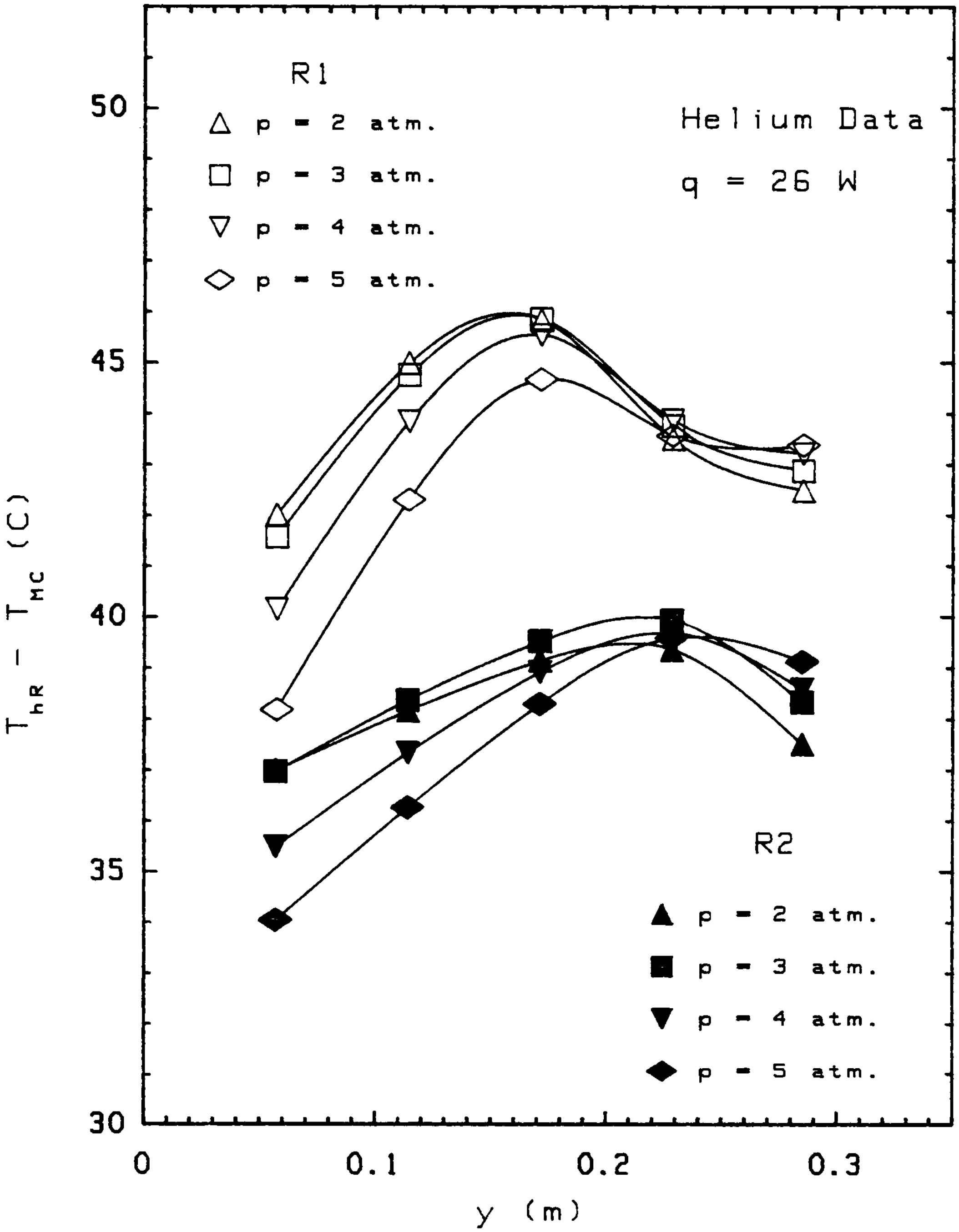

Figure C.1: Local temperature difference on rods 1 and 2 at various pressures for helium

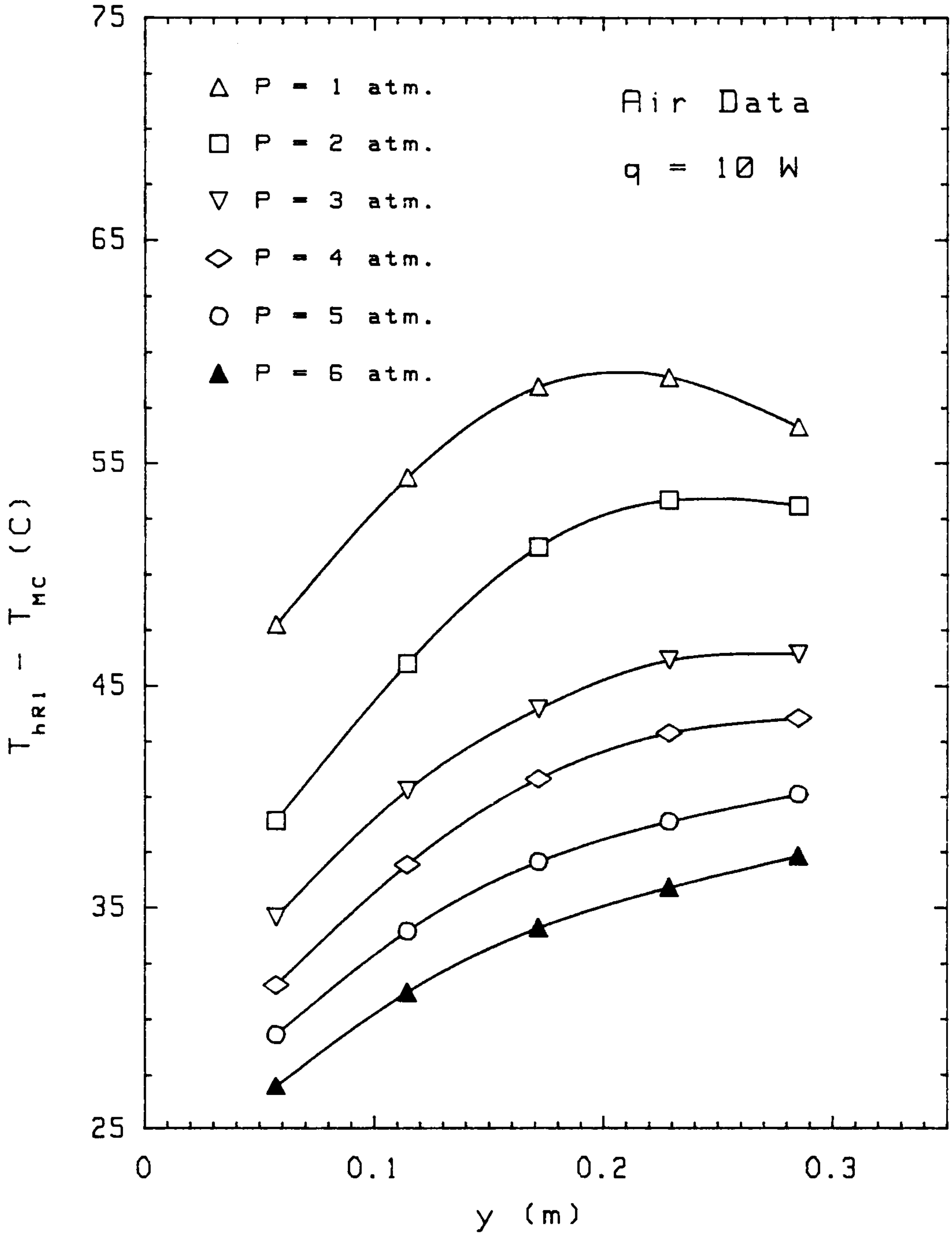

Figure C.2: Local temperature difference on rods 1 and 2 at various pressures for air (a) Rod 1 (b) Rod 2

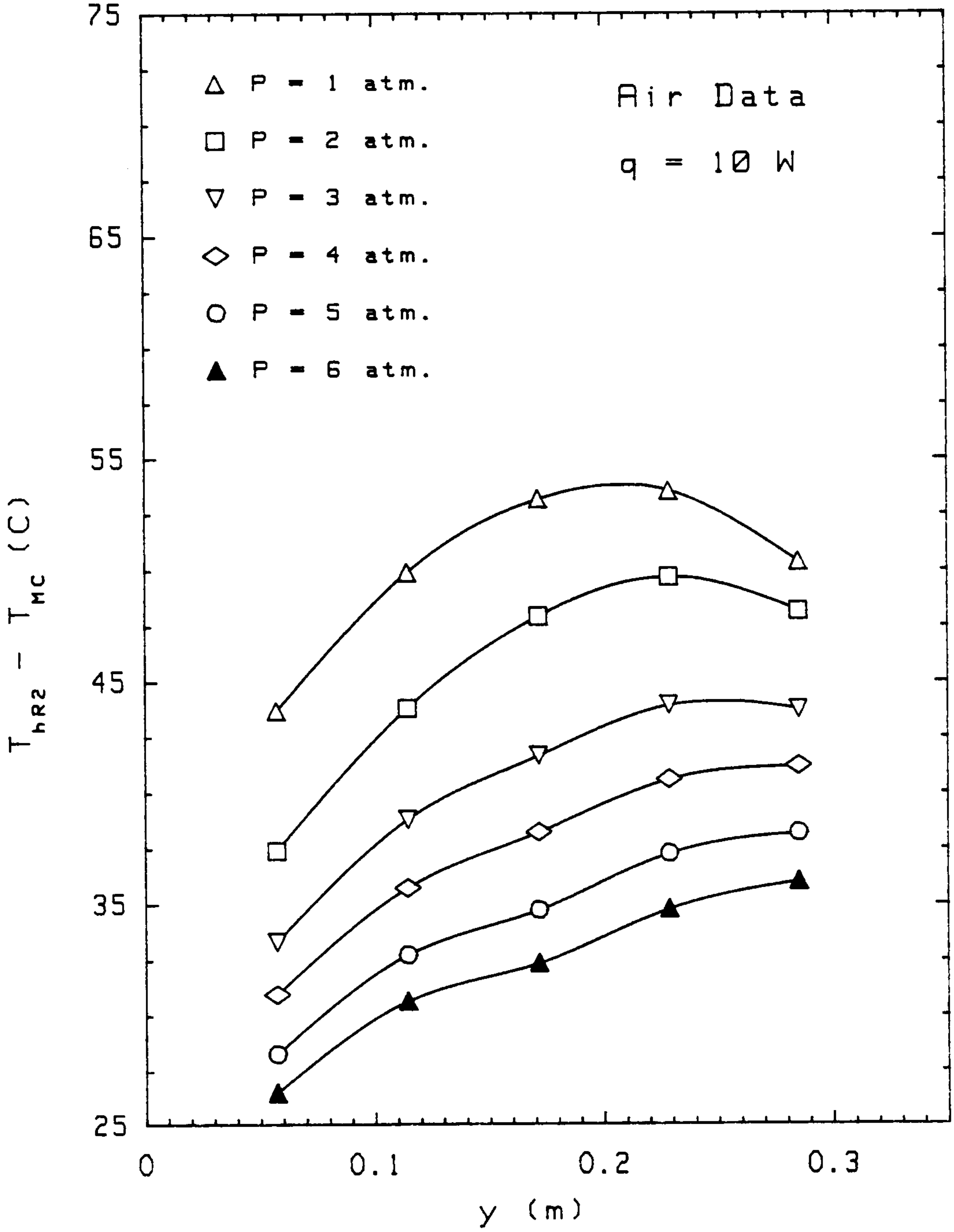

Figure C.2 (Continued)

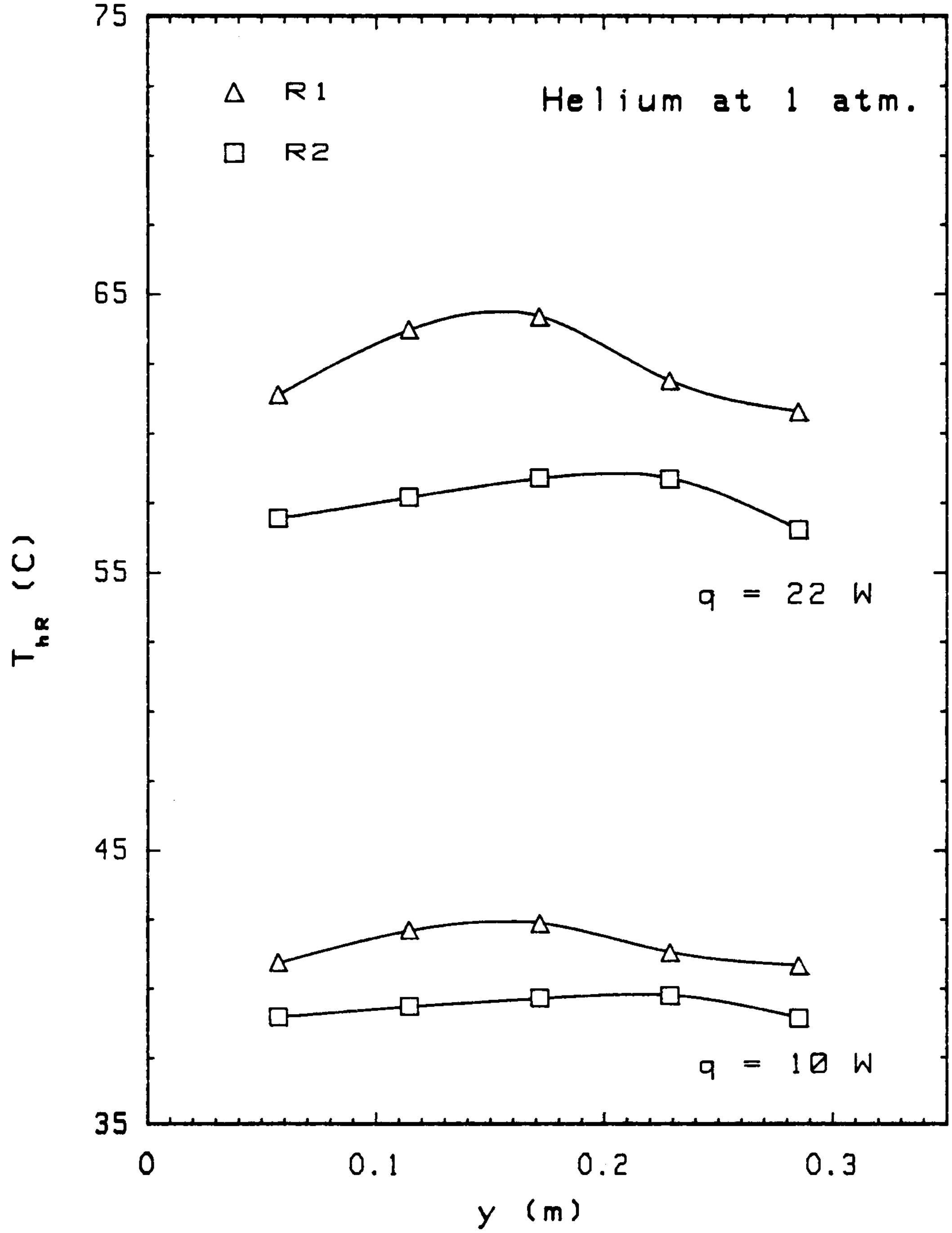

Figure C.3: Temperature profiles on rods for helium at 1 atm.

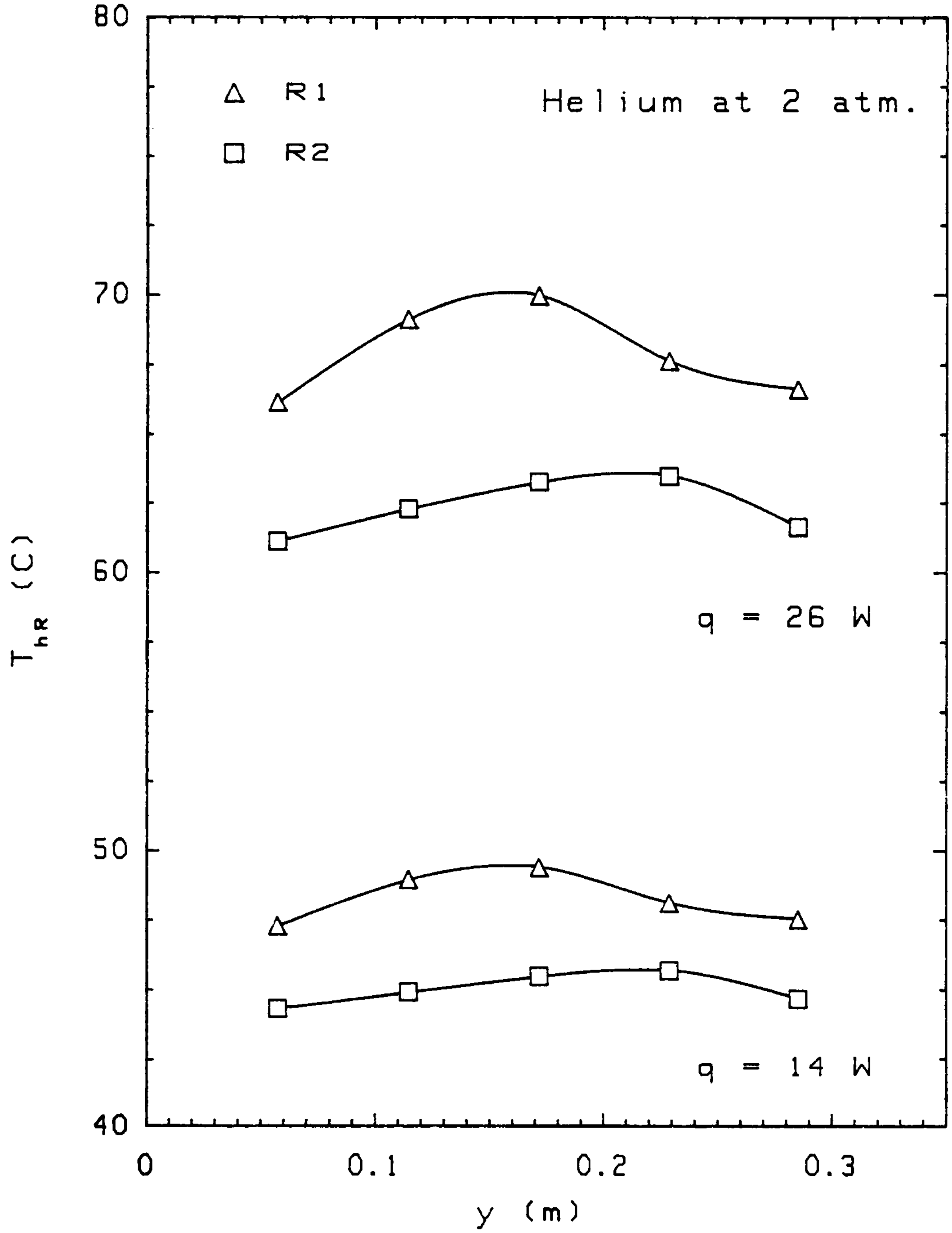

Figure C.4: Temperature profiles on rods for helium at 2 atm.

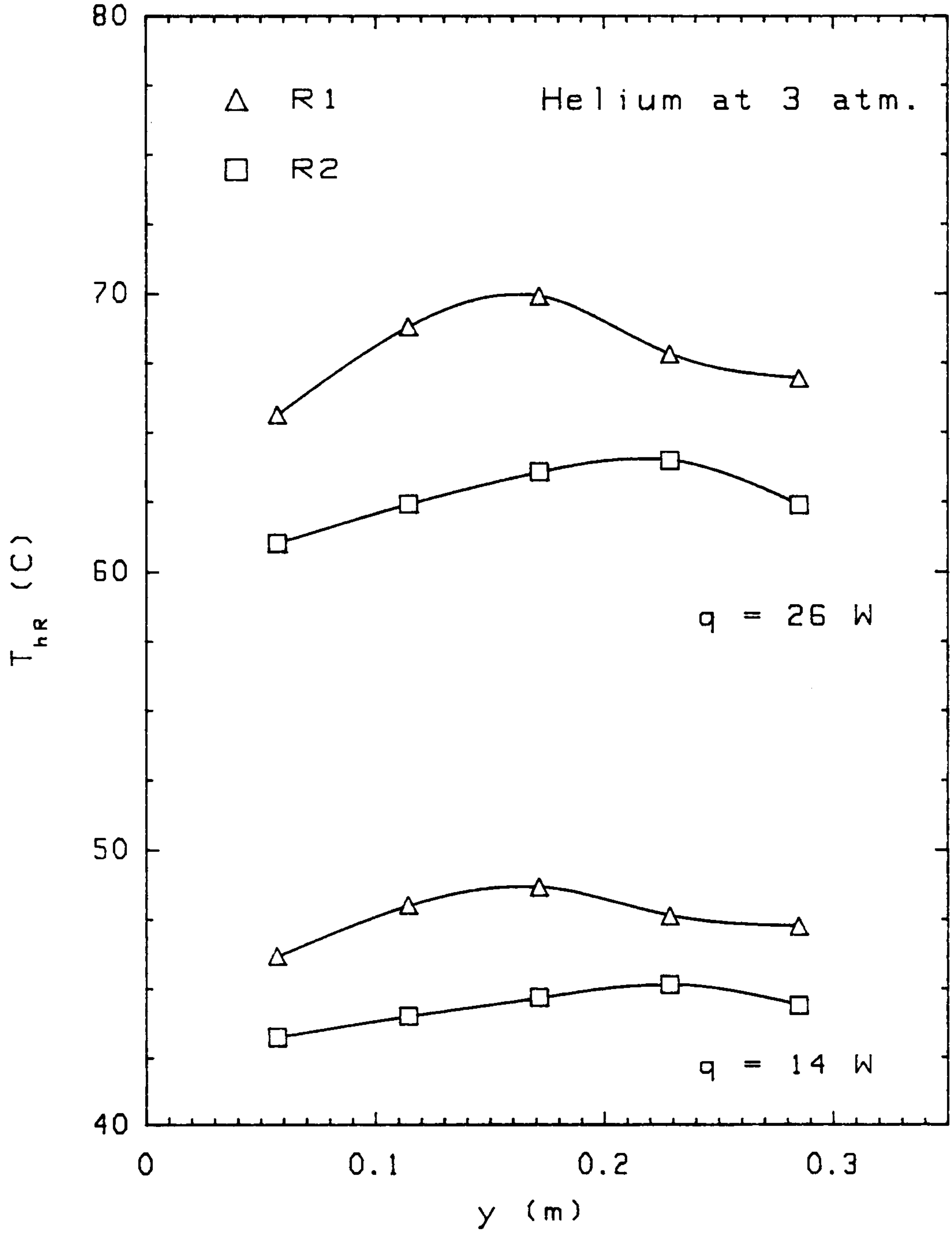

Figure C.5: Temperature profiles on rods for helium at 3 atm.

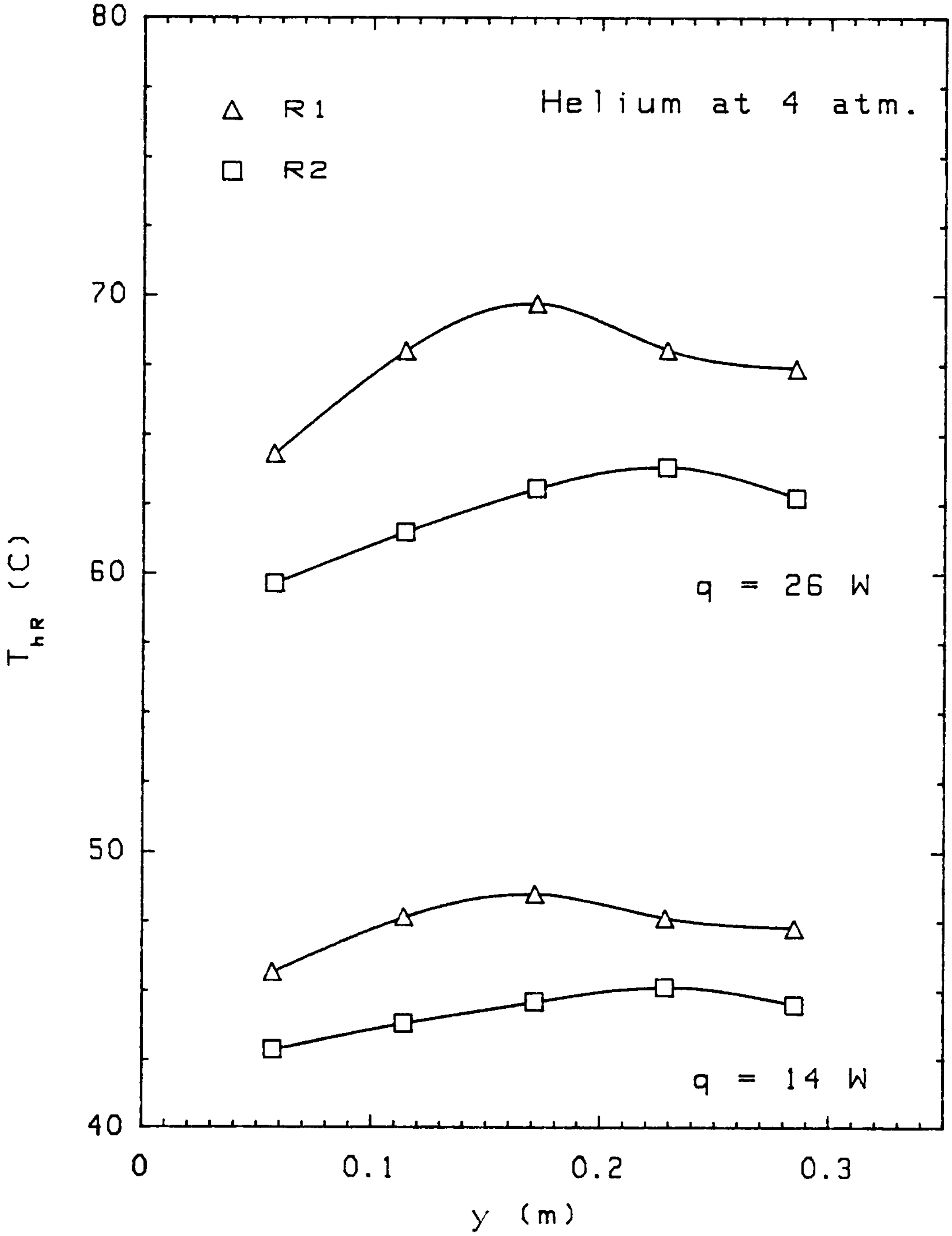

Figure C.6: Temperature profiles on rods for helium at 4 atm.

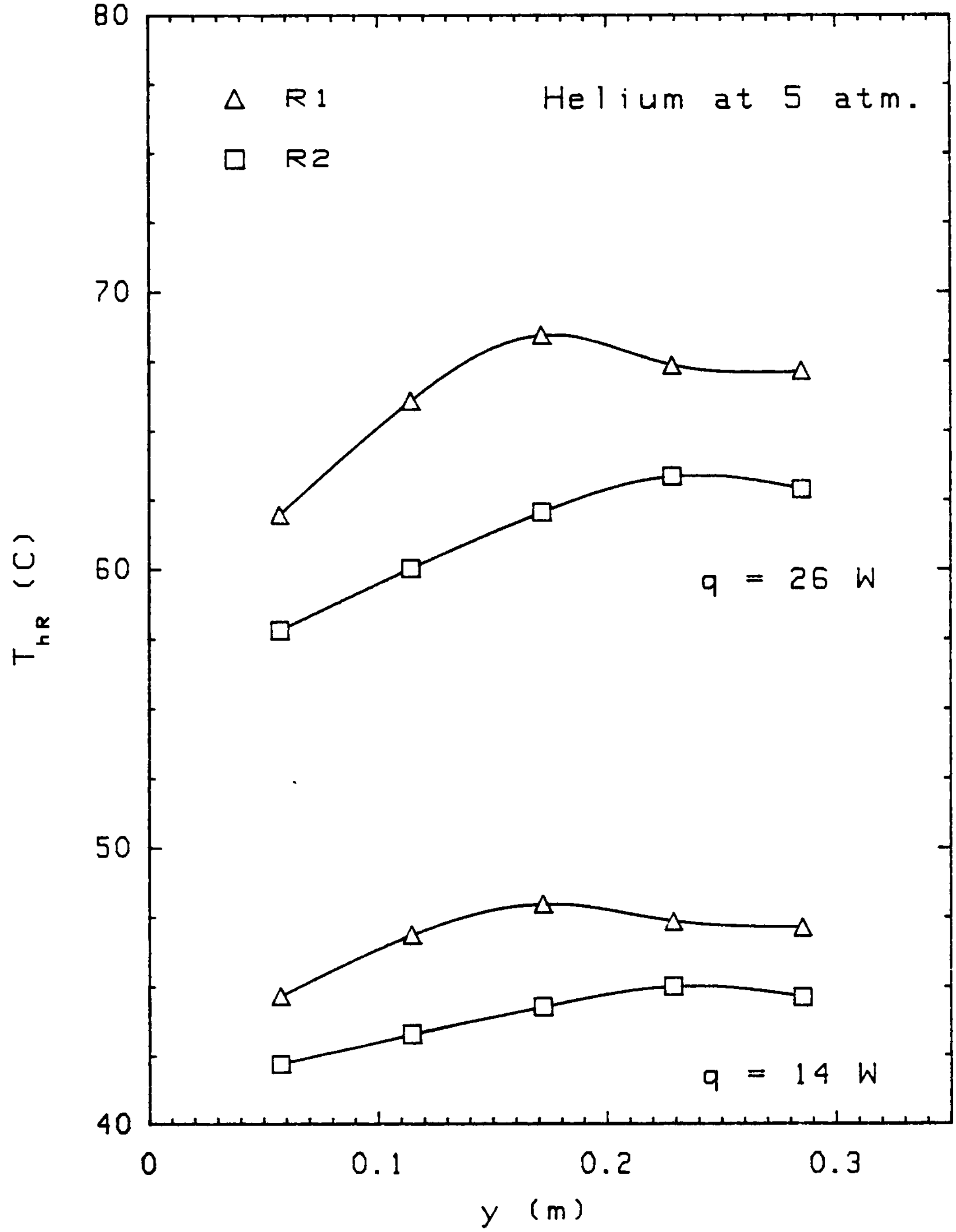

Figure C.7: Temperature profiles on rods for helium at 5 atm.

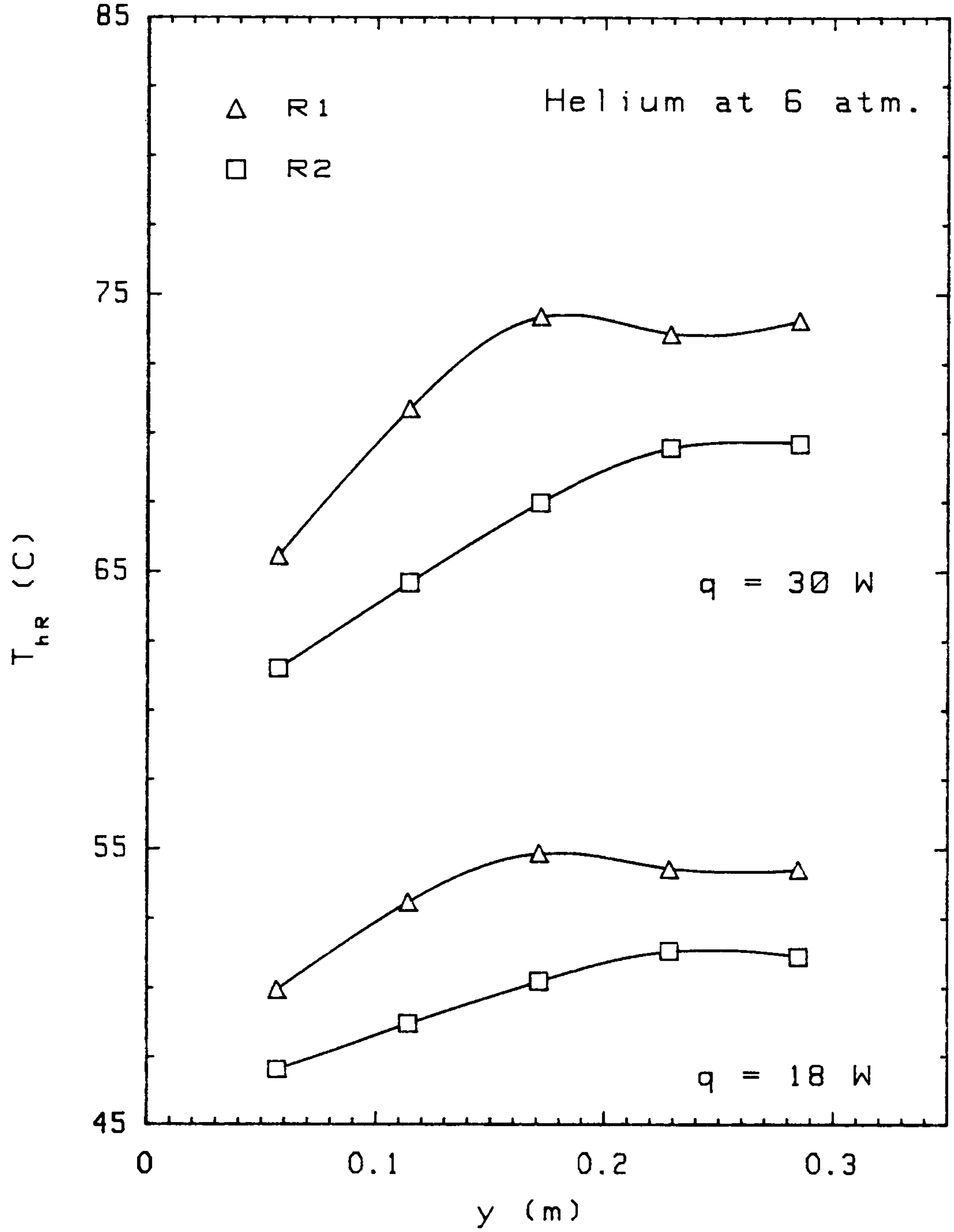

Figure C.8: Temperature profiles on rods for helium at 6 atm.

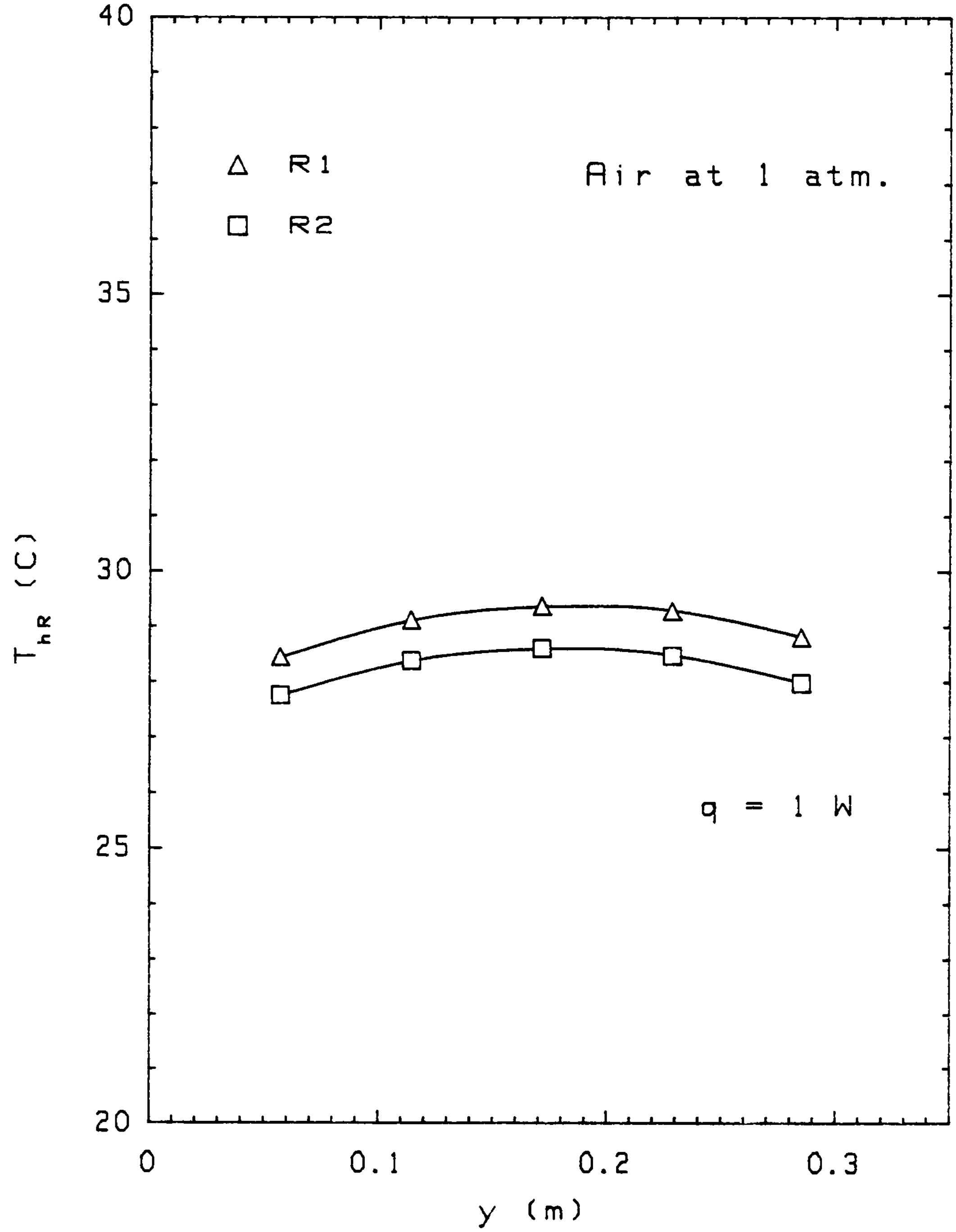

Figure C.9: Temperature profiles on rods for air at 1 atm. (a) 1 W (b) 10 W

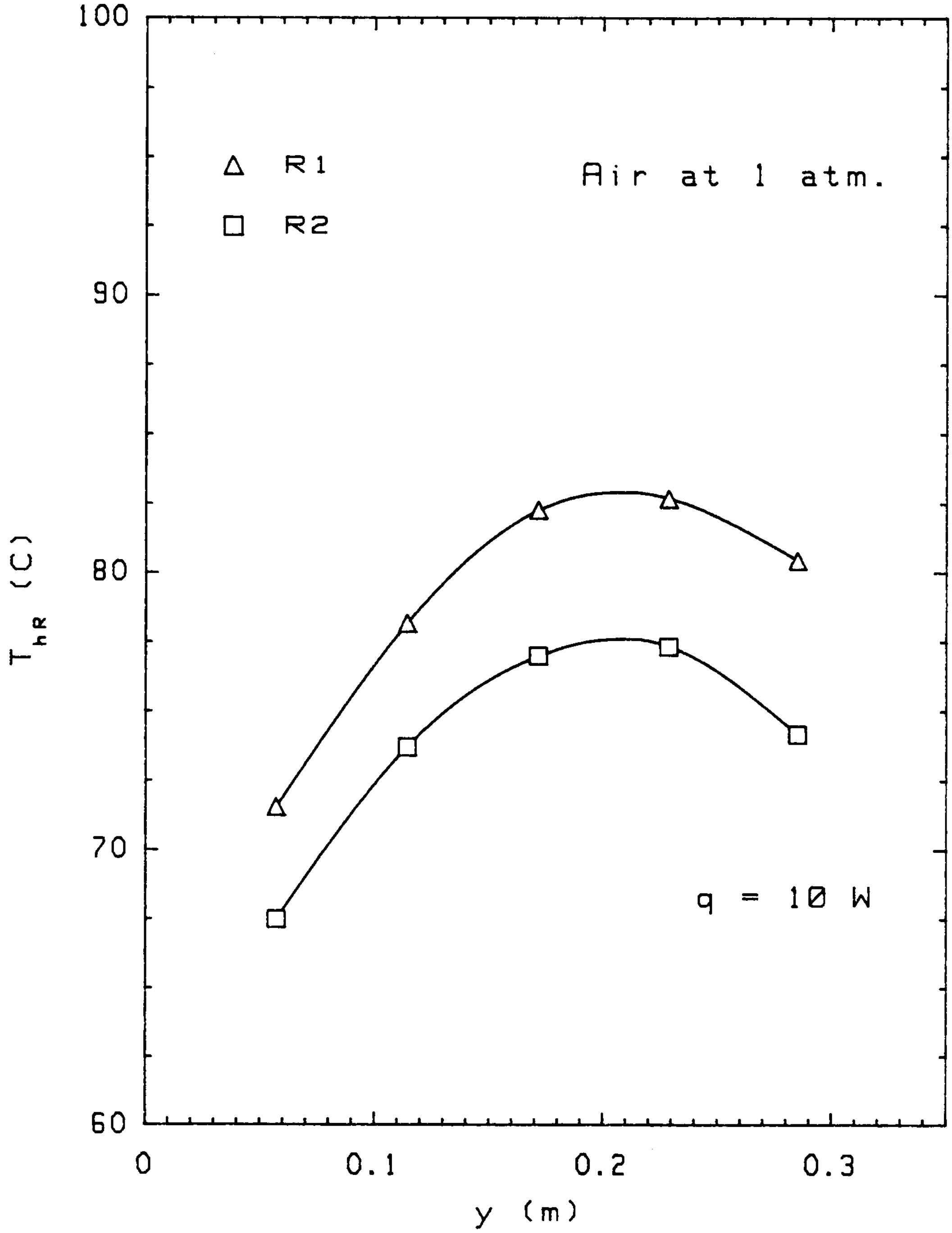

Figure C.9 (Continued)

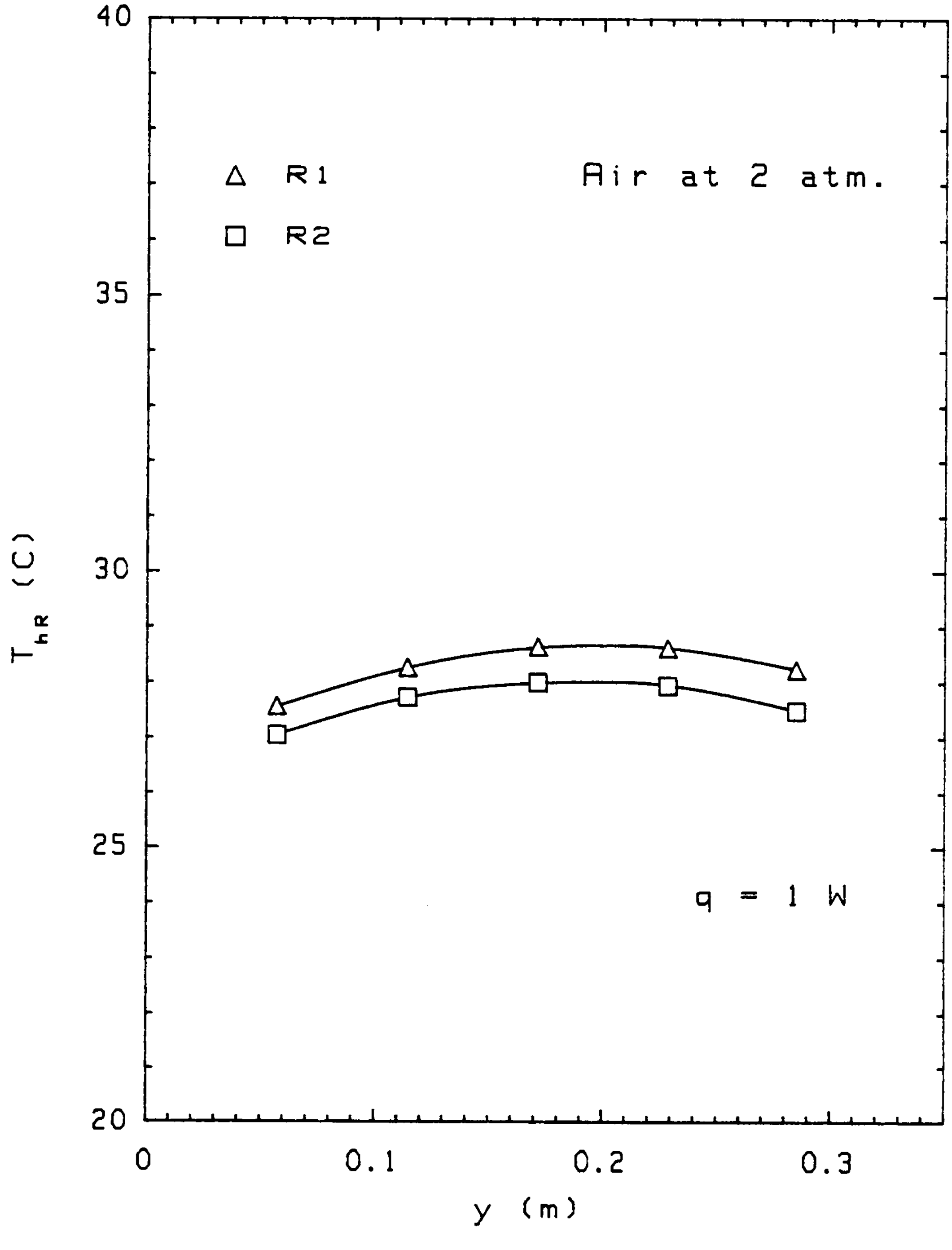

Figure C.10: Temperature profiles on rods for air at 2 atm. (a) 1 W (b) 10 W

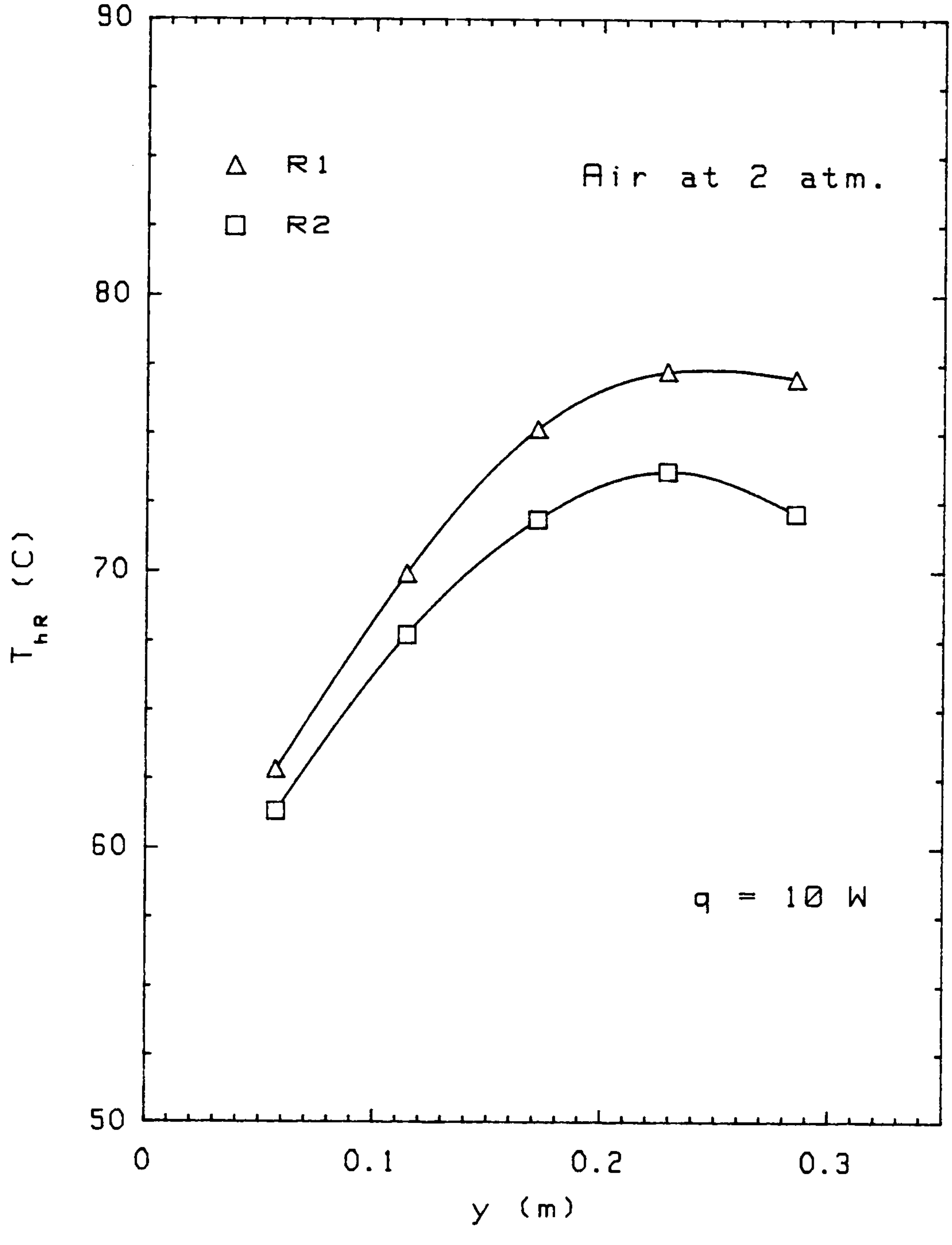

Figure C.10 (Continued)

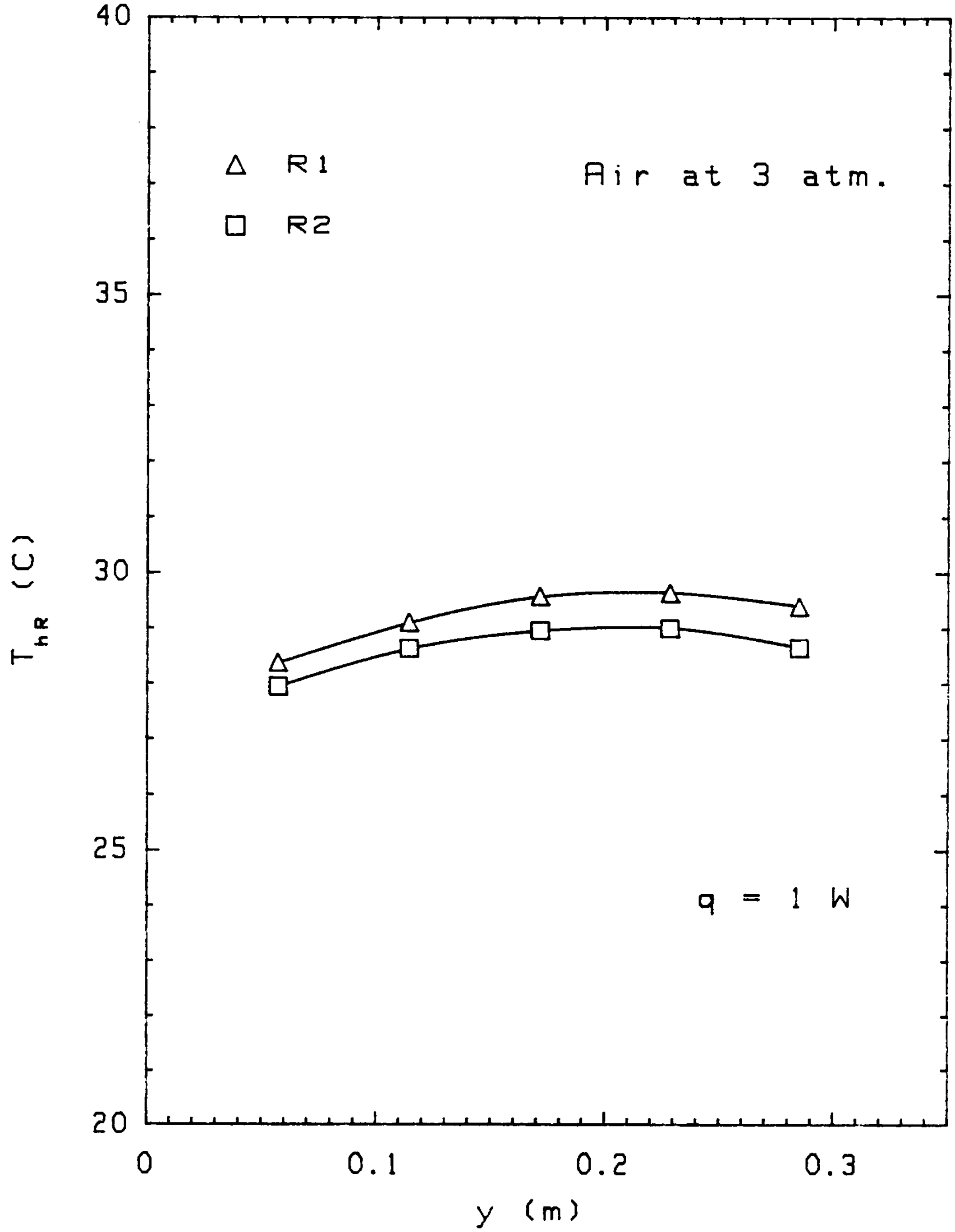

Figure C.11: Temperature profiles on rods for air at 3 atm. (a) 1 W (b) 12 W

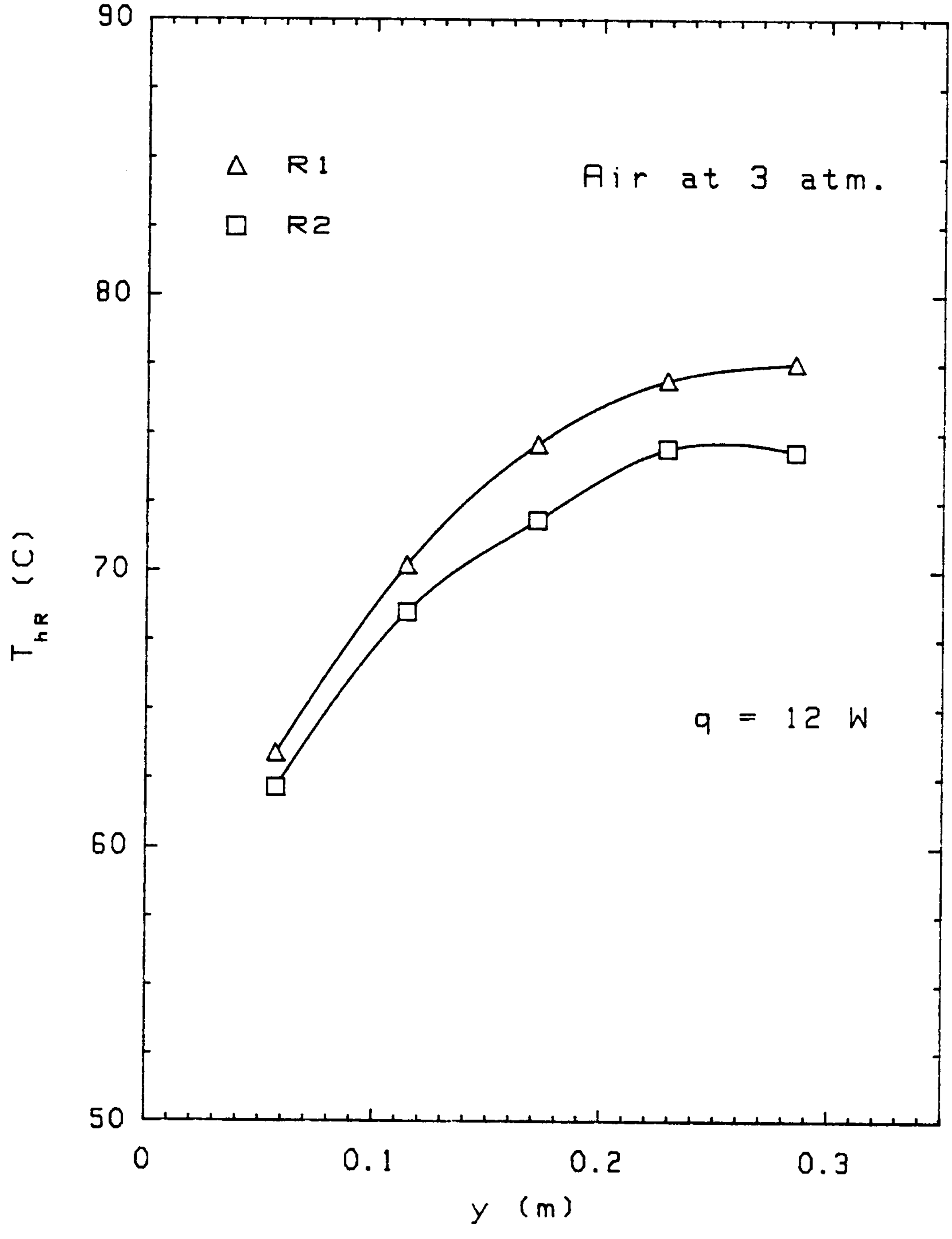

Figure C.11 (Continued)

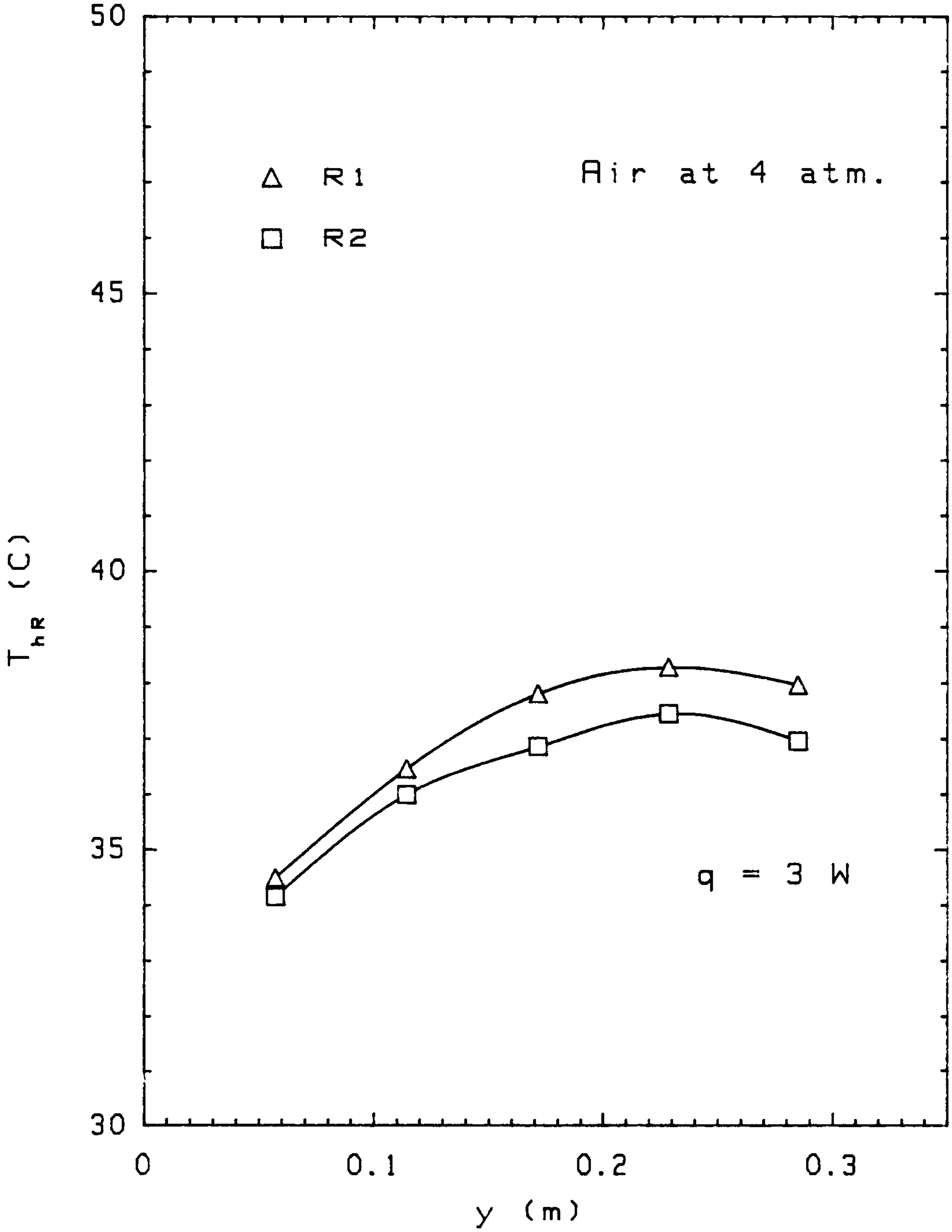

Figure C.12: Temperature profiles on rods for air at 4 atm. (a) 3 W (b) 14 W

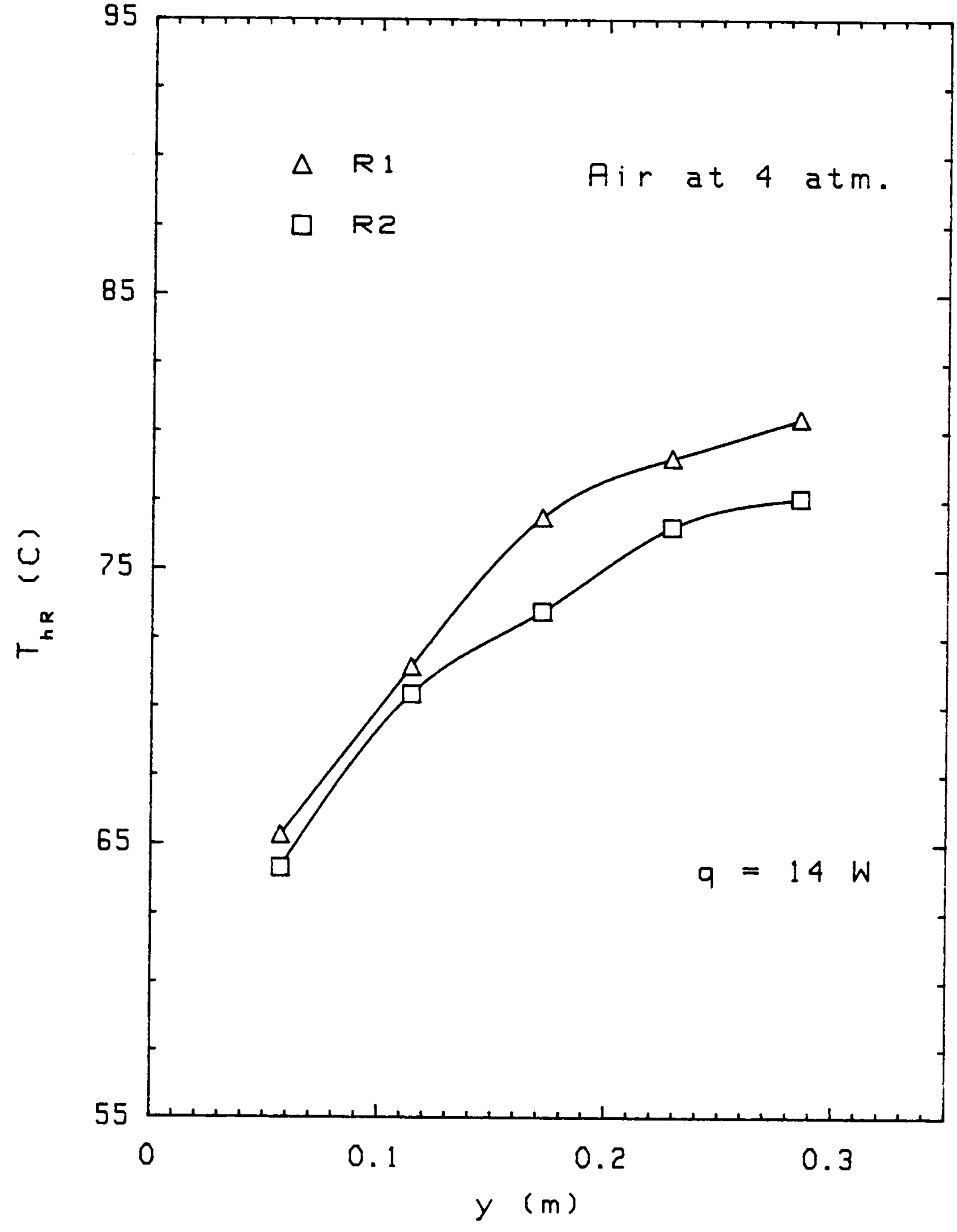

Figure C.12 (Continued)

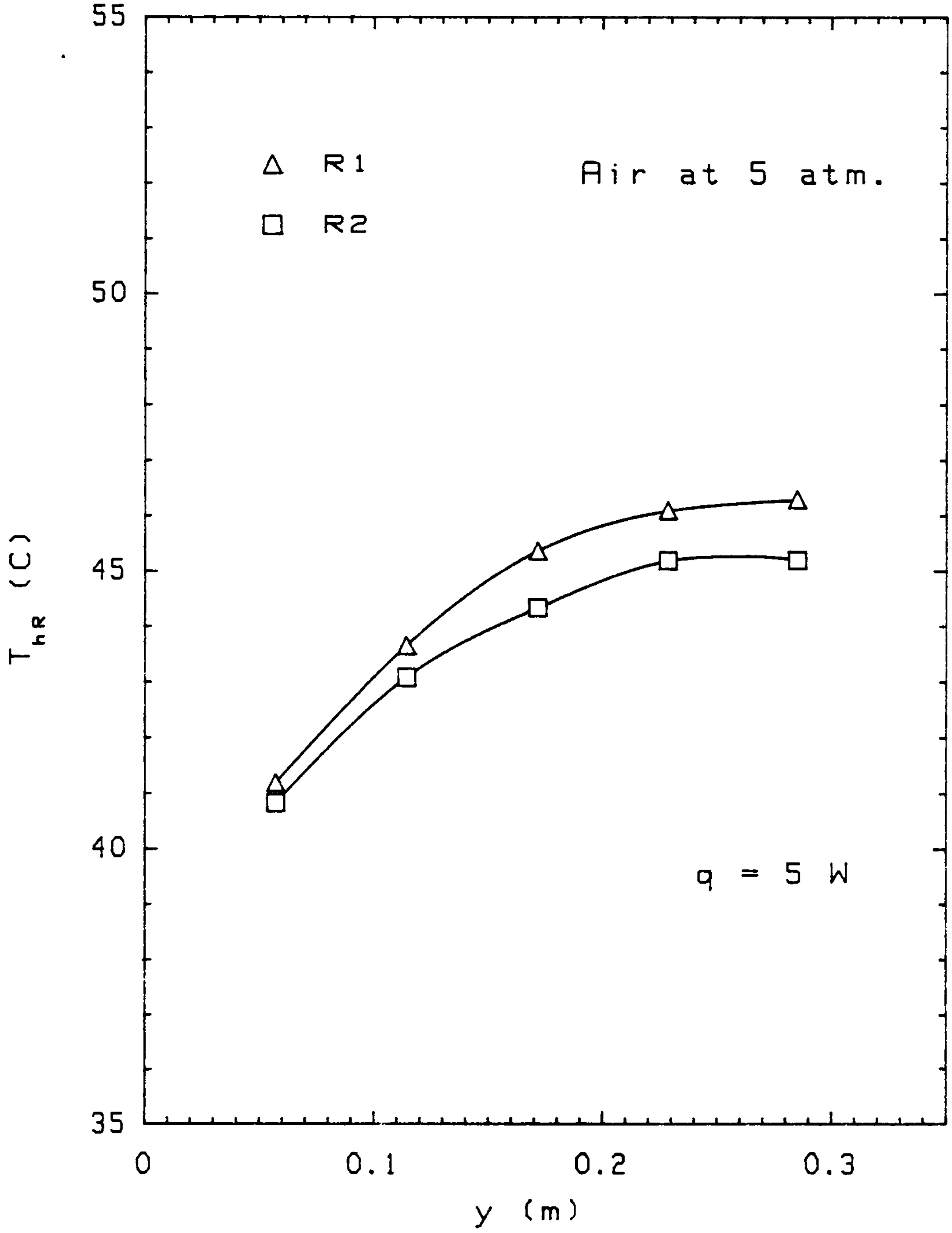

Figure C.13: Temperature profiles on rods for air at 5 atm. (a) 5 W (b) 15 W

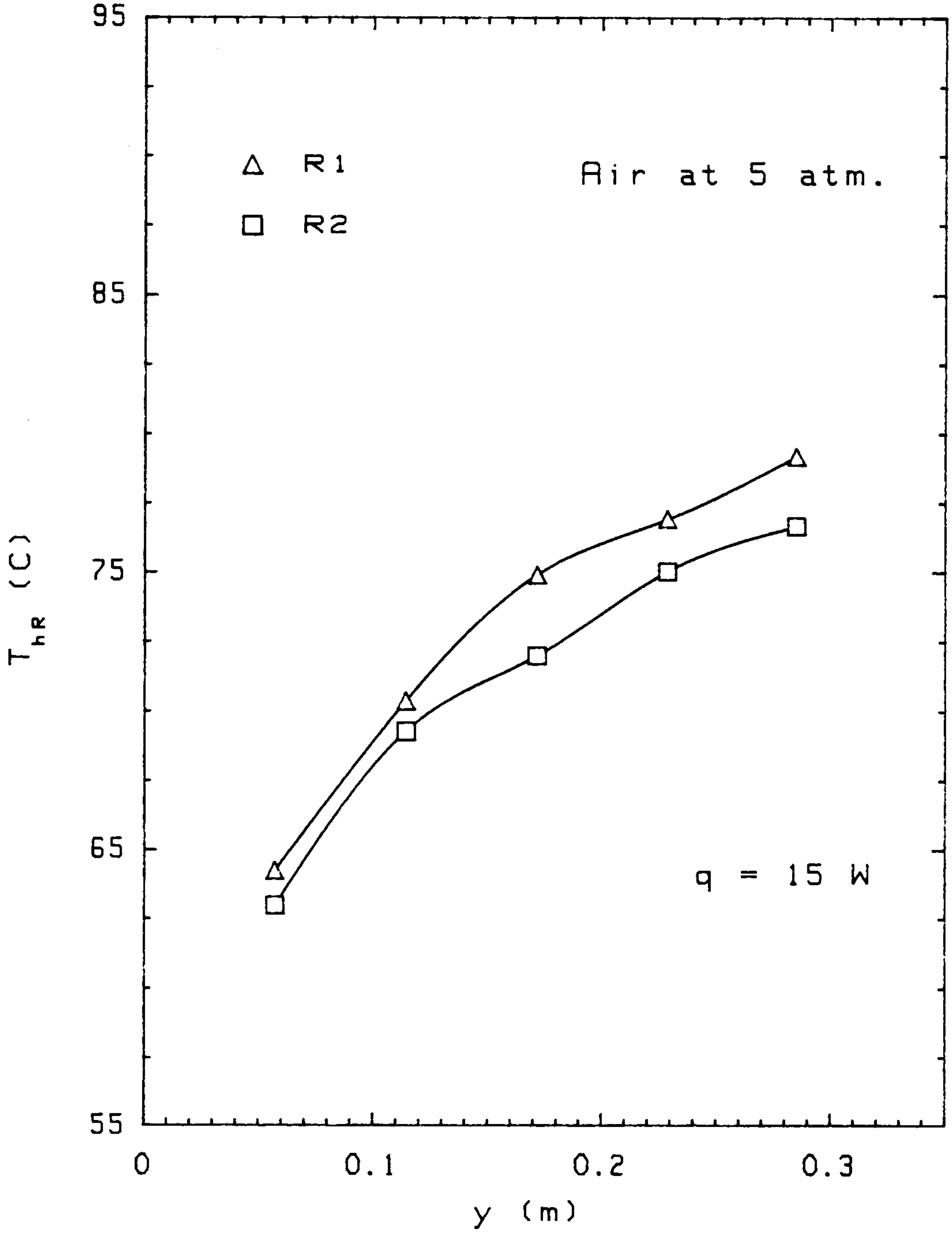

Figure C.13 (Continued)

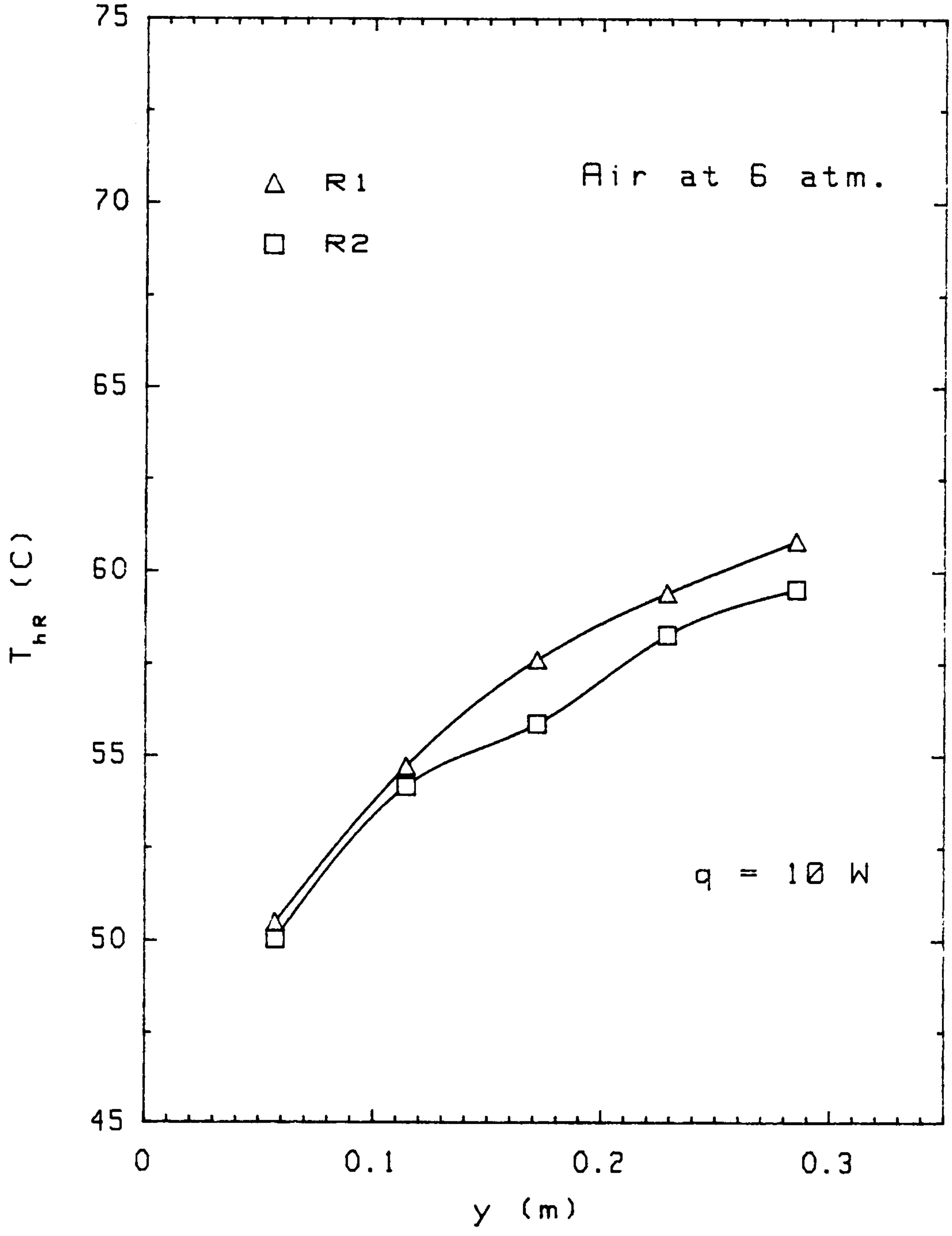

Figure C.14: Temperature profiles on rods for air at 6 atm. (a) 10 W (b) 18 W

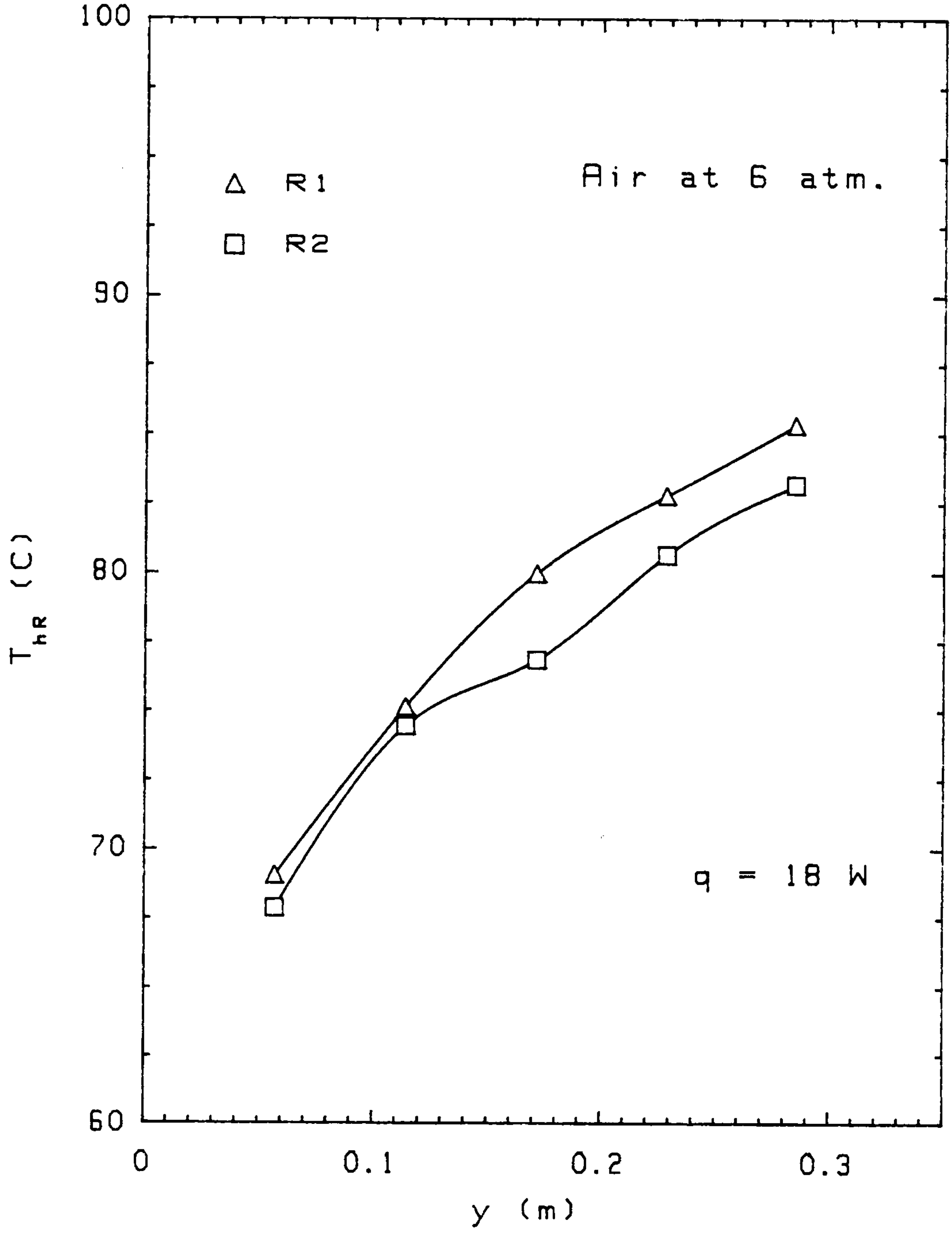

Figure C.14 (Continued)

Appendix D

INSTRUMENTS AND EQUIPMENT

Table D.1: Instruments

Sl.no.	*Item*	*Manu–facturer*	*Range*	*Accuracy*
1.	Ammeter	Keithley–instruments	$20\mu A$ *to* $200ma$	$0.8\%Rdg + 15D$
2.	Voltmeter	Keithley–instruments	$20mV$ *to* $1000V$	$0.5\%Rdg + 15D$
3.	Constant–temp. bath	MGW LAUDA (MT–6)	-20 *to* $120^0\ C$	$\pm\ 0.01\ C$
4.	Vacuum–gage	NRC equip. corp.	1 *to* $2500\mu m$	$14\ mV$ Full scale
5.	Pressure–gage	De Vilbiss company	0 *to* $100PSI$	$\pm\ 0.2\ PSI$

Table D.2: Associated equipment

Sl.no.	*Item*	*Manufacturer*
1.	$35mm$ Camera Single lens reflex	Minolta XG–M
2.	Data acquisition/control system(200 channels)	Hewlett–Packard 3497A
3.	Digital voltmeter	Hewlett–Packard 3456A
4.	Variacs (3)	Oak–Ridge national–laboratory
5.	Vacuum pump	Sargent–Welch scientific company
6.	Cool–arc welder	Laboratory–apparatus co.
7.	Ice–point reference	Kaye instruments model $K - 140/4$
8.	Regulator	De Vilbiss company

Appendix E

ANALYSIS OF EXPERIMENTAL ERRORS

The uncertainities in Nu_{Td} and Ra_d are calculated, following the method of Kline and McClintock. The assumptions and equations used in these analyses are presented below.

Assumptions

$$w_V = 0.005\ volts.$$

$$w_L = w_d = 0.000254\ m.$$

$$w_T = 0.2\ C.$$

$$w_{\Delta T} = w_{T_f} = 0.28284\ C.$$

$$R = 116.720\ \Omega.$$

Equations

Power input per rod :

$$q = \frac{V^2}{A_d R}$$

$$w_q = [(w_V \partial q \partial V)^2 + (w_R \frac{\partial q}{\partial R})^2 + (w_{A_d} \frac{\partial q}{\partial A_d})^2]^{\frac{1}{2}}$$

$$\frac{w_q}{q} = [(2\frac{w_V}{V})^2 + (\frac{w_R}{R})^2 + (\frac{w_{A_d}}{A_d})^2]^{\frac{1}{2}}.$$

Total heat transfer coefficient :

$$h_{Td} = \frac{q}{\Delta T}$$

$$w_{h_{Td}} = [(w_q \frac{\partial h_{Td}}{\partial q})^2 + (w_{\Delta T} \frac{\partial h_{Td}}{\partial \Delta T})^2]^{\frac{1}{2}}$$

$$\frac{w_{h_{Td}}}{h_{Td}} = [(\frac{w_q}{q})^2 + (\frac{w_{\Delta T}}{\Delta T})^2]^{\frac{1}{2}}.$$

Total Nusselt number :

$$Nu_{Td} = \frac{h_{Td} d}{k}$$

Note : w_k is negligible.

$$w_{Nu_{Td}} = [(w_{h_{Td}} \frac{\partial Nu_{Td}}{\partial h_{Td}})^2 + (w_d \frac{\partial Nu_{Td}}{\partial d})^2]^{\frac{1}{2}}$$

$$\frac{w_{Nu_{Td}}}{Nu_{Td}} = [(\frac{w_{h_{Td}}}{h_{Td}})^2 + (\frac{w_d}{d})^2]^{\frac{1}{2}}.$$

Rayleigh number :

$$Ra_d = \frac{g\beta d^3 \Delta T}{\alpha\nu}$$

Note : w_g, w_α and w_ν are negligible.

$$\beta = \frac{1}{T_f}$$

$$w_{Ra_d} = [(w_{T_f} \frac{\partial Ra_d}{\partial T_f})^2 + (w_d \frac{\partial Ra_d}{\partial d})^2 + (w_{\Delta T} \frac{\partial Ra_d}{\partial \Delta T})^2]^{\frac{1}{2}}$$

$$\frac{w_{Ra_d}}{Ra_d} = [(\frac{w_{T_f}}{T_f})^2 + (\frac{w_d}{d})^2 + (\frac{w_{\Delta T}}{\Delta T})^2]^{\frac{1}{2}}.$$

Table E.1: Uncertainty in Nusselt and Rayleigh numbers

% Uncertainty	Helium		Air	
	Lowest P and q	Highest P and q	Lowest P and q	Highest P and q
Nu_{Td}	3.09	1.72	2.52	1.80
Ra_d	3.98	3.04	3.60	3.09

Table E.2: Accuracy of temperature measurements

Temperature Range in C	*Percentage of Data Points in the Range*	$T_{NBS} - T_{HP}$
25 - 60	49.55	−0.078
60 – 70	29.35	+0.171
70 – 85	21.10	+0.280

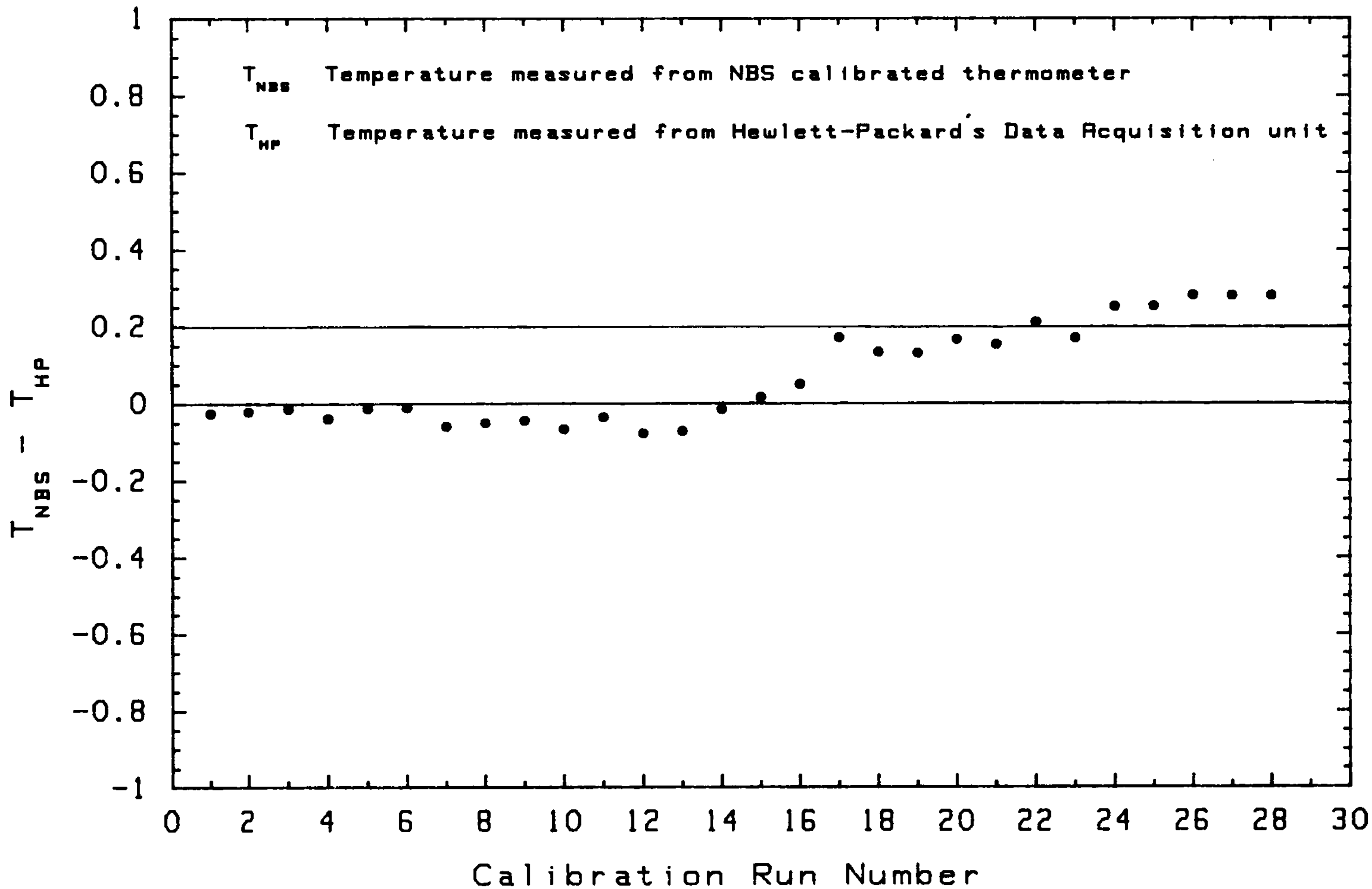

Figure E.1: Calibration of temperature measurements

Appendix F

ANALYSIS OF APPLICATION OF RESULTS TO THE ACTUAL CANISTER.

The maximum temperature on the actual canisters is estimated by using the generalized correlations for different values of power generation, percentage radiation and liner temperatures. The following are the equations to obtain the maximum temperature.

The generalized correlation :

$$Nu_D = a\,(Ra_D)^b$$

where, a and b are known constants.

$$(Nu_D)^{1+b} = a\,(Ra_D\,Nu_D)^b$$

$$\begin{aligned} Ra_D\,Nu_D &= \frac{g\beta}{\alpha\nu}D^3(T_{MR} - T_{MC})\frac{h_D D}{k} \\ &= \frac{g\beta}{\alpha\nu}D^3\frac{Q\,r\,D}{A_T k} \end{aligned}$$

where, r is the percentage radiation.

$$Nu_D = x\,(Ra_D\,Nu_D)^y$$

where,

$$x = a^{\frac{1}{1+b}} \quad and \quad y = \frac{b}{1+b}$$

Since,

$$\begin{aligned} Q\,r &= h_D A_T (T_{MR} - T_{MC}) \\ &= Nu_D \frac{k}{D} A_T (T_{MR} - T_{MC}) \\ &= x\,(Ra_D\ Nu_D)^y \frac{k}{D} A_T (T_{MR} - T_{MC}) \end{aligned}$$

The characteristic temperature difference,

$$(T_{MR} - T_{MC}) = \frac{Q\,r}{A_T \frac{k}{D}} \frac{1}{x\,(Ra_D\ Nu_D)^y}$$

Using the correlation,

$$\frac{(T_{MAX} - T_{MC})}{(T_{MR} - T_{MC})} = u\,(Ra_D)^v$$

where, u and v are known constants,

T_{MAX} is obtained.

Table F.1: Maximum temperature on canisters at $T_{MC} = 20\ C$

Q	T_{MAX} in C Cask with Fins			T_{MAX} in C Cask without Fins		
W	0%	20%	50%	0%	20%	50%
500	30.75	28.99	26.26	40.16	36.79	31.42
1000	38.76	35.68	30.75	55.63	49.66	40.16
2000	52.76	47.38	38.76	83.02	72.45	55.63

Table F.2: Maximum temperature on canisters at $T_{MC} = 30\ C$

Q	T_{MAX} in C Cask with Fins			T_{MAX} in C Cask without Fins		
W	0%	20%	50%	0%	20%	50%
500	40.82	39.05	36.21	50.26	46.85	41.46
1000	48.89	45.79	40.83	65.79	59.77	50.26
2000	62.99	57.57	48.89	93.24	82.63	65.76

Table F.3: Maximum temperature on canisters at $T_{MC} = 40\ C$

Q	T_{MAX} in C Cask with Fins			T_{MAX} in C Cask without Fins		
W	0%	20%	50%	0%	20%	50%
500	50.90	49.11	46.25	60.31	56.91	51.50
1000	59.02	55.90	50.90	75.88	69.87	60.31
2000	73.21	67.75	59.02	103.46	92.82	75.86

Table F.4: Maximum temperature on canisters at $T_{MC} = 50\ C$

Q	T_{MAX} in C Cask with Fins			T_{MAX} in C Cask without Fins		
W	0%	20%	50%	0%	20%	50%
500	60.97	59.17	56.29	70.38	66.97	61.54
1000	69.14	66.00	60.97	86.09	79.98	70.38
2000	83.43	77.94	69.14	113.68	102.99	86.01

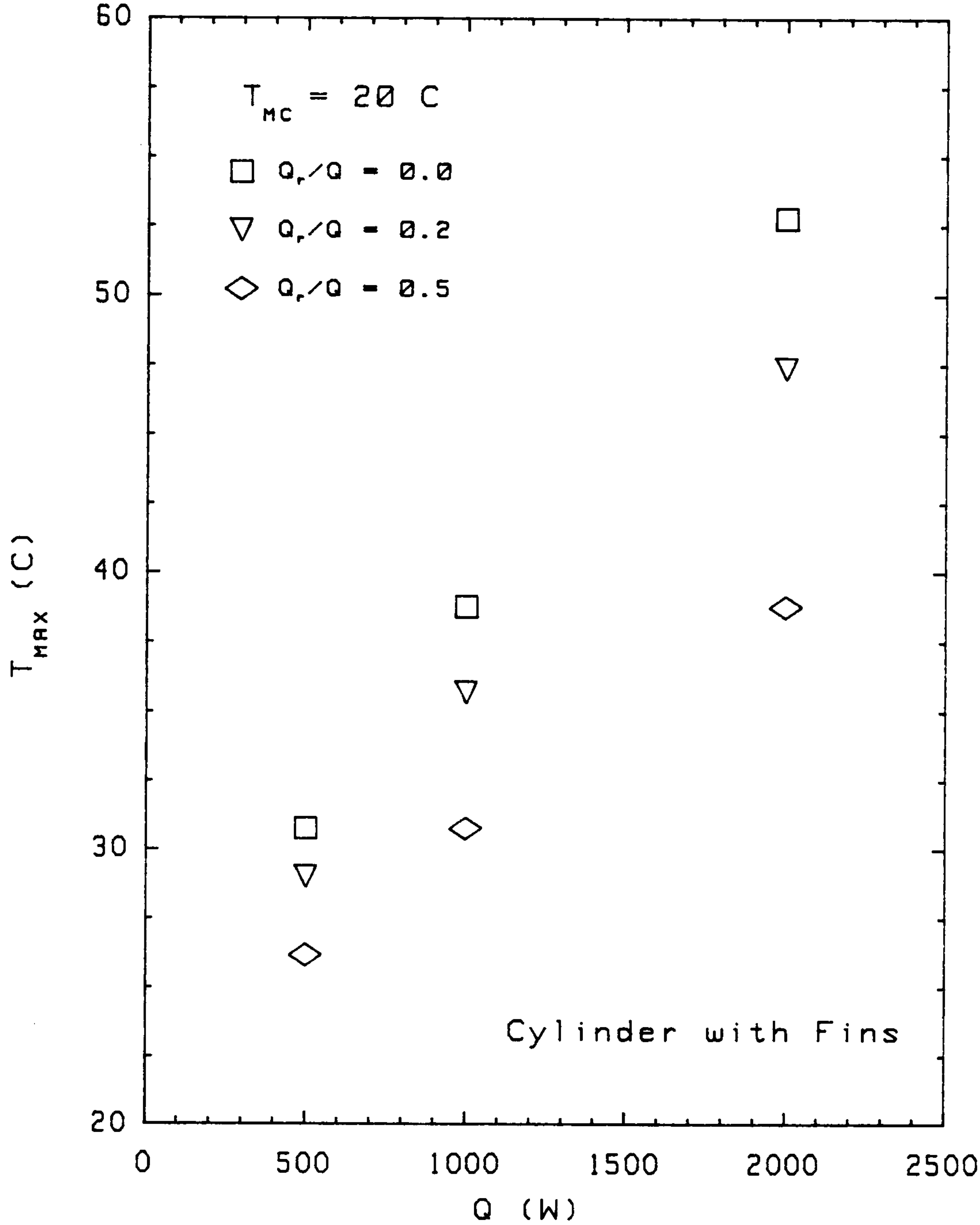

Figure F.1: Maximum temperature distribution on canisters (with fins) at $T_{MC} = 20\ C$

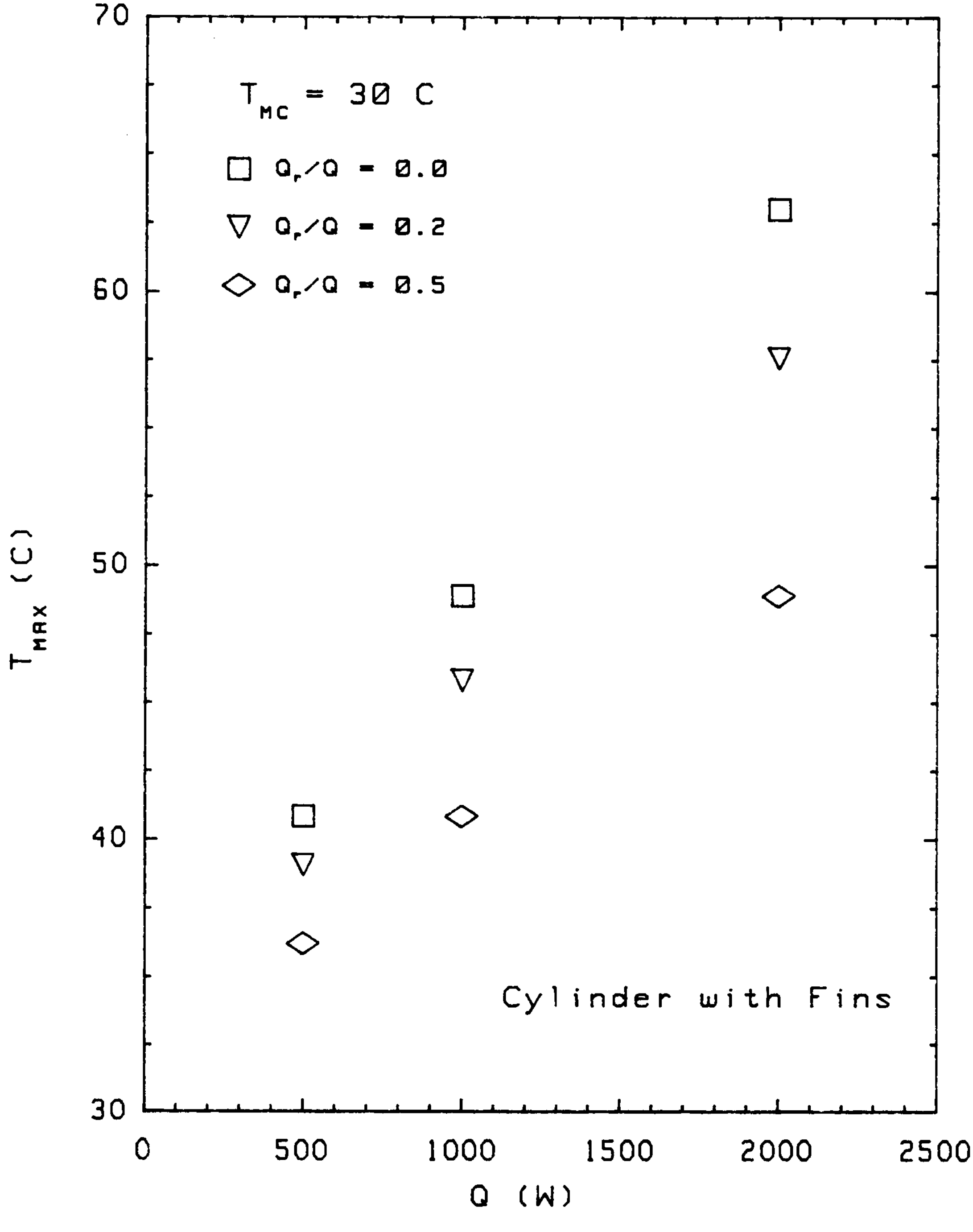

Figure F.2: Maximum temperature distribution on canisters (with fins) at $T_{MC}\ =\ 30\ C$

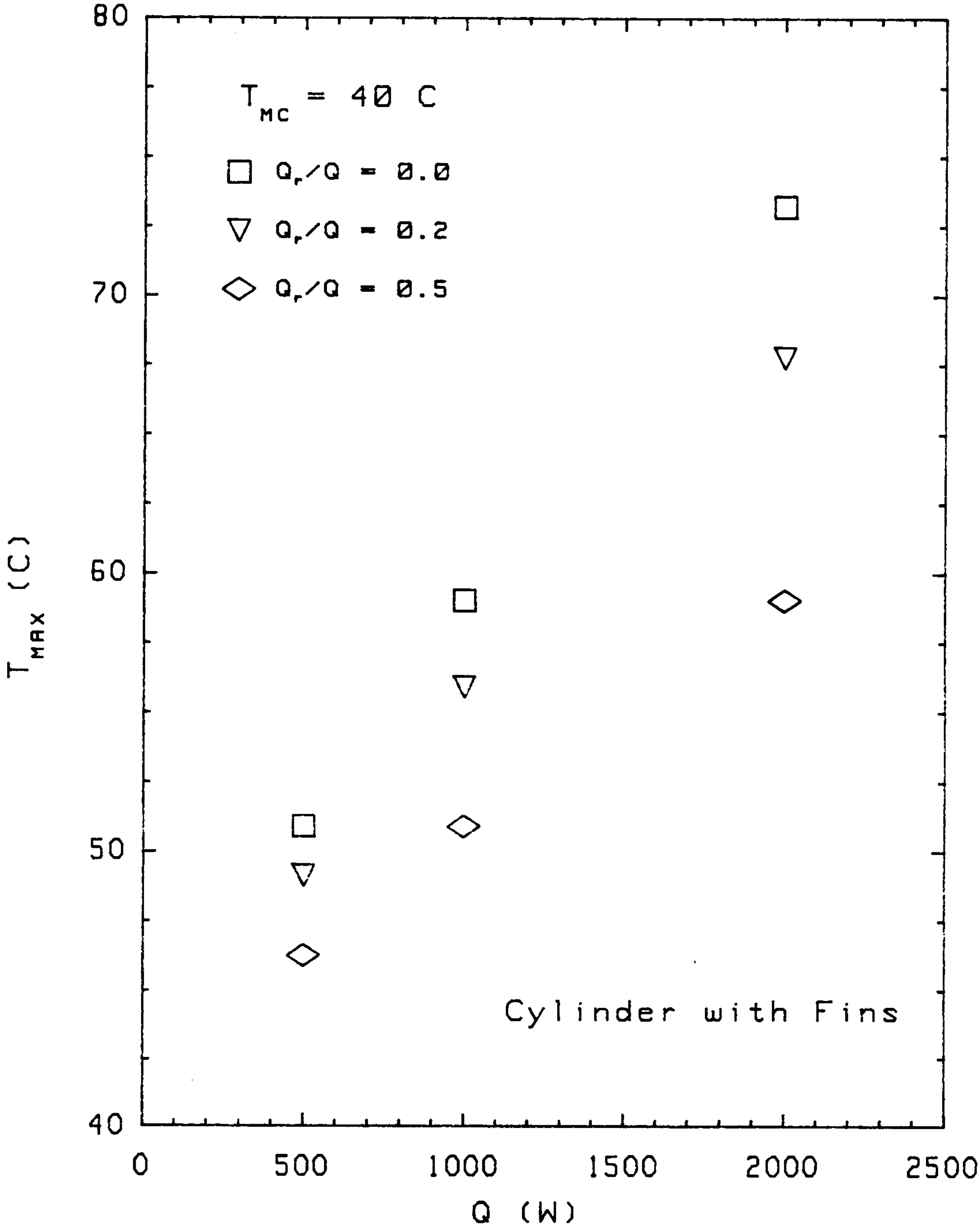

Figure F.3: Maximum temperature distribution on canisters (with fins) at $T_{MC} = 40\ C$

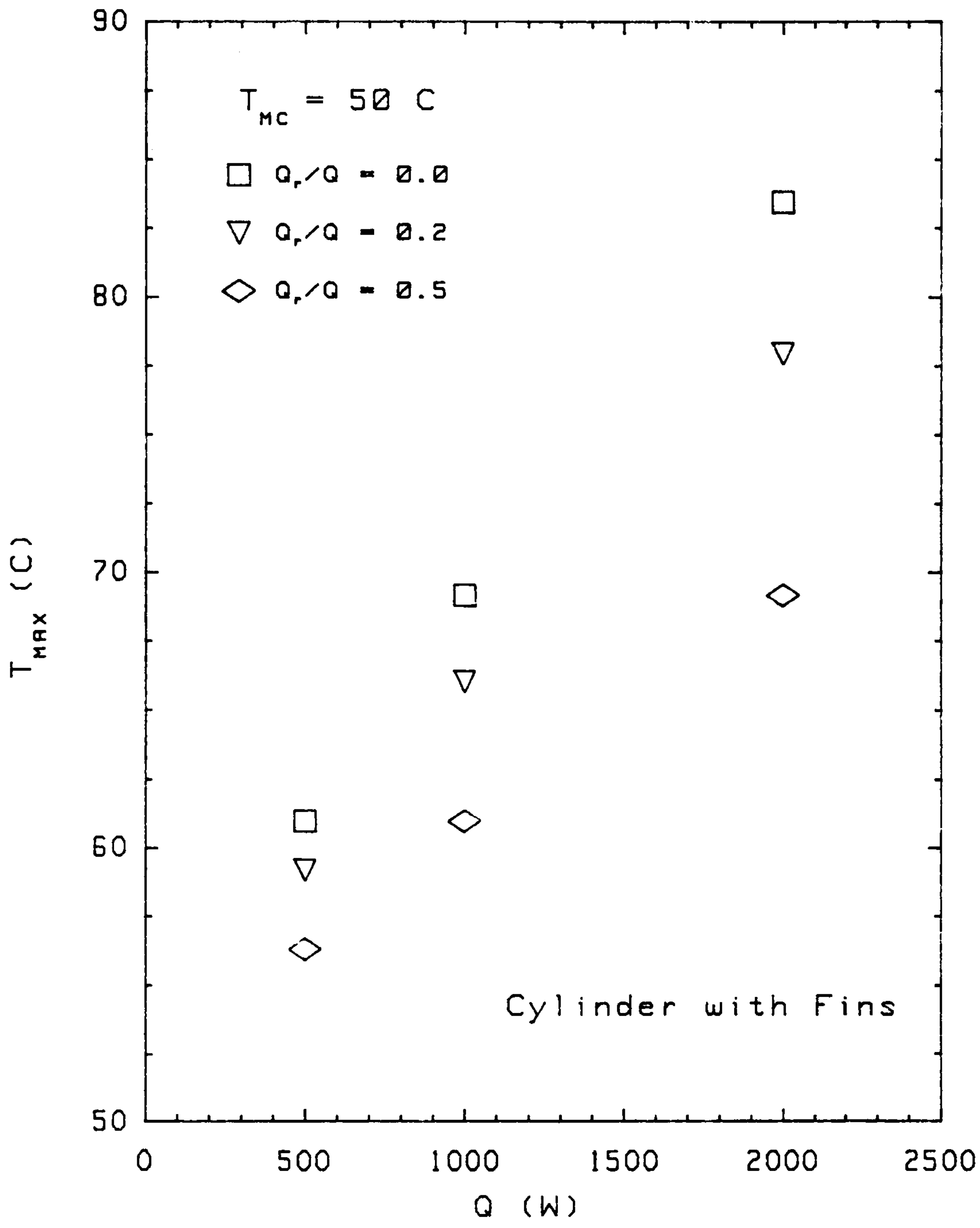

Figure F.4: Maximum temperature distribution on canisters (with fins) at $T_{MC} = 50\ C$

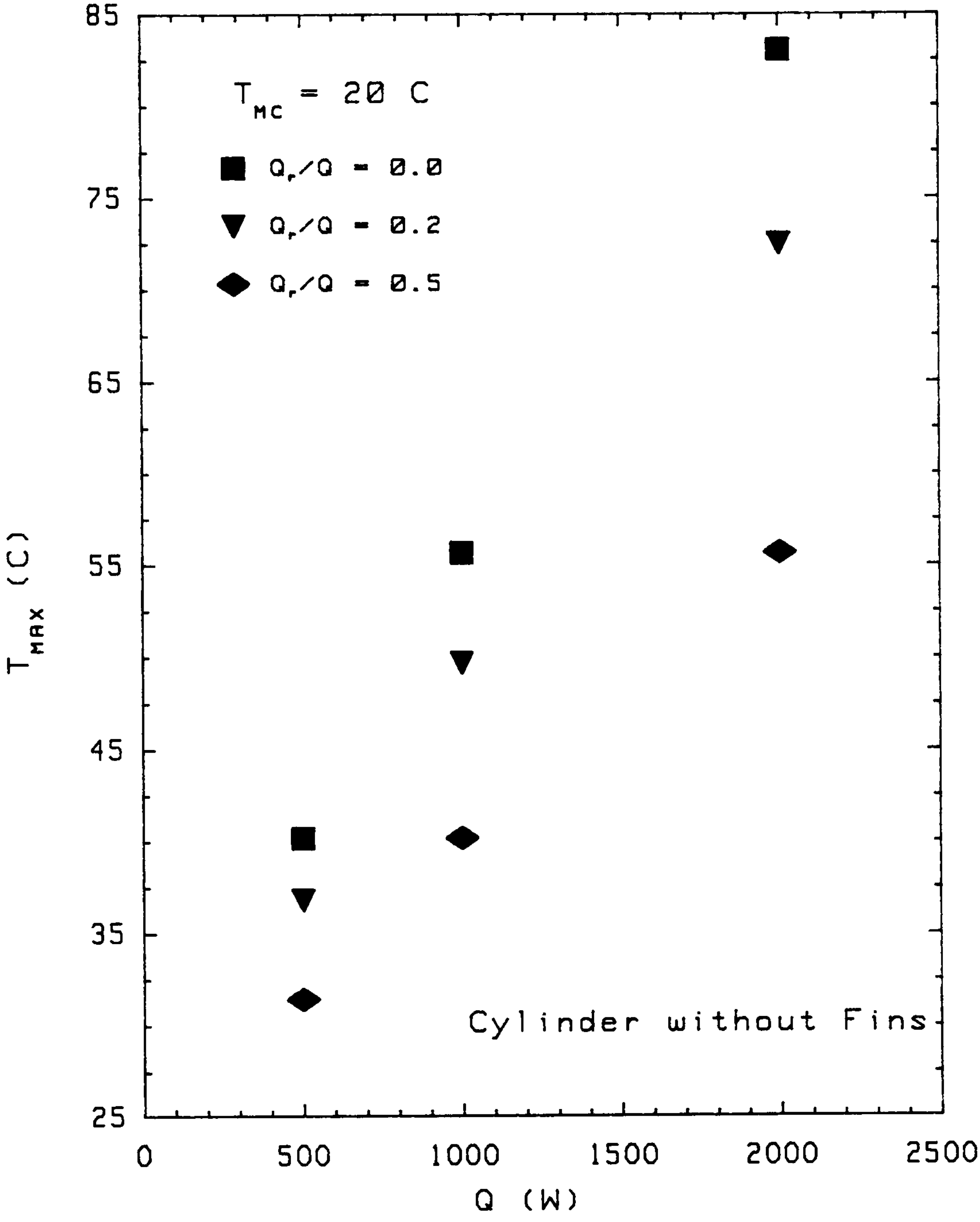

Figure F.5: Maximum temperature distribution on canisters (without fins) at $T_{MC} = 20\ C$

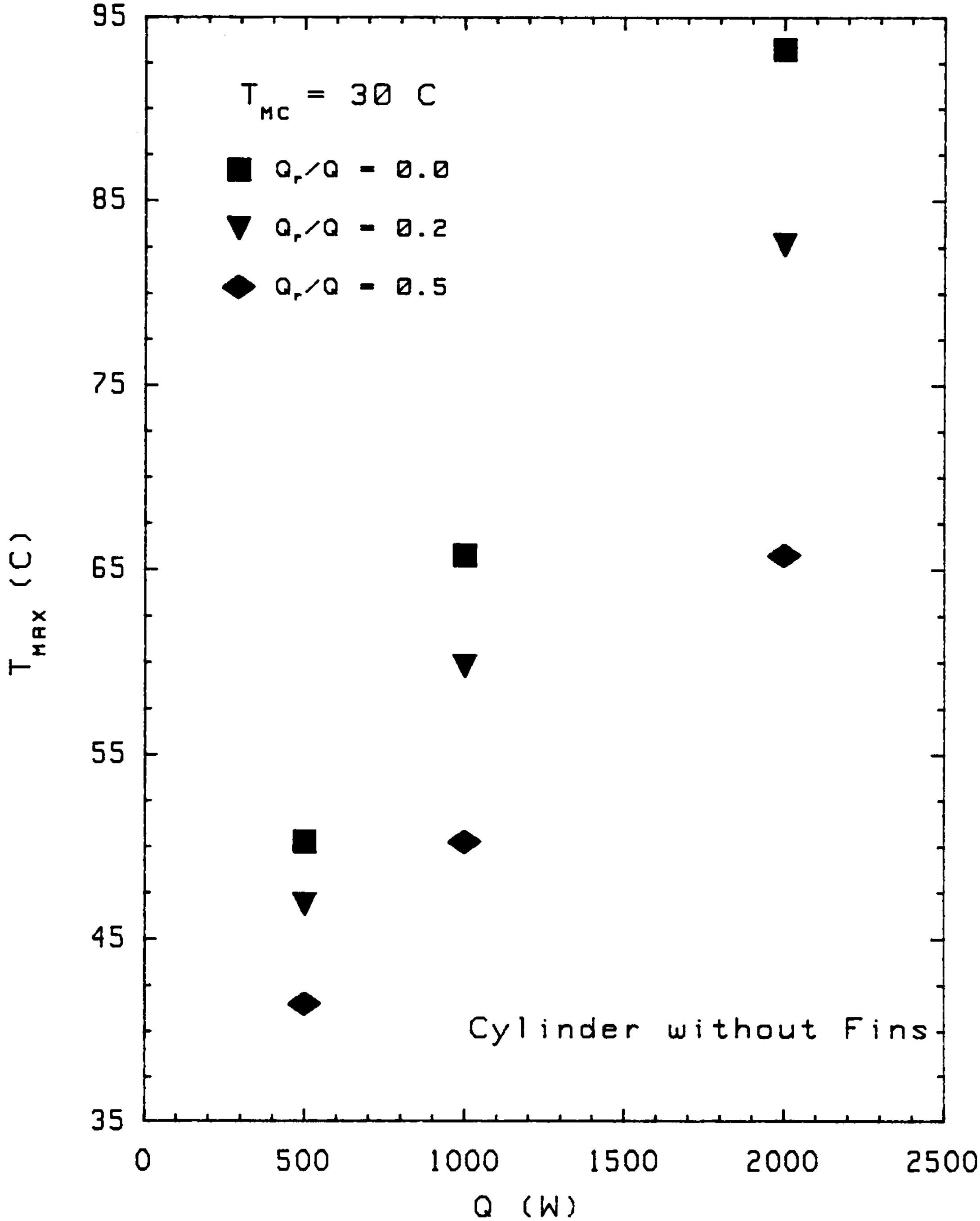

Figure F.6: Maximum temperature distribution on canisters (without fins) at $T_{MC} \ = \ 30 \ C$

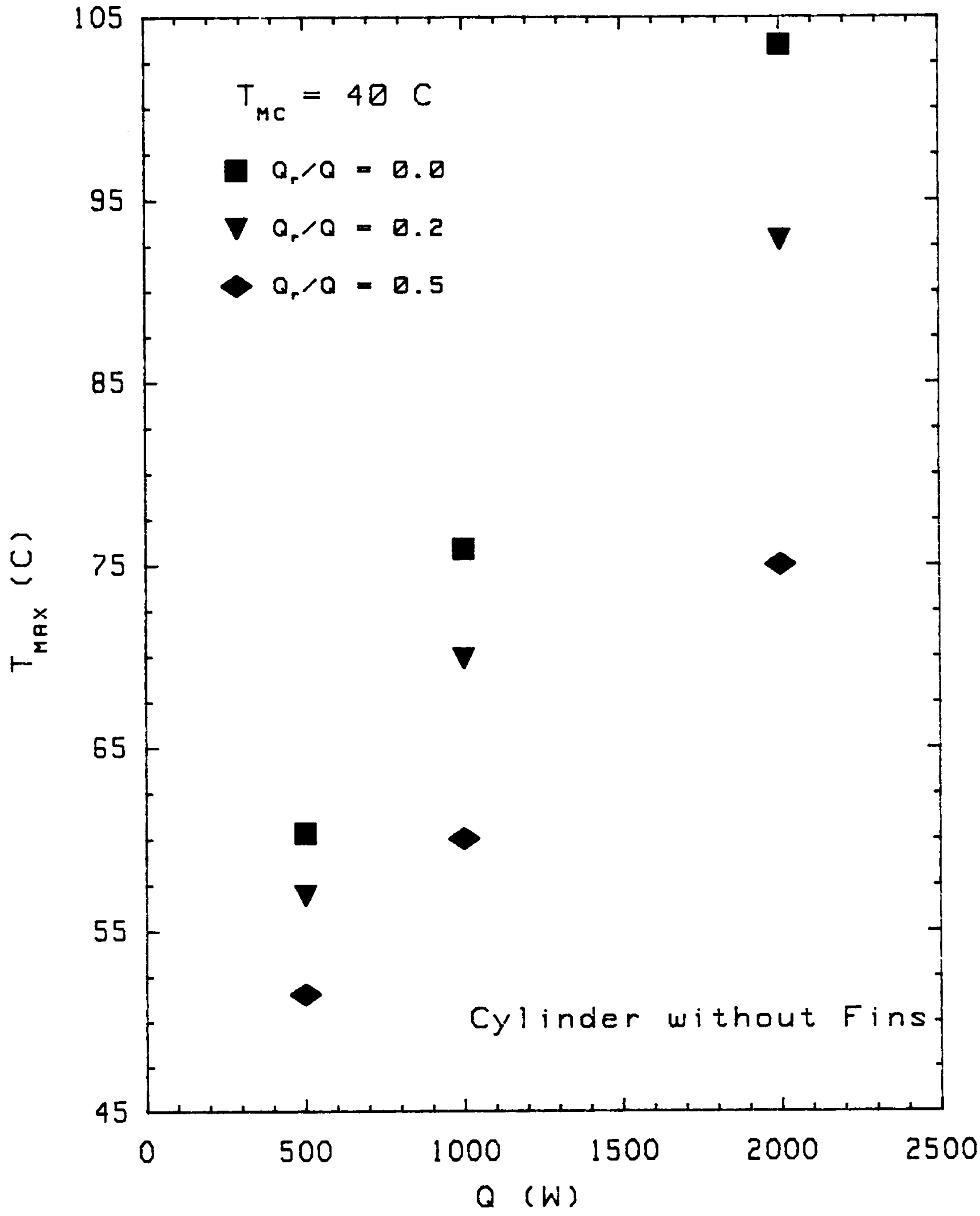

Figure F.7: Maximum temperature distribution on canisters (without fins) at $T_{MC} = 40\ C$

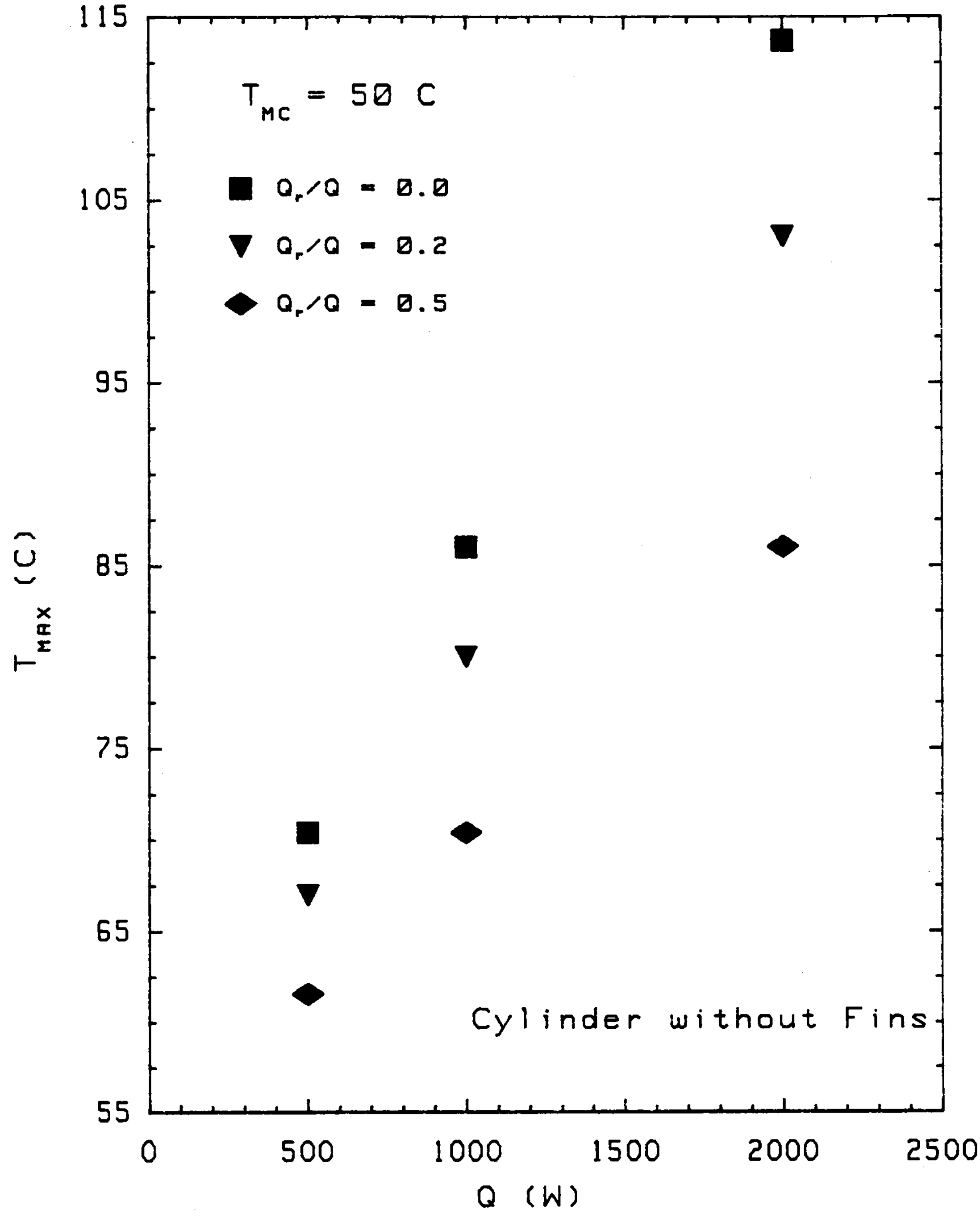

Figure F.8: Maximum temperature distribution on canisters (without fins) at $T_{MC} = 50\ C$

VITA

M. Satishchandra Arya was born in Bangalore, India on May 9, 1962. He attended elementary, high schools and pre–university in that city and graduated in June of 1979. The following September he entered Bangalore University and was awarded the Bachelor of Science in Mechanical Engineering in October of 1984.

After working for one year in a small–scale industry manufacturing ferrous and non–ferrous castings, he was admitted to the Bradley Unviersity, Peoria and began work on his Master's degree. After a semester, he joined The University of Tennessee, Knoxville and accepted a research assistantship in the fall of 1986. He received the Master of Science in Mechanical Engineering in August of 1988.